MONTE CARLO SIMULATION OF TWO-PHOTON PROCESSES

P.H.W.M. DAVERVELDT

STELLINGEN

1. De laagste-orde Feynmandiagrammen, waarbij een Z_0 deeltje uitgewisseld wordt in plaats van een foton, geven bij LEP energieën een significante bijdrage aan de werkzame doorsnede van vier-leptonproductieprocessen, indien de QED bijdrage gedomineerd wordt door Feynmandiagrammen met twee tijdachtige fotonen.
   Hoofdstuk V van dit proefschrift.

2. De methode, die Defrise et al. toepassen om stralingscorrecties op twee-fotonprocessen te berekenen, kan niet gebruikt worden om een "event"-generator te construeren.
   M. Defrise et al., Phys. Rev. D23 (1981) 663.

3. De anomale vervalswijze van het Z_0 deeltje, $Z_0 \rightarrow \mu^+\mu^-\gamma$, zoals gemeten door het UA1 samenwerkingsverband in 1983, kan zowel wat betreft totale als partiële vervalsbreedten uitstekend verklaard worden door het bestaan van geëxciteerde muonen met een massa van slechts enkele GeV te postuleren.
   UA1 Coll. G. Arnison et al., Phys. Lett. 135B (1984) 250.

4. Een geschikte keuze van de constanten, die de koppeling van een geëxciteerd muon aan het Z_0 deeltje en aan het foton beschrijven, verhindert dat eerdere metingen van het anomaal magnetisch moment van het muon en van het proces $e^+e^- \rightarrow \mu^+\mu^-\gamma$ het bestaan van een geëxciteerd muon uitsluiten.

5. Voor de depolarisatie van een roterende spin, die diffundeert op een roos-ter, waarvan aan elk punt een random rotatiefrequentie is toegekend, kan eenvoudig een niet-triviale exacte ondergrens afgeleid worden. Vooral voor diffusieprocessen op roosters van hogere dimensie, waarvoor geen exacte resultaten bekend zijn, kan deze ondergrens van belang zijn.
   R. Czech en K.W. Kehr, Phys. Rev. Lett. 53 (1984) 1783.

6. De interpretatie van de metingen van de weerstand, die een bol ondervindt bij beweging langs de as van een snel roterende vloeistof, kan aanzienlijk bemoeilijkt worden door het optreden van secundaire stromingen.

7. De bewering van James, dat het maximum van twee uniform verdeelde random getallen verdeeld is volgens een wortelfunctie, is niet juist.
F. James, Rep. Prog. Phys. 43 (1980) 1145.

8. Wanneer Mason en Mazur de experimentele metingen van het viscomagnetisch effect bij Knudsengetal Kn ≈ 0.8 proberen te verklaren in het kader van het zogenaamde "Dusty Gas Model", zijn zij genoodzaakt om aan te nemen dat er productie van polarisatie optreedt ten gevolge van de interacties tussen de gasmoleculen en de wand. Deze veronderstelling is niet langer noodzakelijk, wanneer de productie van polarisatie in de grenslaag op een correcte manier beschreven wordt.
E.A. Mason en E. Mazur, Physica 130A (1985) 437.

9. In vele gevallen is het waarnemen van de Zeemansplitsingen van verontreinigingen in halfgeleiders met behulp van optisch gedetecteerde magnetische resonantie niet mogelijk, daar de recombinatie tussen donoren en acceptoren niet stralend plaatsvindt. In deze gevallen kunnen electron-spinecho experimenten wellicht uitkomst bieden.
F.C. Bos, Proefschrift Leiden (1985).

10. De werkzame doorsnede van processen, waarbij een muonpaar uitgezonden wordt door middel van de uitwisseling van één foton, kan beschreven worden door "bremsstrahlung" van een massief foton met massa W en een massadistributie :

$$f(W^2)\, dW^2 = \frac{\alpha}{6\pi} \frac{\beta\,(3-\beta^2)}{W^2}\, dW^2, \quad \beta = \left(1 - \frac{4\,m_\mu^2}{W^2}\right)^{\frac{1}{2}}.$$

11 Wanneer "events" volgens waarschijnlijkheidsdistributies met een ingewikkelde piekstructuur gegenereerd moeten worden, verdient een op maat gemaakte "event"-generator de voorkeur boven "general purpose" integratieprogramma's.
Hoofdstuk II van dit proefschrift.

12. Het is ongewenst dat het rechterlijk ambt tegelijkertijd uitgeoefend wordt met een politiek ambt.

P.H.W.M. Daverveldt Leiden, 18 september 1985

MONTE CARLO SIMULATION OF TWO-PHOTON PROCESSES

MONTE CARLO SIMULATION OF TWO-PHOTON PROCESSES

Proefschrift

ter verkrijging van de graad
van Doctor in de Wiskunde en Natuurwetenschappen
aan de Rijksuniversiteit te Leiden,
op gezag van de Rector Magnificus Dr. J.J.M. Beenakker,
Hoogleraar in de faculteit der Wiskunde en Natuurwetenschappen,
volgens besluit van het College van Dekanen
te verdedigen op woensdag 18 september 1985
te klokke 16.15 uur

door

Petrus Henricus Wilhelmus Marie Daverveldt

geboren te Geldrop in 1958

Druk: NKB-Offset BV — Bleiswijk

Promotiecommissie:

Promotor: Prof. Dr. F.A. Berends

Referent : Dr. R.H.P. Kleiss

Overige leden: Prof. Dr. K.J.F. Gaemers
Prof. Dr. P.W. Kasteleyn
Prof. Dr. P. Mazur

Het in dit proefschrift beschreven onderzoek werd uitgevoerd als onderdeel van het onderzoeksprogramma van de Stichting voor Fundamenteel Onderzoek der Materie (F.O.M.) welke financiëel gesteund wordt door de Nederlandse Organisatie voor Zuiver-Wetenschappelijk Onderzoek (Z.W.O.).

Aan mijn ouders

Aan Marie-Jeanne

CONTENTS

CHAPTER I

OUTLINE

During the last two decades e^+e^- collider experiments provided physicists with a wealth of important discoveries concerning elementary particle physics. Although the main attention was focussed on processes like $e^+e^- \to \mu^+\mu^-$, $e^+e^- \to e^+e^-$ or $e^+e^- \to$ hadrons, where the incoming beams interacted through the annihilation in (or the exchange of) one photon, the interest in processes such as $e^+e^- \to e^+e^-\mu^+\mu^-$, $e^+e^- \to e^+e^+e^-e^-$ or $e^+e^- \to e^+e^-$ hadrons, growed steadily. These reactions can be characterized by the fact that the dominant contribution to the total cross section comes from Feynman diagrams with two spacelike virtual photons which are almost real (also called multiperipheral or t-channel diagrams). Therefore these processes are commonly called two-photon processes. We shall use here this terminology as well, but do not mean to exclude other types of diagrams where the virtual photons can be for instance timelike.

In these same years the availability of sufficient computer power and the development of dedicated simulation programs made it possible for the Monte Carlo simulation technique to become one of the most successful tools to confront experimental results with theoretical predictions.

It is the purpose of this thesis to explain in detail how the Monte Carlo approach can be applied to establish the comparison between two-photon experiments and theory. We argue that the concept of a Monte Carlo event generator is best suited for this comparison. For we do not merely want to calculate the total or a differential cross section corresponding to a specific experimental set-up, but also we want to be able to simulate the experiment in all its details, that is, we want to produce unweighted events. Due to the increasing experimental accuracy with which two-photon reactions are being measured, these experiments are now no longer exclusively sensitive to the multiperipheral Feynman diagrams, but also to corrections which arise from other Feynman diagrams. Consequently, the Monte Carlo event generators used for the comparison should take into account these corrections. They can be classified in two categories.

Firstly, there are the contributions from all $O(\alpha^4)$ diagrams other than the multiperipheral ones. Here, as usual, α stands for the electromagnetic

coupling constant. Calculation of a subclass of O (α^4) diagrams namely those with two timelike virtual photons, yields at the same time a lowest order description of 'exotic' processes, such as $e^+e^- \to \mu^+\mu^-\tau^+\tau^-$, $e^+e^- \to \mu^+\mu^+\mu^-\mu^-$ or $e^+e^- \to \mu^+\mu^- q\bar{q}$, which are, strictly speaking, not two-photon reactions. Still they are nowadays of great interest because experimentalists seem to be able, despite the small cross sections involved, to track them down in their detectors.

The second category consists of the radiative corrections to two-photon processes. Then we consider reactions such as $e^+e^- \to e^+e^-\mu^+\mu^-(\gamma)$, which are of order α^5.

The further outline of this thesis is as follows. In chapter II we shall describe the main motives for and objectives of two-photon research. Furthermore, we shall define the kinematics and pay attention to some special kinematical regions. Also a popular approximation for the exact differential cross section will be reviewed. Finally, those aspects of the Monte Carlo technique that are of relevance for the simulation of two-photon reactions will be recapitulated. In the next chapter we shall discuss the calculation of the complete lowest order cross section for processes with four leptons in the final state and for reactions such as $e^+e^- \to e^+e^- q\bar{q}$, $e^+e^- \to \mu^+\mu^- q\bar{q}$. This calculation poses two problems. First of all, we have to determine the exact matrix element squared of a large number (up to 36) Feynman diagrams. Secondly, we have to generate events according to a multi-differential cross section which has very many (up to 657) different peaks in phase-space. Moreover, in order to ensure numerical stability of the event generator, we are forced to use different sets of kinematical variables. In chapter IV radiative corrections to the multiperipheral diagrams are considered. We shall explain in detail the distinction between soft and hard photon corrections which turns out to be somewhat more tricky than in the case of radiative corrections to one-photon processes. Finally, in chapter V we present some results which were obtained by using the event generators described in chapters III and IV. Also we discuss cross sections of four-lepton production processes at LEP energies. When we want to simulate these reactions we must take into account interactions which are mediated through either a photon or a Z_0 particle. The necessary modifications of the event generation procedure described in chapter III are outlined in appendix E.

CHAPTER II

INTRODUCTION

1. History

A phenomenon, which clearly exhibits the difference between classical and quantum electrodynamics (QED), is the scattering of light by light. While the former theory forbids the interaction between electromagnetic fields, the latter predicts non-zero cross sections for photon-photon interactions. In lowest order of perturbation theory photon-photon scattering is described by the box diagram (see fig. 1).

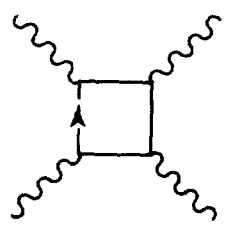

fig. 1

The first calculation of this diagram with electrons going along the internal lines, was already performed in the thirties. For visible light the invariant mass squared of the colliding photons is smaller than 40 eV^2 and the resulting cross section is smaller than 10^{-29} nanobarn [1,2]. Also the first calculations of the interaction between two virtual photons date back to the thirties [3-5]. With the arrival of the first e^+e^- colliding beam facilities in 1960, theorists like Low, Calogero and Zemach, realized that these machines offered the possibility to test photon-photon scattering experimentally [6,7]. However, due to the lack of beam energy and luminosity of the early machines, it lasted another decade before the first experimental results were published [8,9]. Since then experimental as well as theoretical interest in two-photon physics has steadily increased and two-photon research has produced many important results which help us to get a better understanding of the

interactions between elementary particles. These results are discussed extensively in the many reviews and monographs that exist [10-16].

2. Relevance and characteristics of two-photon processes

A remarkable feature of two-photon processes is the fact that their total cross section increases logarithmically with beam energy E_b. This clearly distinguishes two-photon reactions from the one-photon annihilation processes for which the cross section decreases with $1 / E_b^2$. Theoretically, despite the fact that the two-photon reactions are of order α^4, their cross section dominates the cross section arising from one-photon processes, for beam energies greater than a few GeV. However, since most of the cross section is experimentally inaccessible, it turns out that for experiments the cross-over between one- and two-photon reactions takes place at approximately 17 GeV [17]. The reasons for the loss of experimentally observable cross section are twofold.

First of all, the virtual photons radiated by the beams, can be regarded as bremsstrahlung. Therefore they are strongly aligned with the beams and have an energy spectrum which is proportional to $1 / \omega$ (ω is the photon energy). Thus most photons will have a low energy. Secondly, the differential cross section for $\gamma\gamma \to \ell^+\ell^-$ in the CM system can be expressed as follows :

$$\frac{d\sigma}{d\vec{\Omega}} = \frac{\alpha^2 a}{W^2}\left[\frac{2 a^2 \sin^2\Theta - a^4 \sin^4\Theta + 1 - a^4}{(1 - a^2\cos^2\Theta)^2}\right], \quad a = \left(1 - \frac{4 m_\ell^2}{W^2}\right)^{\frac{1}{2}}. \qquad (2.1)$$

Here the angle Θ denotes the polar angle with respect to the $\gamma\gamma$ direction. W^2 is the invariant mass squared of the photons. For the notations and conventions used we refer to appendix A.

Consequently, this cross section is strongly peaked along the photon direction in the $\gamma\gamma$ CM system. Thus even in the case when neither the electron nor the scattered positron are required to be detected ('no-tagging' case), only a small part of the cross section can be observed, since also the produced lepton pair tends to disappear down the beam pipe. Nevertheless at high PETRA and PEP energies two-photon physics can be explored experimentally.

We now have to distinguish between the leptonic processes $e^+e^- \to e^+e^-\ell^+\ell^-$ and the hadronic two-photon reactions $e^+e^- \to e^+e^-$hadrons. The first are

interesting in their own right because they provide higher order tests of QED [17-22]. Moreover at high energies, they may form an important background to other reactions of interest. Also they will establish a calibration for the study of the hadronic two-photon processes. These are of even greater importance since they test Quantum Chromo Dynamics (QCD), which is still a less well established theory than QED. More specifically, they provide a means to study hadronic states with a charge conjugation number C equal to + 1, whereas the one-photon hadron reactions only produce C = -1 hadron systems.

It is outside the scope of this thesis to present a general review of the status of this research field. Therefore we confine ourselves to a listing of the most important areas of investigation. They are :

- total hadronic cross section $\sigma_{\gamma\gamma \rightarrow \text{hadrons}}$
- hadron pair production
- resonance production
- hard scattering processes
- photon structure functions

Again we refer to the many reviews and the proceedings of two-photon conferences for detailed information on the results that were obtained [23-29].

However, we want to make a few remarks concerning the hadronic two-photon processes. The multiperipheral photon-photon scattering in these reactions can theoretically be described by a combination of two models viz. the Quark Model [30] and the Vector Dominance Model (VDM). In the Quark Model the photons have a pointlike QED coupling to quarks. The hadronic two-photon processes now proceed in two steps. Firstly the photons produce a $q\bar{q}$ pair. This interaction is completely described by QED and therefore similar to the leptonic two-photon reactions. Subsequently the quarks fragment into hadrons (see fig. 2). This fragmentation process is described by QCD. The pointlike coupling is thought to dominate the photon-photon interactions whenever large momentum transfers occur. These high momentum transfers are accomplished in two cases (see fig. 3). In the first case the momentum transfer between the photon and quarks is large (Q^2, $q^2 \approx 0$, $\Delta^2 \ll 0$) and we investigate two jet production with high transverse momentum with respect to the photon-photon collision axis [31]. In the other case (q^2, $\Delta^2 \approx 0$, $Q^2 \ll 0$) we study deep inelastic electron-photon scattering [32-37] (see fig. 4). Then one of the beam particles

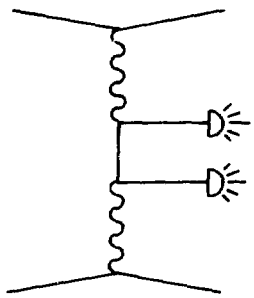

fig. 2

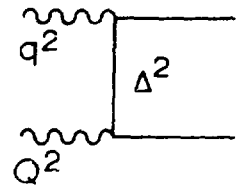

fig. 3

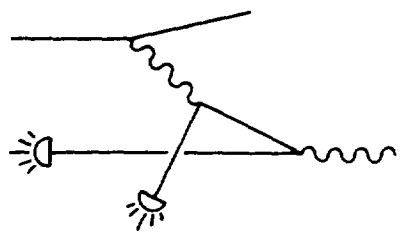

fig. 4

scatters over a large angle and thus produces a photon which is far off mass shell. This photon probes the nearly real photon which is radiated by the other beam particle, scattering over a very small angle. It thereby measures the quark content of the quasi-real photon. To express this more precisely we argue that the differential cross section for the multiperipheral electron-photon scattering can be written in the following form (see appendix C) :

$$d\sigma_{e\gamma \to e\,X} = \frac{4\,\alpha^2 E'}{Q^4\,y}\left\{ (1-y)\,F_2(x\,,Q^2) + x\,y^2 F_1(x\,,Q^2) \right\} d\vec{\Omega}\,dE'\ ,$$

$$y = 1 - \frac{E'}{E}\cos^2(\tfrac{1}{2}\,\Theta)\ ,\quad x = \frac{-\,Q^2}{W^2 - Q^2}\ ,\quad W^2 = p_X^2\ . \qquad (2.2)$$

Here E' and $d\vec{\Omega} = d\cos\Theta\, d\phi$ denote respectively the energy and solid angle of the beam particle which is scattered over a large angle. Q^2 stands for the momentum squared of the photon which is far off mass shell. F_1 and F_2 are the so-called structure functions of the quasi-real photon. In the Quark Model we

can interpret F_2, in analogy to deep inelastic electron-nucleon scattering, as a measure of the momentum weighted sum over the momentum distributions of the quarks inside the quasi-real photon.

$$F_2(x, Q^2) = \sum_i x\, e_i^2\, f_i(x, Q^2) \quad . \tag{2.3}$$

Here $f_i(x, Q^2)$ stands for the probability to find a quark of type i and charge e_i with a momentum fraction x in the photon. Omitting QCD corrections [38] we can calculate the functions F_1 and F_2 explicitly. The resulting structure functions depend not only on x but also on Q^2 and therefore exhibit scaling violation. This is completely opposed to the case of deep inelastic electron-nucleon scattering where because of the limited transverse momenta of the quarks inside the nucleon, we find indeed a scaling behaviour and the Callan-Gross relation between F_1 and F_2 : $F_2 = 2 \times F_1$.

At low $|Q^2|$ the pointlike coupling does not provide us with a good description of the hadron production. Instead we should use non-perturbative QCD. However, since this theory is still not solved completely, we have to rely on effective theories like VDM. In VDM, which is known to work rather well for real or quasi-real photons, the photons first transform into a sum over vector meson states such as ρ, ω, ϕ (see fig. 5). Subsequently these vector mesons interact and produce the hadrons in the final state. As a consequence of VDM scaling behaviour is recovered.

From the above we see that Monte Carlo programs which are needed for an appropriate simulation of hadronic two-photon processes, depend on the model which is considered to describe the process. In the case of large momentum transfer it is clear that the simulation of $e^+e^- \to e^+e^- q\bar{q}$ plays a key role.

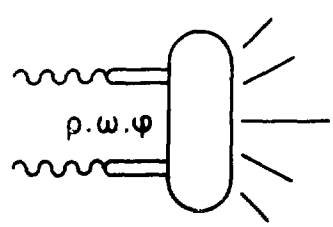

fig. 5

We then have to add to the $e^+e^-q\bar{q}$ generator a Monte Carlo program which describes the fragmentation of the quarks into jets. Thus we obtain an event generator for the complete process. This gives us another motivation to study $e^+e^- \to e^+e^-\ell^+\ell^-$. Having constructed an event generator for this process we only have to insert the appropriate charge and colour factors to obtain the event generator for $e^+e^- \to e^+e^-q\bar{q}$.

3. Helicity structure and Weizsäcker-Williams Approximation

In this section we shall review multiperipheral two-photon scattering in more detail. We consider the following two-photon process :

$$e^+(p_+)\ e^-(p_-) \to e^+(q_+)\ e^-(q_-)\ \mu^+(k_+)\ \mu^-(k_-) \qquad (2.4)$$

Here p_+ and p_- denote the four-momenta of the incoming beam particles, q_+ and q_- the four-momenta of the scattered particles and finally k_+ and k_- the four-momenta of respectively the produced anti-muon and muon. Since we only consider unpolarized beams and do not measure the spins of the outgoing particles the spin indices have been omitted. The dynamics of this process is in lowest order (α^4) described by 12 Feynman diagrams. However, in many cases, e.g. when one is interested in the total cross section, it is sufficient to consider only the 2 multiperipheral graphs which are depicted in fig. 6. The calculation of the complete lowest order will be discussed in the next chapter.

We now want to discuss the exact differential cross section corresponding to the multiperipheral Feynman graphs. This can be done in several ways. We choose to describe the so-called helicity structure of the two-photon cross

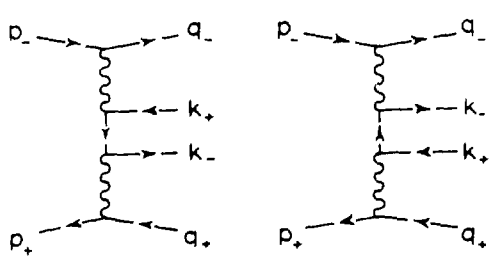

fig. 6

section. This helicity structure relates the cross section for two-photon reactions to the cross section for the processes : $\gamma^*(Q_+,\lambda_+)\ \gamma^*(Q_-,\lambda_-) \rightarrow \mu^+(k_+)\ \mu^-(k_-)$ with various choices for the photon polarizations λ_+ and λ_- [15,16]. Here Q_+ and Q_- denote the four-momenta of the virtual photons. This relation is interesting for the following reasons.

First of all, the helicity structure is in particular useful when we study hadronic two-photon reactions. It allows us to split off that part of the process which is completely determined by QED and to concentrate on the process which produces the hadrons : $\gamma^*\gamma^* \rightarrow$ hadrons. Moreover, it allows for an easy interpretation of the cross section in terms of photon structure functions. In the case of leptonic two-photon reactions this formalism is not really necessary since the multiperipheral process is calculable from QED (see next chapter) [39,40].

The second reason concerns the approximations for the cross section which were widely used before Monte Carlo integration became the fashion. Most of these approximations are variations on the so-called Weizsäcker-Williams Approximation (WWA) [3,4] which describes the two-photon cross section for $e^+e^- \rightarrow e^+e^-X$ as a convolution of the cross section for the process $\gamma\ \gamma \rightarrow X$ and so-called flux factors. These flux factors, which are calculable from QED, can be interpreted as probability densities for the emission of a photon with a four-momentum Q by the incoming beam particle. On the basis of the helicity structure it can easily be shown how the WWA can be derived and which are the conditions that have to be met in order to ensure its validity.

The derivation of the helicity structure of the two-photon cross section has already been known for a long time. Therefore we shall just present the result here and refer to appendix B for a résumé. The exact multiperipheral differential cross section for the process $e^+e^- \rightarrow e^+e^-X$ equals :

$$
\begin{aligned}
d\sigma = \frac{\alpha^2}{16\,\pi^4} \frac{|\vec{k}|\ W}{[(p_+\cdot p_-)^2 - m_e^4]^{\frac{1}{2}}\ Q_+^2\ Q_-^2} \\
\{\ \rho_+^{00}\rho_-^{00}\sigma_{LL}(Q_+^2,Q_-^2,W^2) + 2\ \rho_+^{00}\rho_-^{++}\sigma_{LT}(Q_+^2,Q_-^2,W^2) + 2\ \rho_+^{++}\rho_-^{00}\sigma_{TL}(Q_+^2,Q_-^2,W^2) + \\
4\ \rho_+^{++}\rho_-^{++}\sigma_{TT}(Q_+^2,Q_-^2,W^2) + 2\ |\rho_+^{+-}|\,|\rho_-^{+-}|\cos(2\tilde{\phi})\ \tau_{TT} - \\
8\ |\rho_+^{+0}|\,|\rho_-^{+0}|\cos\tilde{\phi}\ \tau_{TL}\ \}\ \frac{d^3\vec{q}_+}{q_+^0}\ \frac{d^3\vec{q}_-}{q_-^0}\ .
\end{aligned}
\tag{2.5}
$$

The variables which are used in eq. (2. are defined in appendix B. Now a few remarks are in order. The angle $\tilde{\phi}$ can be nterpreted as the angle between the scattering planes of the colliding ele- on and positron in the CM (centre of momentum) frame of the photons [16]. After integration over $\tilde{\phi}$ the τ terms vanish. The τ_{TT} can be related to the cross sections $\sigma_{//}$ and $\sigma_{\perp}$ for photons with linear transverse polarizations which are respectively parallel or perpendicular to each other : $\tau_{TT} = \sigma_{//} - \sigma_{\perp}$ [16]. In the limit of Q_+^2 and Q_-^2 approaching zero all terms with an index L vanish which is to be expected since only transverse degrees of freedom of real photons propagate. Because of the $1 / (Q_+^2 Q_-^2)$ behaviour of $d\sigma$ the virtual photons tend to be quasi-real. The minimum of $|Q_\pm^2|$ is obtained when the lepton which emits the photon scatters over zero angle and equals :

$$|Q_\pm^2|_{min} = m_e^2 \frac{(1 + |\vec{p}_\pm| - q_\pm^o - |\vec{q}_\pm|)^2}{(1 + |\vec{p}_\pm|)(q_\pm^o + |\vec{q}_\pm|)} = m_e^2 \frac{(1 - q_\pm^o)^2}{q_\pm^o} + O(m_e^4). * \quad (2.6)$$

We are now able to derive the WWA. To this end we first take the limit of Q_+^2 and Q_-^2 going to zero in all σ and τ terms in eq. (2.5). This leaves us with the σ_{TT} and τ_{TT} terms. The latter vanishes after integration over $\tilde{\phi}$. Therefore we only keep the σ_{TT} term. Next we approximate the factors $|\vec{k}| W$ and ρ. We assume that $|Q_+^2|, |Q_-^2| \ll W^2$. This allows us to write :

$$|\vec{k}| W = \tfrac{1}{2} W^2 = 2 \omega_+ \omega_- \quad , \quad \omega_\pm = 1 - q_\pm^o \quad , \quad \rho_\pm^{++} = \frac{(\omega_\pm - 1)^2 + 1}{\omega_\pm^2} + \frac{2 m_e^2}{Q_\pm^2} \quad ,$$

$$d\sigma = \frac{\alpha^2}{4\pi^2} \frac{1}{Q_+^2} \left(\frac{(\omega_+ - 1)^2 + 1}{\omega_+} + \frac{2 m_e^2 \omega_+}{Q_+^2}\right) \frac{1}{Q_-^2} \left(\frac{(\omega_- - 1)^2 + 1}{\omega_-} + \frac{2 m_e^2 \omega_-}{Q_-^2}\right)$$
$$\sigma_{TT}(0,0,W^2)\, d\omega_+ d\omega_- dQ_+^2 dQ_-^2 \quad . \quad (2.7)$$

Performing the Q^2 integrations we find the WWA :

$$d\sigma = N(\omega_+)\, N(\omega_-)\, \sigma_{TT}(0,0,W^2)\, d\omega_+ d\omega_- \quad , \quad (2.8)$$

$$N(\omega) = \frac{\alpha}{2\pi} \frac{1}{\omega} \left[((\omega - 1)^2 + 1) \ln\left(\frac{|Q^2|_{max}}{|Q^2|_{min}}\right) - 2(1 - \omega)\left(1 - \frac{|Q^2|_{min}}{|Q^2|_{max}}\right)\right].$$

*Throughout this thesis we use the beam energy E_b as unit of energy.

The cross section factorizes into a product of σ_{TT} and two flux factors which are fully determined by the four-momenta occurring at one vertex.

4. Special kinematical regions

In this section we shall briefly discuss the three kinematical situations that are often distinguished by experimentalists viz. those corresponding to the no-tagging, single-tagging and double-tagging cases. Tagging refers to the detection of a scattered beam particle in the final state.

In the no-tagging case only the produced $\ell^+\ell^-$ are measured. Since in current two-photon experiments tagging at angles of order m_e / E_b is hardly possible, it is justified to assume that the beam particles scatter over zero angle and produce quasi-real photons. Consequently in the no-tagging case we can safely neglect non-multiperipheral diagrams. Moreover WWA is expected to be a good approximation.

In the single-tagging case, apart from the $\ell^+\ell^-$, either the e^+ or the e^- is detected. For convenience we assume that the e^+ is tagged while there is an anti-tag cut on the e^-, that is, the e^- is explicitly not seen in the detector. Now in general the multiperipheral diagrams alone will not constitute a good description of the process. At low W^2 the effect of the so-called bremsstrahlung diagrams cannot be ruled out (see also the next chapter) [41]. Even for those event configurations where the multiperipheral diagrams do indeed dominate the cross section, the situation is no longer as simple as in the no-tagging case. Taking the limit of Q_-^2 approaching zero in the σ and τ terms in eq. (2.5), we are left with three terms. Again the τ term drops out after the $\tilde{\phi}$ integration, which is necessitated since we do not detect the e^-. Consequently we find :

$$d\sigma = \frac{\alpha^2}{4\pi^2} \frac{|\vec{k}|\, W}{[(p_+ \cdot p_-)^2 - m_e^4]^{\frac{1}{2}} Q_+^2 Q_-^2} 4\, \rho_+^{++} \rho_-^{++} |\vec{q}_+||\vec{q}_-|$$
$$\{ \sigma_{TT}(Q_+^2, 0, W^2) + \varepsilon\, \sigma_{LT}(Q_+^2, 0, W^2) \}\, dq_+^{\circ} dq_-^{\circ} d\cos\Theta_+ d\cos\Theta_- \,, \qquad (2.9)$$

$\varepsilon = \dfrac{\rho_+^{00}}{2\,\rho_+^{++}}$, $\Theta_\pm$ are the scattering angles of the $e^\pm$.

This formula is the starting point to derive eq. (2.2) which relates $d\sigma$ to the

photon structure functions F_1 and F_2 (see appendix C).
Finally, we consider the double-tagging case. Then all the four-momenta of the particles in the final state are measured which requires the beam particles to scatter over a large angle ($\theta >> m_e / E_b$) . It is the most complicated case to treat theoretically. First of all, it is no longer evident that the multiperipheral diagrams will yield a satisfactory description of the process. We obviously have to account for the other diagrams contributing in lowest order. Secondly, even if the multiperiheral diagrams dominate the process, we can no longer afford to take the limit of Q_+^2 or Q_-^2 approaching zero but have to deal with all six terms in eq. (2.5). Moreover, the τ terms, which spoil the factorization of the cross section, can no longer be integrated out when the experiment at issue is not $\tilde{\phi}$ symmetric.

5. Monte Carlo technique

It is not the purpose of this section to give an exhaustive review of the Monte Carlo technique. Many excellent monographs and reviews do exist which describe the essential ideas in great detail [42-44]. Therefore we want to restrict ourselves to the discussion of the so-called event generator. Furthermore we shall outline two methods which are often used to construct these generators.

Before elucidating the notion of the event generator we recall the principal goals which are achieved by the application of the Monte Carlo approach. The comparison between theoretical predictions and experimental results is generally performed at the cross section level. To this end experimentalists need to know how much cross section for a specific process can be attributed to their experimental set-up according to the theory. Therefore the exact differential cross section has to be integrated over the phase-space which is prescribed by the experiment. This poses some severe problems. Firstly, the complexity of experiments is nowadays so enormous that it is virtually impossible to carry out analytically the required integrations. Even when one would succeed in doing this, the result would be highly dependent on the experiment at issue and therefore one would have to start all over again whenever the experimental configuration is changed. This problem becomes worse when we are interested in differential cross sections with respect to specific variables. To obtain these differential cross

sections we, in general, have to make a change of phase-space variables. As a consequence, a Jacobian must be inserted which will complicate the integrations even more. Finally, when one wants to include detector inefficiencies, which are of a statistical nature, then analytical methods will no longer help and we shall have to perform a real detector simulation on the computer. In principle all these problems can be handled by the so-called event generator. An event generator is a simulation program which generates randomly 'unweighted' events. Unweighted means that the four-momenta of the final state particles are distributed according to the exact differential cross section. Moreover it yields a Monte Carlo estimate for the total cross section. Using an event generator we easily obtain the differential cross section of any kinematical variable by just binning the generated events according to the value of that variable. Finally, since the generated events are intrinsically the same as the measured ones, we can easily perform a detector simulation. We now present the Monte Carlo theory in a nutshell.

Suppose that the differential cross section is written symbolically as :

$$d\sigma = \frac{d\sigma}{d\vec{x}}(\vec{x})\, d\vec{x} \ .$$

Here $\vec{x}$ denotes the kinematical variables which span phase-space. A Monte Carlo estimate for $\sigma = \int d\sigma$ is defined as follows :

$$\sigma' = \frac{1}{N} \sum_{i=1}^{N} \frac{d\sigma}{d\vec{x}}(\vec{X}_i) \int d\vec{x} \ , \text{ with } \vec{X}_i \text{ uniformly distributed random vectors.}$$

According to the Monte Carlo theory σ' has the following properties :

- For large N σ' converges to σ .
- The expectation value for σ' equals σ .
- For large N it is normally distributed.
- Its standard deviation is given by $\left(\frac{V}{N}\right)^{\frac{1}{2}}$, with V the variance of $\frac{d\sigma}{d\vec{x}}(\vec{x})$.

Therefore the standard deviation and, therefore, the error in the calculation can be reduced by either enlarging N or by making the variance of the function that is to be integrated by the Monte Carlo method, smaller. Of course, the latter option is favored, since it pays off much better than the former one. From now on we shall drop the distinction between the exact cross section and its Monte Carlo estimate and denote both by σ .

We now briefly discuss two methods, which are widely used to decrease the variance and to generate unweighted events. The first method requires ideally little or no preliminar information on the function that is to be integrated, since it is self-learning or adaptive [45]. It makes uses of stratified sampling. This means that the integration space is divided into a large number of subvolumes. Next a Monte Carlo estimate for the integral in each subvolume is made. After summation we obtain an estimate for the total integral which has generally a smaller standard deviation than a crude one which is obtained without the division of phase-space. Subsequently the boundaries of the subvolumes are adjusted such that each subvolume contributes equally to the total integral. This procedure is repeated several times until the desired accuracy is achieved. Events are generated in four steps. Firstly, a subvolume is selected at random. Next an event is generated randomly within the subvolume. Thereupon the weight of the event is calculated. This weight is defined as the ratio of the differential cross section corresponding to the generated event over the maximum differential cross section within the chosen subvolume. Finally, a rejection algorithm is applied : if a random number, equi-distributed between 0 and 1, is smaller than the weight, the event is accepted, otherwise it is rejected. This approach has clearly the advantage of being a general-purpose one : in principle, the event generation can start immediately when the differential cross section of a process is given. However, in practice, there are some difficulties that have to be solved. First of all, two-photon reactions are remarkable for the strong peaking behaviour of the matrix element squared, which may vary over more than 30 orders of magnitude. In general, these peaks cannot be handled by the adaptive integration program. As a consequence, mappings of the integration variables have to be chosen which soften this peaking behaviour. The choice of these mappings requires some apriori knowledge about the matrix element squared. Thereby the approach looses its nice quality of being process-independent. Moreover, different cuts which are applied to the events, may ask for different mappings which further restricts the generality. Secondly, it is not always possible to find mappings which deal with all the occurring peaks. If the number of peaks is limited it is usually not too difficult to find these mappings. For example, when we consider the multiperipheral scattering of the process $e^+e^- \to e^+e^-\ell^+\ell^-$ in the no-tagging case and apply the cut $W^2 > W^2_{min} >> 4\ m^2_\ell$, one may choose $\ell n(-Q^2_+)$ and $\ell n(-Q^2_-)$ as integration variables. This choice flattens the peaks considerably and the adaptive approach will yield

accurate results [46]. However, when we take more Feynman diagrams into account, we encounter severe problems. The number of different peaks increases enormously so that one set of integration variables can only describe well a limited number of peaks. Then the remaining peaking behaviour must be accounted for by the automatic integration program which may turn out to be very difficult. This problem is enlarged by the fact that the chosen integration variables may often be inappropriate to describe these remaining peaks. This has to be prevented since we always have to beware of numerical instabilities during the calculation. Numerical instability implies an enormous loss of accuracy in the final numerical result because of dramatic cancellations during the evaluation.

The alternative approach, which is favored by us, is based on importance sampling. Events are first generated according to an approximation which is assumed to be analytically integrable over phase-space and moreover must exhibit the same peaking structure as the exact expression. Next the events are assigned a weight which is equal to the ratio of the exact over the approximate differential cross section. Upon the application of a rejection algorithm we are left with unweighted events. Now a few remarks can be made. Of course, this method is highly dependent on the process at issue. Different processes, even different experimental cuts may require different approximations and consequently different event generators. So the first drawback remains. However the second problem can be solved by the use of the superposition principle for the Monte Carlo simulation of distributions. We divide the exact differential cross section $d\sigma$ into several pieces $d\sigma_i$, each of which has its own characteristic peaking structure. Next we design for each piece a separate subgenerator. Then we are allowed to choose for each subgenerator that set of integration variables that describes best the occurring peaks. When we now want to generate events which are distributed according to $d\sigma$, we first select a subgenerator at random. The probability for the subgenerator with label i to be used, is chosen to be proportional to the corresponding approximate total cross section $\tilde{\sigma}_i$. Next we generate the event and assign a weight to it which equals $W_i = d\sigma_i / d\tilde{\sigma}_i$ when the subgenerator with label i was selected. Upon the application of a rejection algorithm we are left with events distributed according to $d\sigma$. The exact total cross section can be calculated by the use of the weights W_i. It equals :

$$\sigma = \int d\sigma = \sum_{i=1}^{N} \int d\sigma_i = \sum_{i=1}^{N} \langle W_i \rangle_{d\tilde{\sigma}_i} \tilde{\sigma}_i = \langle W \rangle \tilde{\sigma} \quad ,$$

$$\tilde{\sigma} = \sum_{i=1}^{N} \tilde{\sigma}_i \quad , \quad \tilde{\sigma}_i = \int d\tilde{\sigma}_i \ (i=1,..,N) \ . \qquad (2.10)$$

Here $\langle W_i \rangle_{d\tilde{\sigma}_i}$ stands for the average of W_i for events which are distributed according to $d\tilde{\sigma}_i$, $\langle W \rangle$ denotes the average of the weights for events which are generated according to the following algorithm :

if $\sum_{j=1}^{i-1} \tilde{\sigma}_j / \tilde{\sigma} \leq \eta < \sum_{j=1}^{i} \tilde{\sigma}_j / \tilde{\sigma}$ then the event is generated according to $d\tilde{\sigma}_i$ (η is a random number equi-distributed between 0 and 1).

Finally, we want to comment on the efficiency of an event generator. We define the efficiency as the ratio of the mean weight over the maximum weight that occurred during the generation. It is clear that with this definition the efficiency becomes a measure of the number of produced unweighted events in a certain time interval.

References

1. H. Euler and B. Kockel, Naturwiss. 23 (1935) 246.
2. K. O. Mikaelian, Phys. Lett. 115B (1982) 267.
3. C. F. von Weizsäcker, Z. Phys. 88 (1934) 612.
4. E. Williams, Kgl. Danske Vidensk Selskab. Mat.-Fiz. Medd. 13 (1935) N4; Phys. Rev. 45 (1934) 729.
5. L. Landau and E. Lifshitz, Z. Phys. Sow. 6 (1934) 244.
6. F. Low, Phys. Rev. 120 (1960) 582.
7. F. Calogero and C. Zemach, Phys. Rev. 120 (1960) 1860.
8. C. Bacci et al., Nuovo Cim. Lett. 3 (1972) 709.
9. G. Barbiellini et al., Phys. Rev. Lett. 32 (1974) 385.
10. H. Cheng and T.T. Wu, Phys. Rev. Lett. 23 (1969) 1311; Phys. Rev. D1 (1970) 2775.
11. A. Jaccarini, N. Arteaga-Romero, J. Parisi and P. Kessler, Compt. Rend. 269B (1969) 153,1129; Nuovo Cim. Lett. 4 (1970) 933.
12. V.E. Balakin, V.M. Budnev and I.F. Ginzburg, Zh.E.T.F.Pis'ma 11 (1970) 559 (JETP Lett. 11 (1970) 388).
13. S.J. Brodsky, T. Kinoshita and H. Terazawa, Phys. Rev. Lett. 25 (1970) 972; Phys. Rev. D4 (1971) 1532.
14. H. Terazawa, Rev. Mod. Phys. 45 (1973) 615.
15. G. Bonneau, M. Gourdin and F. Martin, Nucl. Phys. B54 (1973) 573.
16. V.M. Budnev, I.F. Ginzburg, G.V. Meledin and V.G. Serbo, Phys. Rep. 15 (1975) 181. (this review contains a rather complete bibliography of the early theoretical work).
17. MARK-J Coll., B. Adeva et al., Phys. Rev. Lett. 48 (1982) 721.
18. CELLO Coll., H.-J. Behrend et al., Phys. Lett. 126B, (1983) 384.
19. M. Pohl, Proceedings of the 5th Intern. Workshop on Photon Photon Collisions, Aachen, ed. Ch. Berger, Lecture Notes in Phys. Vol. 191, Springer Verlag (1983).

20. P. Colas, Thèse 3^{e} cycle, LPNHE Université de Paris (1983).
21. E. Fernandez et al., Phys. Rev. D28 (1983) 2721.
22. PLUTO Coll., Ch. Berger et al., Z. Physik C 27 (1985) 249.
23. Proceedings of the Intern. Conference on Two-Photon Interactions, Lake Tahoe, Calif. (1979), ed. J.F. Gunion.
24. Proceedings of the Intern. Workshop on Photon-Photon Collisions, Amiens, ed. G. Cochard and P. Kessler, Lecture Notes in Physics Vol. 134, Springer Verlag (1980).
25. Proceedings of the 4th Intern. Colloquium on Photon-Photon Interactions, Paris (1981), Ed. G.W. London (Singapore, World Scientific).
26. Proceedings of the 5th Intern. Workshop on Photon-Photon Collisions, Aachen, Ed. Ch. Berger, Lecture Notes in Physics Vol. 191, Springer Verlag (1983).
27. W. Wagner, Aachen PITHA 83/03 (based on lectures given at the 7th Nordic Meeting on Elementary Particle Physics, Spatind (1982).
28. H. Kolanoski, Springer Tracts of Modern Physics, Vol. 105 (1984).
29. J.H. Field, preprint LPNHE Université de Paris (1984).
30. J.D. Bjorken and E.A. Paschos, Phys. Rev. 185 (1969) 1975.
31. S.J. Brodsky, T.A. DeGrand, J.F. Gunion and J.H. Weis, Phys. Rev. D19 (1979) 1418.
32. S.J. Brodsky, T. Kinoshita and H. Terazawa, Phys. Rev. Lett. 27 (1971) 280.
33. T.F. Walsh, Phys. Lett. 36B (1971) 121.
34. T.F. Walsh and P. Zerwas, Phys. Lett. 44B (1973) 195.
35. R.L. Kingsley, Nucl. Phys. B60 (1973) 45.
36. R.P. Worden, Phys. Lett. 51B (1974) 57.
37. M.A. Ahmed and G.G. Ross, Phys. Lett. 59B (1975) 369.
38. E. Witten, Nucl. Phys. B120 (1977) 189.
39. R. Bhattacharya, J. Smith and G. Grammer Jr., Phys. Rev. D15 (1977) 3267.
40. J.A.M. Vermaseren in ref. 24.
41. F.A. Berends, P.H. Daverveldt, R. Kleiss, Z. Physik C 22 (1984) 239.
42. F. James, Rep. Prog. Phys. 43 (1980) 1145. and references quoted there.
43. T.M. Hammersley and. D.C. Handscomb, Monte Carlo Methods, Methuen, London (1964).
44. R. Kleiss, PhD Thesis, Univ. of Leiden (1982).
45. G.P. Lepage, Journ. Comp. Phys. 27 (1978) 192
46. J.A.M. Vermaseren, Nucl. Phys. B229 (1983) 347.

CHAPTER III

COMPLETE LOWEST ORDER CALCULATIONS

1. Introduction

In the previous chapter we reviewed calculations of the cross section for $e^+e^- \to e^+e^-\ell^+\ell^-$ ($\ell = e, \mu, \tau$), which were based on two multiperipheral Feynman graphs. The resulting event generators were widely used to describe the multiperipheral scattering for $e^+e^- \to e^+e^-\mu^+\mu^-$ and $e^+e^- \to e^+e^-\tau^+\tau^-$ [1]. Even the multiperipheral scattering for $e^+e^- \to e^+e^+e^-e^-$ was simulated in this way, although it is described by eight Feynman diagrams [1].

In this chapter we shall show how these calculations can be extended so that all Feynman diagrams contributing in lowest order are taken into account. To this end we describe in detail the algorithm which is used to calculate the exact matrix element squared. Furthermore it is outlined how events can be generated according to the exact differential cross section. We shall illustrate the calculations involved by considering :

$$e^+(p_+)\ e^-(p_-) \to e^+(q_+)\ e^-(q_-)\ e^+(k_+)\ e^-(k_-)\ , \tag{3.1}$$

because it is the most complicated four-lepton production process. In this case as many as 36 Feynman diagrams contribute. Moreover, because of the small ratio of electron mass over beam energy high demands are made upon the numerical stability of the event generator. We can describe other processes, such as $e^+e^- \to e^+e^-\mu^+\mu^-$, $e^+e^- \to e^+e^-q\bar{q}$, $e^+e^- \to \mu^+\mu^-\mu^+\mu^-$, $e^+e^- \to \mu^+\mu^-\tau^+\tau^-$, $e^+e^- \to \mu^+\mu^-q\bar{q}$ by selecting the contributing Feynman graphs out of the 36 mentioned above and by inserting appropriate charge factors for the quarks.

The reasons why we want to perform these calculations are twofold. Firstly, it was already argued in the previous chapter that, as soon as we apply tagging conditions to two-photon processes, the contributions from non-multiperipheral diagrams may become sizeable. Sometimes they can even dominate. This happens for example in the single-tagging case at low W^2. Nowadays two-photon experiments have acquired so many data, even when single- or double-tagging cuts are applied, that they really become sensitive to effects which can certainly be attributed to non-multiperipheral graphs and

maybe to multiperipheral interferences that were not taken into account in the calculations described in the previous chapter for the $e^+e^+e^-e^-$ case [1,2]. Furthermore events of the type : $e^+e^- \to \mu^+\mu^+\mu^-\mu^-$ and $e^+e^- \to \mu^+\mu^-q\bar{q}$ have been observed experimentally [3,4]. The analysis of all this data requires Monte Carlo event generators which take in account all the lowest order Feynman diagrams.

The second motivation is of a theoretical nature. The complete calculation of a matrix element squared consisting of 36 Feynman diagrams with all masses included is highly challenging. Until now there exists only a calculation valid in those experimental circumstances where the masses of the particles can be neglected [5]. However as soon as the peaks in the differential cross section become observable the masses have to be incorporated which complicates the calculation considerably. The way this problem is tackled resembles in many ways the method discussed in ref. [5]. Again the calculation is performed at the amplitude level using a suitable set of spinor definitions. Now also much attention has to be paid to the numerical stability of the calculation. Furthermore the event generation poses some problems of itself. In the $e^+e^+e^-e^-$ case the multi-differential cross section has 657 different peaks in a seven dimensional phase-space, which all have to be carefully accounted for. Moreover in order to ensure numerical stability different sets of integration variables have to be used to describe the structure of the occurring peaks. These two complications force us to think of other methods of solution than the conventional use of multi-purpose integration programs. We therefore follow the procedure described in sect. 5 of the previous chapter and treat the cross section as the square of an amplitude, which consists of a sum of specifically chosen subamplitudes. Each subamplitude squared is generated by a subgenerator in which the phase-space variables have been chosen such that the peaking structure is properly taken into account. The interference between the subamplitudes is taken care of by imposing a weight on the events.

The rest of this chapter is organized as follows. In sect. 2 we describe in detail the exact calculation of the matrix element squared. We show that the contributing amplitudes all decompose into scalar factors with no more repeated indices to be summed over. It turns out that the numerical calculation can be speeded up by examining carefully (for a given momentum configuration of the final state particles) which parts of the amplitude can be considered as negligible. In sect. 3 the exact cross sections corresponding

to the subamplitudes will be derived. Special attention is given to numerical stability. In the subsequent sections (4-7) we describe briefly four subgenerators which generate efficiently events in the no-tagging case. For the single- and double-tagging case we designed separate generators. These will be reviewed in appendix D. In sect. 8 it is shown how the exact total cross section is obtained. Since we want the event generators to be also useful for the description of four lepton production processes at LEP energies, we present in appendix E a calculation of the complete matrix element squared corresponding to all lowest order diagrams with either photon or Z_0 exchanges. The Z_0 exchange complicates the calculations in several ways. First of all, the number of contributing Feynman diagrams increases with a factor four. Secondly, the vector and axial couplings of the Z_0 together with its more involved propagator make the calculation of each individual diagram more difficult. Finally the peaking structure of the matrix element squared may change drastically when a Z_0 replaces a time-like photon. Again we constructed separate event generators for the single- and double-tagging case.

2. The exact matrix element

In this section the exact calculation of the matrix element squared will be discussed. The process (3.1) is described by 36 Feynman diagrams which are depicted in fig. 7. Because of this large number of graphs and the complicated current structure the standard way of calculating these matrix elements squared i.e. spin summing and calculating traces is not feasible. Therefore we follow the same lines as in ref. [5] and perform the calculation on the amplitude level which implies that now no spin summing is allowed. That is, we have to choose different spin states for all the occurring particles, we calculate the corresponding amplitude, then square it and sum over these spin states. Before the procedure can be presented we have to group the 36 diagrams in a systematic way. This is done in a way completely analogous to the one used in ref. [5]. Each diagram is assigned a group number which specifies the connection between the spinors $u(p_-)$, $v(q_+)$, $v(k_+)$ and the conjugate spinors $\bar{v}(p_+)$, $\bar{u}(q_-)$, $\bar{u}(k_-)$. The contraction between the three currents which occur in the amplitude is fixed by a permutation number. The diagrams in group 2, 4 and 6 carry a minus sign, due to Fermi statistics, relative to the diagrams in group 1, 3 and 5. After this assignment each

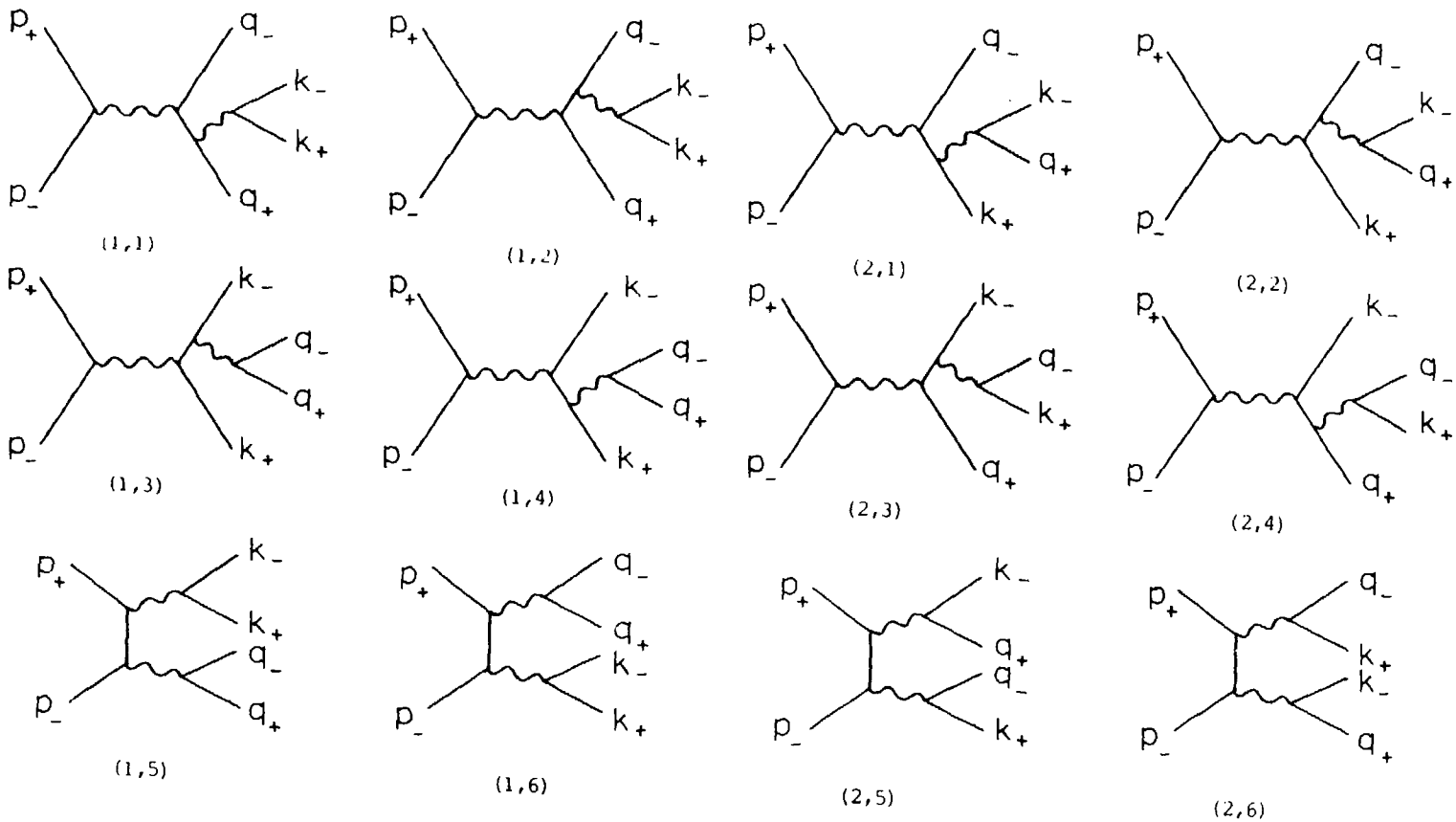

Fig. 7

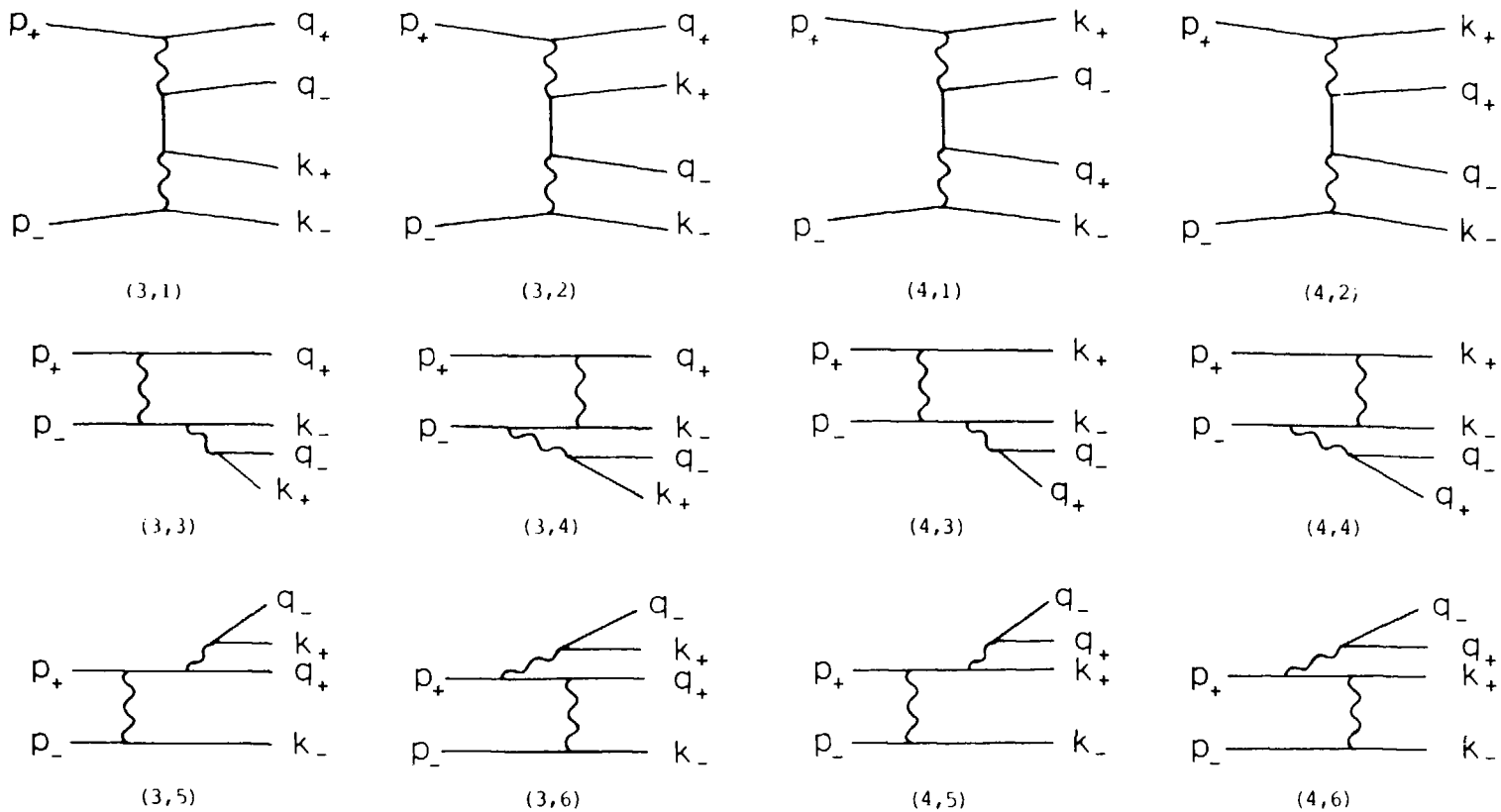
p+
q+
q-
k+
p-
k-
(3,1)
p+
q+
k+
q-
p-
k-
(3,2)
p+
k+
q-
q+
p-
k-
(4,1)
p+
k+
q+
q-
p-
k-
(4,2)
p+
q+
p-
k-
q-
k+
(3,3)
p+
q+
p-
k-
q-
k+
(3,4)
p+
k+
p-
k-
q-
q+
(4,3)
p+
k+
p-
k-
q-
q+
(4,4)
q-
k+
p+
q+
p-
k-
(3,5)
q-
k+
p+
q+
p-
k-
(3,6)
q-
q+
p+
k+
p-
k-
(4,5)
q-
q+
p+
k+
p-
k-
(4,6)

Fig. 7 (cont'd)

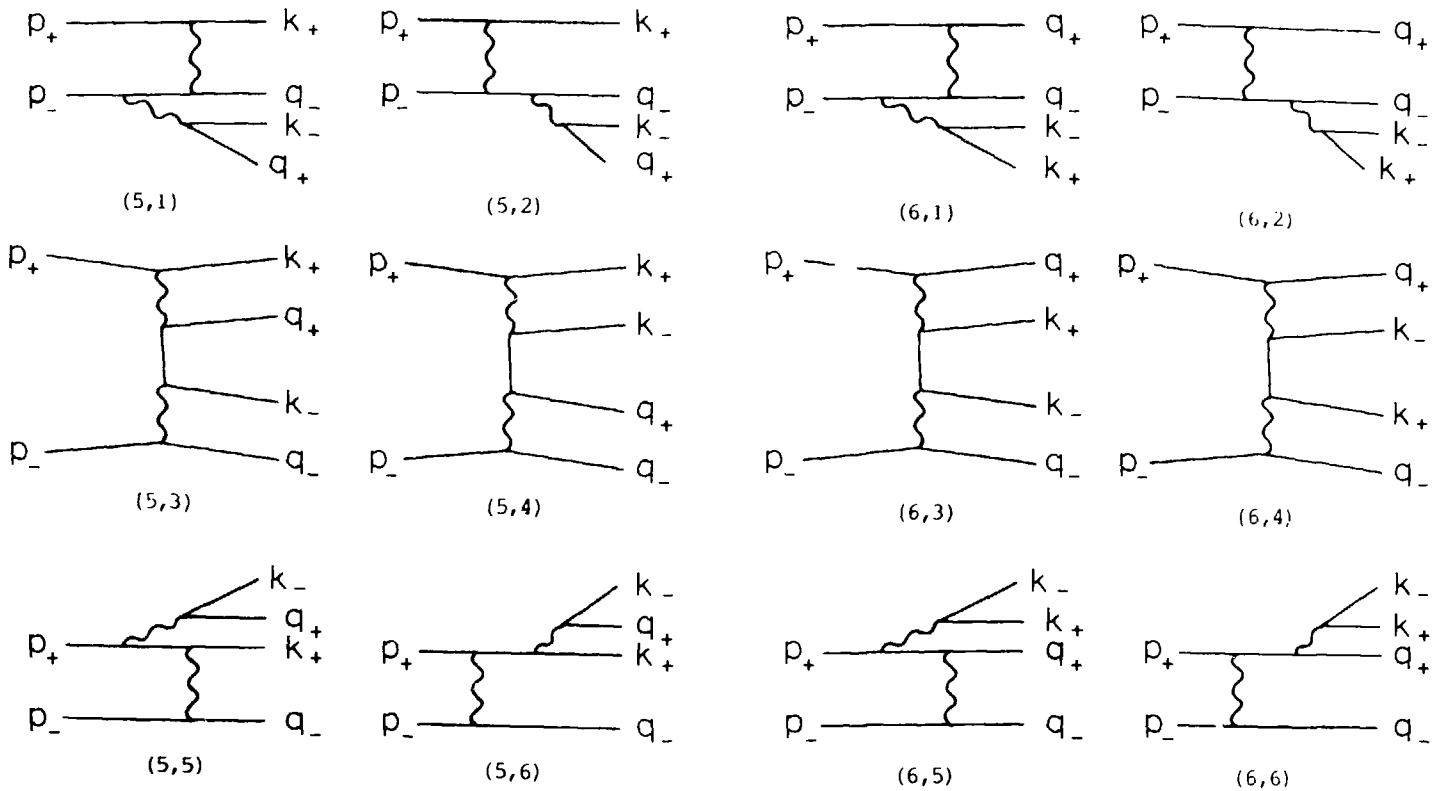
p+ k+
p- q- k- q+
(5,1)
p+ k+
p- q- k- q+
(5,2)
p+ q+
p- q- k- k+
(6,1)
p+ q+
p- q- k- k+
(6,2)
p+ k+ q+ k- p- q-
(5,3)
p+ k+ k- q+ p- q-
(5,4)
p+ q+ k+ k- p- q-
(6,3)
p+ q+ k- k+ p- q-
(6,4)
k- q+ p+ k+ p- q-
(5,5)
k- q+ p+ k+ p- q-
(5,6)
k- k+ p+ q+ p- q-
(6,5)
k- k+ p+ q+ p- q-
(6,6)

Fig. 7 (cont'd)

diagram can be referred to in a unique way which makes a systematic treatment easy.

For a given diagram we define the amplitude as follows :

$$M\,(p_1,\lambda_1,p_2,\lambda_2,p_3,\lambda_3,p_4,\lambda_4,p_5,\lambda_5,p_6,\lambda_6) = \frac{-\,i\,e^4\,T\,(p_1,\lambda_1,p_2,\lambda_2,p_3,\lambda_3,p_4,\lambda_4,p_5,\lambda_5,p_6,\lambda_6)}{(b_1p_1+b_2p_2)^2\,((b_3p_3+b_1p_1+b_2p_2)^2-m_3^2)\,(b_5p_5+b_6p_6)^2} \qquad (3.2)$$

p_1,p_2,p_3,p_4,p_5,p_6 is a permutation of the four-momenta p_+,p_-,q_+,q_-,k_+,k_- determined by the group and permutation number of the chosen diagram.

$b_i = b\,(p_i) \equiv \begin{cases} +1 & \text{if } p_i \text{ is one of the outgoing momenta.} \\ -1 & \text{if } p_i \text{ is one of the incoming momenta.} \end{cases}$

$m_i = m(p_i) \equiv$ mass corresponding to four-momentum p_i.

If we now adopt the calculational convention that anti-particles have negative mass we are allowed to use u spinors for both particles and anti-particles. The spinorial part T of the amplitude is given by :

$$T(p_1,\lambda_1,p_2,\lambda_2,p_3,\lambda_3,p_4,\lambda_4,p_5,\lambda_5,p_6,\lambda_6) = \bar{u}_{\lambda_1}(p_1)\,\gamma_\mu u_{\lambda_2}(p_2)\,\bar{u}_{\lambda_5}(p_5)\,\gamma_\nu u_{\lambda_6}(p_6)$$

$$\bar{u}_{\lambda_3}(p_3)\,\gamma^\mu(b_3(\not{p}_3+m_3)+b_2(\not{p}_2+m_2)+b_1(\not{p}_1+m_1))\,\gamma^\nu u_{\lambda_4}(p_4) \qquad (3.3)$$

Here we used $b_1m_1+b_2m_2=0$. The indices λ carried by the spinors denote the spin state of the particle. The polarization axis of a given spinor we leave undefined for the moment (for massless particles, λ reduces to a helicity assignment).

Our aim is to decompose the spinorial expression eq. (3.3) into scalar factors which can be evaluated in a fast and efficient way. First we have to get rid of the repeated indices μ and ν. To this end we define :

$$Z(p_1,\lambda_1,p_2,\lambda_2,p_3,\lambda_3,p_4,\lambda_4) = \bar{u}_{\lambda_1}(p_1)\,\gamma^\mu u_{\lambda_2}(p_2)\,\bar{u}_{\lambda_3}(p_3)\,\gamma_\mu u_{\lambda_4}(p_4) \qquad (3.4)$$

Using $\sum_{\lambda=\pm1} u_\lambda(p)\,\bar{u}_\lambda(p) = \not{p} + m$ we now write :

$$T(p_1,\lambda_1,p_2,\lambda_2,p_3,\lambda_3,p_4,\lambda_4,p_5,\lambda_5,p_6,\lambda_6) =$$

$$\sum_{\lambda=\pm 1} \{\, b_3\, Z(p_1,\lambda_1,p_2,\lambda_2,p_3,\lambda_3,p_3,\lambda)\, Z(p_3,\lambda,p_4,\lambda_4,p_5,\lambda_5,p_6,\lambda_6) +$$

$$b_1\, Z(p_1,\lambda_1,p_2,\lambda_2,p_3,\lambda_3,p_1,\lambda)\, Z(p_1,\lambda,p_4,\lambda_4,p_5,\lambda_5,p_6,\lambda_6) +$$

$$b_2\, Z(p_1,\lambda_1,p_2,\lambda_2,p_3,\lambda_3,p_2,\lambda)\, Z(p_2,\lambda,p_4,\lambda_4,p_5,\lambda_5,p_6,\lambda_6) \,\} \quad (3.5)$$

The repeated indices are fully contained in the Z expressions. Thus from now on, it is sufficient to consider the arbitrary Z expression (3.4). Choosing a suitable spinor definition up to an overall complex phase we shall show that for every possible choice of $\lambda_1,\lambda_2,\lambda_3$ and λ_4 the Z function factorizes in complex scalar products between the spinors. Notice that we cannot use conservation of helicity, since we do not deal with massless particles. It turns out that only 2 out of the 16 possibilities of λ's give a zero result (in the case of helicity conservation, 12 out of the 16 combinations give zero).

We define the spinors in two steps. First of all we choose two four-vectors which satisfy the following conditions :

$$k_o \cdot k_o = 0, \quad k_1 \cdot k_1 = -1, \quad k_o \cdot k_1 = 0. \quad (3.6)$$

Moreover k_o must differ from all other four-vectors which determine the event i.e. $p_i \cdot k_o \neq 0$ for all p_i. Since generally for the processes considered all the particles tend to go along the beam directions (assumed to be the z axis) a safe choice for k_o and k_1 is therefore : $k_o = (1,1,0,0)$ and $k_1 = (0,0,1,0)$. Now so-called basic spinors are fixed up to a complex phase by the equations :

$$u_-(k_o)\, \bar{u}_-(k_o) = \omega_- \not{k}_o,$$

$$u_+(k_o) = \not{k}_1\, u_-(k_o),$$

$$\omega_\lambda = \tfrac{1}{2}(1 + \lambda\, \gamma^5) \;, \quad \lambda = \pm 1 \;. \quad (3.7)$$

Next we express the spinors $u(p_i)$ in terms of the basic ones :

$$u_\pm(p_i) = (\not{p}_i + m_i)\, u_\mp(k_o) \;/\; \eta_i \quad ; \quad \eta_i = \sqrt{2 p_i \cdot k_o} \quad (3.8)$$

It is easily checked that these spinors satisfy Dirac's equation and this

definition corresponds to a specific choice for the polarization axis s^μ: $s^\mu = \frac{p^\mu}{m} - \frac{m}{p.k_o} k_o^\mu$. Notice that the limit $m \to 0$ in eq. (3.8) is regular and that the spinor reduces to a spinor with a helicity. We now define the scalar S and T products between the spinors, which will be used to build up the Z expressions :

$$S\ (p_1,p_2) \equiv \bar{u}_+(p_1)\ u_-(p_2),$$

$$T\ (p_1,p_2) \equiv \bar{u}_-(p_1)\ u_+(p_2). \qquad (3.9)$$

Expressing the $u_\pm$ spinors in terms of the basic ones we find :

$$S\ (p_1,p_2) = \bar{u}_-(k_o)(\not{p}_1 + m_1)(\not{p}_2 + m_2)\not{k}_1 u_-(k_o)\ /\ (\eta_1\eta_2)$$

$$= Tr\ \omega_-\not{k}_o\not{p}_1\not{p}_2\not{k}_1\ /\ (\eta_1\eta_2)$$

$$= 2\ (p_1.k_o p_2.k_1 - p_1.k_1 p_2.k_o - i\ \varepsilon(k_o,k_1,p_1,p_2))\ /\ (\eta_1\eta_2) \qquad (3.10)$$

where $\varepsilon(k_o,k_1,p_1,p_2)$ is the Levi Civita tensor ($\varepsilon_{0123} = 1$) fully contracted with the vectors k_o,k_1,p_1,p_2. With the above choice of k_o and k_1 the resulting expressions equal :

$$S\ (p_1,p_2) = (p_1^y + i\ p_1^z)\ \frac{\eta_2}{\eta_1} - (p_2^y + i\ p_2^z)\ \frac{\eta_1}{\eta_2}\ ,$$

$$T\ (p_1,p_2) = -\ S\ (p_1,p_2)^*. \qquad (3.11)$$

The S and T products play here a similar role as in ref. [5]. There the conditions on k_o and k_1 were different. Consequently, there the products S and T are not anti-symmetric, as in this case. The present choice for k_o, k_1 seems to minimize the computational efforts. Again an elegant relationship between S,T and the four-vector dot product may be derived which stresses the fundamental role these two quantities play :

$$2\ p_i.\ p_j = S\ (p_i,p_j)\ T\ (p_j,p_i) + \mu_i^2\eta_j^2 + \mu_j^2\eta_i^2 \quad ; \quad \mu_i = \frac{m_i}{\eta_i}. \qquad (3.12)$$

Now we arrive at the final part of the calculation. All that is left to do is to express Z for arbitrary spin polarizations $\lambda_1,\lambda_2,\lambda_3,\lambda_4$ in terms of S

and T. To this end we first split the spinor $u_\lambda(p)$ into two parts :

$$u_\lambda(p_i) = \alpha_\lambda(p_i) + \mu_i u_{-\lambda}(k_o) \quad ; \quad \alpha_\lambda(p_i) = \not{p}_i u_{-\lambda}(k_o) \; / \; \eta_i \tag{3.13}$$

Notice that also holds :

$$\bar{\alpha}_+(p_1)\; \alpha_-(p_2) = S\;(p_1,p_2) \; ; \; \bar{\alpha}_-(p_1)\; \alpha_+(p_2) = T\;(p_1,p_2) \tag{3.14}$$

Inserting eq. (3.13) in eq. (3.4) we find the following result :

$$\begin{aligned}
Z\;(p_1,\lambda_1,p_2,\lambda_2,p_3,\lambda_3,p_4,\lambda_4) = \\
&\bar{\alpha}_{\lambda_1}(p_1)\; \gamma^\mu \alpha_{\lambda_2}(p_2)\; \bar{\alpha}_{\lambda_3}(p_3)\; \gamma_\mu \alpha_{\lambda_4}(p_4) + \\
&\mu_1 \bar{u}_{-\lambda_1}(k_o)\; \gamma^\mu \alpha_{\lambda_2}(p_2)\; \bar{\alpha}_{\lambda_3}(p_3)\; \gamma_\mu \alpha_{\lambda_4}(p_4) + \\
&\mu_2 \bar{\alpha}_{\lambda_1}(p_1)\; \gamma^\mu u_{-\lambda_2}(k_o)\; \bar{\alpha}_{\lambda_3}(p_3)\; \gamma_\mu \alpha_{\lambda_4}(p_4) + \\
&\mu_3 \bar{\alpha}_{\lambda_1}(p_1)\; \gamma^\mu \alpha_{\lambda_2}(p_2)\; \bar{u}_{-\lambda_3}(k_o)\; \gamma_\mu \alpha_{\lambda_4}(p_4) + \\
&\mu_4 \bar{\alpha}_{\lambda_1}(p_1)\; \gamma^\mu \alpha_{\lambda_2}(p_2)\; \bar{\alpha}_{\lambda_3}(p_3)\; \gamma_\mu u_{-\lambda_4}(k_o) + \\
&\mu_1\mu_2 \bar{u}_{-\lambda_1}(k_o)\; \gamma^\mu u_{-\lambda_2}(k_o)\; \bar{\alpha}_{\lambda_3}(p_3)\; \gamma_\mu \alpha_{\lambda_4}(p_4) + \\
&\mu_1\mu_3 \bar{u}_{-\lambda_1}(k_o)\; \gamma^\mu \alpha_{\lambda_2}(p_2)\; \bar{u}_{-\lambda_3}(k_o)\; \gamma_\mu \alpha_{\lambda_4}(p_4) + \\
&\mu_1\mu_4 \bar{u}_{-\lambda_1}(k_o)\; \gamma^\mu \alpha_{\lambda_2}(p_2)\; \bar{\alpha}_{\lambda_3}(p_3)\; \gamma_\mu u_{-\lambda_4}(k_o) + \\
&\mu_2\mu_3 \bar{\alpha}_{\lambda_1}(p_1)\; \gamma^\mu u_{-\lambda_2}(k_o)\; \bar{u}_{-\lambda_3}(k_o)\; \gamma_\mu \alpha_{\lambda_4}(p_4) + \\
&\mu_2\mu_4 \bar{\alpha}_{\lambda_1}(p_1)\; \gamma^\mu u_{-\lambda_2}(k_o)\; \bar{\alpha}_{\lambda_3}(p_3)\; \gamma_\mu u_{-\lambda_4}(k_o) + \\
&\mu_3\mu_4 \bar{\alpha}_{\lambda_1}(p_1)\; \gamma^\mu \alpha_{\lambda_2}(p_2)\; \bar{u}_{-\lambda_3}(k_o)\; \gamma_\mu u_{-\lambda_4}(k_o) + \\
&\mu_1\mu_2\mu_3 \bar{u}_{-\lambda_1}(k_o)\; \gamma^\mu u_{-\lambda_2}(k_o)\; \bar{u}_{-\lambda_3}(k_o)\; \gamma_\mu \alpha_{\lambda_4}(p_4) + \\
&\mu_1\mu_2\mu_4 \bar{u}_{-\lambda_1}(k_o)\; \gamma^\mu u_{-\lambda_2}(k_o)\; \bar{\alpha}_{\lambda_3}(p_3)\; \gamma_\mu u_{-\lambda_4}(k_o) +
\end{aligned}$$

$$\mu_1\mu_3\mu_4\bar{u}_{-\lambda_1}(k_o)\ \gamma^\mu\alpha_{\lambda_2}(p_2)\ \ \bar{u}_{-\lambda_3}(k_o)\ \gamma_\mu u_{-\lambda_4}(k_o) +$$

$$\mu_2\mu_3\mu_4\bar{\alpha}_{\lambda_1}(p_1)\ \gamma^\mu u_{-\lambda_2}(k_o)\ \ \bar{u}_{-\lambda_3}(k_o)\ \gamma_\mu u_{-\lambda_4}(k_o) +$$

$$\mu_1\mu_2\mu_3\mu_4\bar{u}_{-\lambda_1}(k_o)\ \gamma^\mu u_{-\lambda_2}(k_o)\ \ \bar{u}_{-\lambda_3}(k_o)\ \gamma_\mu u_{-\lambda_4}(k_o). \qquad (3.15)$$

Because $\bar{\alpha}_{\lambda_1}(p)\ \gamma^\mu\alpha_{\lambda_2}(q)$, $\bar{u}_{\lambda_1}(k_o)\ \gamma^\mu u_{\lambda_2}(k_o)$ and $\bar{\alpha}_{\lambda_1}(p)\ \gamma^\mu u_{\lambda_2}(q)$ are only different from zero when λ_1 equals λ_2, at most four terms out of the 16 in eq. (3.15) contribute for a given configuration of the spinor polarizations Using eqs. (3.7) and (3.13) a straightforward calculation results into :

$$Z\ (p_1,\lambda_1,p_2,\lambda_1,p_3,\lambda_3,p_4,\lambda_3) = \bar{\alpha}_{\lambda_1}(p_1)\ \gamma^\mu\alpha_{\lambda_1}(p_2)\ \bar{\alpha}_{\lambda_3}(p_3)\ \gamma_\mu\alpha_{\lambda_3}(p_4) +$$

$$2\ \mu_1\mu_2\eta_3\eta_4 + 2\ \mu_3\mu_4\eta_1\eta_2$$

$$Z\ (p_1,\lambda_1,p_2,\lambda_1,p_3,\lambda_3,p_4,-\lambda_3) = \mu_4\bar{\alpha}_{\lambda_1}(p_1)\ \gamma^\mu\alpha_{\lambda_1}(p_2)\ \bar{\alpha}_{\lambda_3}(p_3)\ \gamma_\mu u_{\lambda_3}(k_o) - (p_3 - p_4)$$

$$Z\ (p_1,\lambda_1,p_2,-\lambda_1,p_3,\lambda_3,p_4,\lambda_3) = \mu_2\bar{\alpha}_{\lambda_1}(p_1)\ \gamma^\mu u_{\lambda_1}(k_o)\ \bar{\alpha}_{\lambda_3}(p_3)\ \gamma_\mu\alpha_{\lambda_3}(p_4) - (p_1 - p_2)$$

$$Z\ (p_1,\lambda_1,p_2,-\lambda_1,p_3,\lambda_3,p_4,-\lambda_3) = \mu_2\mu_4\bar{\alpha}_{\lambda_1}(p_1)\ \gamma^\mu u_{\lambda_1}(k_o)\ \bar{\alpha}_{\lambda_3}(p_3)\ \gamma_\mu u_{\lambda_3}(k_o) -$$

$$(p_1 - p_2) - (p_3 - p_4) + (p_1 - p_2;\ p_3 - p_4) \qquad (3.16)$$

Now there are still two possibilities : $\lambda_1 = \lambda_3$ and $\lambda_1 = -\lambda_3$. In the former case we can easily get rid of the repeated indices e.g. :

$$\bar{\alpha}_\lambda(p_1)\ \gamma^\mu\alpha_\lambda(p_2)\ \bar{\alpha}_\lambda(p_3)\ \gamma_\mu\alpha_\lambda(p_4) = \bar{\alpha}_\lambda(p_1)\ \gamma^\mu\not{p}_2\omega_{-\lambda}\not{k}_o\not{p}_3\gamma_\mu\alpha_\lambda(p_4) / (\eta_2\eta_3) =$$

$$\bar{\alpha}_\lambda(p_1)\ \gamma^\mu\not{p}_2\not{k}_o\not{p}_3\gamma_\mu\alpha_\lambda(p_4) / (\eta_2\eta_3) = -2\ \bar{\alpha}_\lambda(p_1)\ \not{p}_3\not{k}_o\not{p}_2\alpha_\lambda(p_4) / (\eta_2\eta_3) =$$

$$-2\ \bar{\alpha}_\lambda(p_1)\ \alpha_{-\lambda}(p_3)\ \ \bar{\alpha}_{-\lambda}(p_2)\ \alpha_\lambda(p_4) \qquad (3.17)$$

In the $\lambda_1 = -\lambda_3$ case it is worthwhile noticing that the following identity holds for an arbitrary string of γ matrices $\Sigma = \gamma_1 \cdots \gamma_n$:

$$\bar{u}_{\lambda_1}(p_1)\ \Sigma\ u_{\lambda_2}(p_2) = \lambda_1\lambda_2\ \bar{u}_{-\lambda_2}(p_2)\ \Sigma^R\ u_{-\lambda_1}(p_1) \text{ where } \Sigma^R = \gamma_n \cdots \gamma_1 \qquad (3.18)$$

Using this result and eq. (3.18) we derive e.g. :

$$\bar{\alpha}_\lambda(p_1)\ \gamma^\mu \alpha_\lambda(p_2)\ \bar{\alpha}_{-\lambda}(p_3)\ \gamma_\mu \alpha_{-\lambda}(p_4) = \bar{\alpha}_\lambda(p_1)\ \gamma^\mu \alpha_\lambda(p_2)\ \bar{\alpha}_\lambda(p_4)\ \gamma_\mu \alpha_\lambda(p_3) =$$

$$-2\ \bar{\alpha}_\lambda(p_1)\ \alpha_{-\lambda}(p_4)\ \bar{\alpha}_{-\lambda}(p_2)\ \alpha_\lambda(p_3) \qquad (3.19)$$

In an analogous way we calculate the remaining expressions. The final result is listed in table 1.

Table 1

$$Z(\lambda_1,\lambda_2,\lambda_3,\lambda_4) \equiv Z(p_1,\lambda_1,p_2,\lambda_2,p_3,\lambda_3,p_4,\lambda_4)$$

$$\begin{aligned}
Z(+,+,+,+) &= -2\{s_{13}t_{24} - \mu_1\mu_2\eta_3\eta_4 - \eta_1\eta_2\mu_3\mu_4\}\\
Z(+,+,+,-) &= -2\,\eta_2\{\mu_4 s_{13} - \mu_3 s_{14}\}\\
Z(+,+,-,+) &= -2\,\eta_1\{\mu_4 t_{23} - \mu_3 t_{24}\}\\
Z(+,+,-,-) &= -2\{s_{14}t_{23} - \mu_1\mu_2\eta_3\eta_4 - \eta_1\eta_2\mu_3\mu_4\}\\
Z(+,-,+,+) &= -2\,\eta_4\{\mu_2 s_{31} - \mu_1 s_{32}\}\\
Z(+,-,+,-) &= 0\\
Z(+,-,-,+) &= 2\,(\eta_1\mu_2 - \mu_1\eta_2)(\eta_3\mu_4 - \mu_3\eta_4)\\
Z(+,-,-,-) &= -2\,\eta_3\{\mu_2 s_{41} - \mu_1 s_{42}\}\\
Z(-,+,+,+) &= -2\,\eta_3\{\mu_2 t_{41} - \mu_1 t_{42}\}\\
Z(-,+,+,-) &= 2\,(\eta_1\mu_2 - \mu_1\eta_2)(\eta_3\mu_4 - \mu_3\eta_4)\\
Z(-,+,-,+) &= 0\\
Z(-,+,-,-) &= -2\,\eta_4\{\mu_2 t_{31} - \mu_1 t_{32}\}\\
Z(-,-,+,+) &= -2\{t_{14}s_{23} - \mu_1\mu_2\eta_3\eta_4 - \eta_1\eta_2\mu_3\mu_4\}\\
Z(-,-,+,-) &= -2\,\eta_1\{\mu_4 s_{23} - \mu_3 s_{24}\}\\
Z(-,-,-,+) &= -2\,\eta_2\{\mu_4 t_{13} - \mu_3 t_{14}\}\\
Z(-,-,-,-) &= -2\{t_{13}s_{24} - \mu_1\mu_2\eta_3\eta_4 - \eta_1\eta_2\mu_3\mu_4\}
\end{aligned}$$

Here s_{12} stands for $S(p_1,p_2)$ and so on.

Before finishing the description of the calculation of the matrix element squared let us now recapitulate the subsequent operations which have to be performed in order to evaluate the matrix element squared for a given event with four-momenta p_+,p_-,q_+,q_-,k_+,k_- :

1) Calculate the scalars $S(p,q)$ and $T(p,q)$ using eq. (3.11)
2) Choose the spin polarizations for each particle.

3) Pick one of the 36 diagrams and calculate it using eqs. (3.2) (3.5) and table 1.
4) Repeat step 3 until all the diagrams are calculated while summing the results.
5) Square the result of step 4.
6) Repeat steps 2 through 5 while summing the results.

A few remarks are in order here. The speed with which this algorithm can be executed can be significantly increased if we observe that for an accurate evaluation of the amplitude it sometimes is not really necessary to calculate all diagrams or to take all masses into account. Generally the masses of the particles are not to be neglected whenever we calculate a gauge invariant combination of two diagrams whose denominators are close to zero. But then it makes no sense spending a lot of computer time on the calculation of the contribution of the other diagrams since the total amplitude will be dominated by the diagrams with denominators close to zero. On the other hand when none of the propagators blows up we have to calculate all diagrams but are allowed to think of massless particles. Consequently, in those cases, we can leave out those spin polarization configurations which are suppressed with a mass factor. It is rather straightforward to write a computer routine which determines on the basis of a given momentum configuration, which amplitudes or sets of diagrams can safely be neglected without affecting the result for the cross section.

Next we turn our attention to the numerical stability of the scheme described above. Since we perform the calculation at the amplitude level as contrasted with the cross section level, the numerical stability is improved considerably. However, there may still occur cancellations during the evaluation of eq. (3.2) which must be controlled. Almost all of these cancellations come about when one of the propagators in eq. (3.2) blows up. Therefore we take the following precautions :
when $(b_1p_1+ b_2p_2)^2$ becomes close to 0 we calculate it as follows :

$$(b_1p_1+ b_2p_2)^2= m_1^2+ m_2^2+ 2\, b_1b_2\{ [\, p_{1o}^2(p_{2x}^2+ p_{2y}^2+ m_2^2) + p_{2z}^2(p_{1x}^2+ p_{1y}^2+ m_1^2)\,] \Big/ (\, p_{1o}p_{2o}+ p_{1z}p_{2z}) - p_{1x}p_{2x}- p_{1y}p_{2y}\} \qquad (3.20)$$

when $(b_5p_5+ b_6p_6)^2$ becomes close to 0 it is calculated in a similar way.
when $(b_1p_1+ b_2p_2+ b_3p_3)^2$ approaches 0 either $(b_1p_1+ b_2p_2)^2$ or $(b_5p_5+ b_6p_6)^2$

does the same. In the former case we write $(b_1p_1+ b_2p_2+ b_3p_3)^2=$ $(b_1p_1+ b_2p_2)^2+ 2\ b_3p_3\cdot(b_1p_1+ b_2p_2) + m_3^2$ and calculate the dot product with p_3 using the same trick as in eq. (3.20). In the latter case we calculate $(b_4p_4+ b_5p_5+ b_6p_6)^2$.

When we do not consider $e^+e^- \to e^+e^+e^-e^-$ but another four-lepton production process only a subset of the 36 diagrams has to be calculated e.g. for $e^+e^- \to e^+e^-\mu^+\mu^-$ only groups 1 and 6 (if we assume k_+, k_- to be the four-momenta of respectively the μ^+ and the μ^-), for $e^+e^- \to \mu^+\mu^+\mu^-\mu^-$ only groups 1 and 2, for $e^+e^- \to \mu^+\mu^-\tau^+\tau^-$ only group 1. In the case of a quark pair in the final state the charge of the quark should be inserted. One should be aware of the fact that the power with which this charge occurs in the amplitude equals the number of vertices along the quark line. Finally we want to remark that, as in ref. [5], this algorithm can be easily implemented in a FORTRAN computer program which ensures a fast numerical evaluation.

We remind the reader that the procedure outlined in this section for the calculation of the exact matrix element squared can be extended to Z_0 exchange. This is shown in appendix E.

3. Exact matrix elements squared of subsets of Feynman diagrams

Having calculated the complete exact matrix element squared, we now start with the description of the event generation. As was already emphasized in the introduction we need several subgenerators, each of which takes into account a specific part of the peaking behaviour of the complete matrix element squared. To this end we divide the 36 Feynman graphs in fig. 7 in four groups. The first group consists of the 'multiperipheral' diagrams (3,1), (3,2), (4,1), (4,2), (5,3), (5,4), (6,3) and (6,4). The second, 'bremsstrahlung' group, contains the remaining diagrams with group number 3, 4, 5 or 6. The third consists of 'conversion' graphs (1,5), (1,6), (2,5) and (2,6). The remaining diagrams with group number 1 or 2 make up the so-called 'annihilation' group. It is important to notice that in those four groups diagrams with the same group number form gauge invariant combinations. These we will denote as subgroups. So we may write the matrix element squared as follows :

$$\sum_{\text{spins}} |M|^2 \quad , \quad M = M_{m_3} + M_{m_4} + M_{m_5} + M_{m_6} + M_{b_3} + M_{b_4} +$$

$$M_{b_5} + M_{b_6} + M_{c_1} + M_{c_2} + M_{a_1} + M_{a_2} \qquad (3.21)$$

where M_{m_3} stands for the amplitude of the two multiperipheral diagrams with group number 3 and so on.

Let us now as a first approximation neglect all the interferences between these 12 terms. Consequently the events will then be assigned a weight equal to :

$$\frac{\Sigma \, |M|^2}{\Sigma \{ |M_{m_3}|^2 + |M_{m_4}|^2 + |M_{m_5}|^2 + |M_{m_6}|^2 + |M_{b_3}|^2 + \ldots\ldots\ldots\ldots + |M_{a_2}|^2 \}} \qquad (3.22)$$

Notice that these amplitudes squared of subgroups of Feynman diagrams can be evaluated concurrently with the calculation of $\Sigma \, |M|^2$. When, despite all our precautions, a numerical cancellation occurs during the evaluation of $\Sigma |M|^2$, the effect on the weight will usually be small, since it affects both the numerator and denominator. Now all that is left to do is to generate events according to the denominator of eq. (3.22).

Let us first consider the process $e^+e^- \to e^+e^+e^-e^-$. If we restrict ourselves to experimental cuts which are the same for all particles in the final state the event generation according to the denominator of eq. (3.22) is considerably simplified because then the four gauge invariant subgroups of multiperipheral diagrams all contribute equally to the total cross section. As a consequence, when events have been generated according to one of the four subgroups, the event distribution according to all four subgroups can be obtained after symmetrization of the four-momenta of the final state particles and it is therefore sufficient to consider from now on only one subgroup (provided that we multiply its cross section with the number of subgroups). The same applies to the four bremsstrahlung, two conversion and two annihilation subgroups. Thus, apart from the symmetrization procedure, the subgenerators for $e^+e^- \to e^+e^+e^-e^-$ will be identical to those for $e^+e^- \to e^+e^-\mu^+\mu^-$. Therefore, we will often discuss the latter process instead of the former one. The price which now has to be paid is the fact that those cuts that are not symmetrical with respect to the particles in the final state, can only be put in afterwards ,that is by setting weights equal to zero of those events that do not satisfy these cuts. This may of course reduce the efficiency of the Monte Carlo program. For processes other than eeee production, less than 36 graphs will contribute and the symmetrization

procedure is simplified accordingly.

Using the superposition principle for the Monte Carlo simulation of distributions (as was explained in chapter II), we shall design for each of the differential cross sections corresponding to the four remaining subgroups an approximation which can be integrated analytically over physical phase-space and moreover has the correct peaking structure. As before we account for these approximations by assigning a weight to the generated events. This weight is equal to the ratio of the exact matrix element squared of the subgroup over the approximation used. Since there are at most four Feynman diagrams in a subgroup, it is again feasible to derive an analytical expression for the corresponding matrix element squared. Of course, this has the advantage, that it can be evaluated much faster than the numerical method which was used to obtain the complete matrix element squared.

We first discuss the exact matrix element squared of the multiperipheral subgroup which consists of the graphs (6,3) and (6,4). We write the matrix element M as follows:

$$M = J_e^{\mu}(p_-,q_-)\; X_{\mu}(p_+,q_+,k_+k_-) \;/\; Q_-^2 \;,$$

$$J_e^{\mu}(p_-,q_-) = \bar{u}(q_-)\;\gamma^{\mu}u(p_-) \quad , \quad Q_-^{\mu} = p_-^{\mu} - q_-^{\mu} \;. \tag{3.23}$$

We have to be very cautious when calculating this amplitude. Since the $1 / Q_-^2$ dependence in M would give rise to a $1 / Q_-^4$ dependence in $|M|^2$ and consequently a total cross section proportional to $(E_b / m_e)^2$ which is not observed, the contraction between J_e^{μ} and X_{μ} exhibits dramatic cancellations down to $O(m_e / E_b)$. This point has been discussed extensively by many authors [6]. To avoid these cancellations we adopt a method which makes use of current conservation [7]. First we write the matrix element squared as follows : *

$$\tfrac{1}{4}\;\Sigma\,|M|^2 = L_o^{\mu\nu}(p_-,q_-)\; H_{\mu\nu}(p_+,q_+,k_+,k_-) \;,$$

$$L_o^{\mu\nu}(p_-,q_-) = \tfrac{1}{4}\;\Sigma\, J_e^{\mu}(p_-,q_-)\; J_e^{\nu}(p_-,q_-)^{*}. \tag{3.24}$$

Current conservation yields : $Q_-^{\mu}\, H_{\mu\nu} = 0$. Consequently $L_o^{\mu\nu}$ can now be rewritten in the following form :

* From now on spin sum and average is always implied.

$$L_o^{\mu\nu} = \varepsilon_1^\mu \varepsilon_1^\nu + Q_-^2 g^{\mu\nu} \quad , \quad \varepsilon_1^\mu = p_-^\mu + q_-^\mu + z_1 Q_-^\mu . \tag{3.25}$$

Here z_1 stands for an arbitrary parameter. We now use this freedom of choice in order to make the contraction between $\varepsilon_1^\mu \varepsilon_1^\nu$ and $H_{\mu\nu}$ numerically stable. We can ensure this stability by choosing z_1 in such a way that ε_1^μ becomes of order m_e whenever $|Q_-^2|$ is of order m_e^2. A suitable choice for z_1 is $z_1 = -(p_-^o + q_-^o) / Q_-^o$ so that ε_1^o equals 0. Now $\varepsilon_1^2 = -|\vec{\varepsilon}_1|^2 = 4 m_e^2 + (z_1^2 - 1) Q_-^2 \to 0 (m_e^2)$ when $|Q_-^2| \to 0 (m_e^2)$ and $\varepsilon_1^i \to 0 (m_e)$ $(i = x,y,z)$ in this limit. Notice $\varepsilon_1^2 \to 0 (m_e^4)$ when $|Q_-^2| \to \min |Q_-^2|$. Thus the $1 / Q_-^2$ behaviour of $|M|^2$ is achieved without any huge cancellation. Here we have assumed that $W^2 = (k_+ + k_-)^2 >> m_e^2$. However, the event generator turns out to be numerically stable even when this condition is not fulfilled. Notice that the $g^{\mu\nu}$ term is already numerically stable because of the Q_-^2 in front of it. Of course the contraction of the positron current is dealt with in the same way.

We define $D(p_-, q_-, p_+, q_+, k_-, k_+)$ to be the exact matrix element squared of the multiperipheral subgroup. A straightforward REDUCE [8] calculation yields :

$$D(p_-,q_-,p_+,q_+,k_-,k_+) = \frac{-32}{t_1^2 t_2^2} \left[\frac{\Pi_1}{\Delta_1^2} + \frac{\Pi_2}{\Delta_2^2} + \frac{\Pi_{12}}{\Delta_1 \Delta_2} \right] ,$$

$$\Pi_1 = \left(P_{11}^2 + t_1 \left(\tfrac{1}{4} t_1 + m_1^2 + m_3^2 \right) \right) \left(P_{22}^2 + t_2 \left(\tfrac{1}{4} t_2 + m_2^2 + m_3^2 \right) \right) ,$$

$$\Pi_2 = \left(P_{21}^2 + t_1 \left(\tfrac{1}{4} t_1 + m_1^2 + m_3^2 \right) \right) \left(P_{12}^2 + t_2 \left(\tfrac{1}{4} t_2 + m_2^2 + m_3^2 \right) \right) ,$$

$$\begin{aligned} \Pi_{12} = {} & 2 P_{11} P_{12} P_{21} P_{22} + \Delta \Delta_1 P_{12} P_{21} + \Delta \Delta_2 P_{11} P_{22} + \tfrac{1}{4} \Delta^2 \Delta_1 \Delta_2 - \\ & 2 P_{11} P_{21} t_2 \left(\tfrac{1}{4} t_2 + m_2^2 + m_3^2 \right) - 2 P_{12} P_{22} t_1 \left(\tfrac{1}{4} t_1 + m_1^2 + m_3^2 \right) - \\ & m_1^2 m_2^2 \left(t_1 + t_2 - W^2 \right)^2 - m_1^2 t_2 \left(Q_{12} + Q_{22} \right)^2 - m_2^2 t_1 \left(Q_{21} + Q_{11} \right)^2 - \\ & \tfrac{1}{4} \left(\Delta_2 - \Delta_1 \right)^2 \left(m_2^2 t_1 + m_1^2 t_2 \right) + \frac{1}{16} t_1 t_2 \left[-4 \left(Q_{11} - Q_{21} \right)^2 - \right. \\ & 4 \left(Q_{12} - Q_{22} \right)^2 - 4 \Delta_o^2 - \left(W^2 + t_1 + t_2 \right)^2 - 16 \left(W^2 - t_1 - t_2 \right) m_3^2 - \\ & \left. 16 W^2 \left(m_1^2 + m_2^2 \right) + 32 \left(\tfrac{1}{4} t_1 - m_1^2 - m_3^2 \right) \left(\tfrac{1}{4} t_2 - m_2^2 - m_3^2 \right) \right] \end{aligned}$$

$$P_{11} = k_- \cdot \varepsilon_1 - \tfrac{1}{2} z_1 t_1 \quad , \qquad Q_{11} = k_- \cdot d_1 ,$$

$$P_{12} = k_- \cdot \varepsilon_2 - \tfrac{1}{2} z_2 t_2 \quad , \qquad Q_{12} = k_- \cdot d_2 \ ,$$
$$P_{21} = k_+ \cdot \varepsilon_1 - \tfrac{1}{2} z_1 t_1 \quad , \qquad Q_{21} = k_+ \cdot d_1 \ ,$$
$$P_{22} = k_+ \cdot \varepsilon_2 - \tfrac{1}{2} z_2 t_2 \quad , \qquad Q_{22} = k_+ \cdot d_2 \ ,$$

$$\Delta = \varepsilon_1 \cdot \varepsilon_2 \ , \ \Delta_0 = d_1 \cdot d_2 \ , \ t_1 = (p_- - q_-)^2 , \ t_2 = (p_+ - q_+)^2 ,$$
$$\Delta_1 = (p_- - q_- - k_-)^2 - m_3^2 , \ \Delta_2 = (p_- - q_- - k_+)^2 - m_3^2 , \ W^2 = (k_- + k_+)^2 ,$$
$$d_1 = p_- + q_- \ , \ \varepsilon_1 = d_1 + z_1 (p_- - q_-) \ ,$$
$$d_2 = p_+ + q_+ \ , \ \varepsilon_2 = d_2 + z_2 (p_+ - q_+) \ , \qquad (3.26)$$
z_1 and z_2 are arbitrary numbers.

In this equation we introduced three masses m_1, m_2 and m_3 (belonging to respectively the (p_-,q_-), (p_+,q_+) and (k_-,k_+) fermion lines) in order to obtain a general result which later on will also be used for processes with different masses such as $e^+e^- \to \mu^+\mu^-\tau^+\tau^-$.

All the other matrix elements squared of gauge invariant combinations of two Feynman diagrams can be calculated using eq. (3.26) after interchanging the momenta according to table 2.

Table 2

matrix element squared of diagrams :			
S_m :	(6.3) (6,4)	$\lvert M_m \rvert^2 =$	$D (p_-, q_-, p_+, q_+, k_-, k_+)$
S_{be} :	(6.1) (6.2)	$\lvert M_{be} \rvert^2 =$	$D (-k_+, k_-, p_+, q_+, q_-, -p_-)$
S_{bp} :	(6.5) (6,6)	$\lvert M_{bp} \rvert^2 =$	$D (p_-, q_-, -k_-, k_+, -p_+, q_+)$
S_c :	(1,5) (1,6)	$\lvert M_c \rvert^2 =$	$D (-q_+, q_-, -k_-, k_+, -p_+, -p_-)$
S_{aq} :	(1,3) (1,4)	$\lvert M_{aq} \rvert^2 =$	$D (p_-, -p_+, -q_-, q_+, k_-, k_+)$
S_{ak} :	(1,1) (1,2)	$\lvert M_{ak} \rvert^2 =$	$D (p_-, -p_+, -k_-, k_+, q_-, q_+)$

Using this table and eq. (3.26) the matrix elements squared of the multiperipheral subgroup and the conversion subgroup (graphs (1,5) and (1,6))

are completely determined. The matrix elements squared of the bremsstrahlung subgroup (diagrams (6,1), (6,2), (6,5) and (6,6)) and the annihilation subgroup (diagrams (1,1), (1,2), (1,3) and (1,4)) are calculated by dividing the four Feynman graphs in two gauge invariant subsets respectively S_{be}, S_{bp} and S_{aq}, S_{ak}. Their matrix elements squared are listed in table 2. Next we calculate the interference between the subsets S_{be} and S_{bp}. Using again REDUCE we find the following result :

$$
\begin{aligned}
I\,(p_-,q_-,p_+,q_+,k_-,k_+) = \frac{1}{t_1 t_2 W^4}\,\{\; & 32\,(R_{11}+R_{21})\,(R_{12}+R_{22}) + \\
& \frac{32\,(\tilde{s}^2+\tilde{u}_1\tilde{u}_2-2\,(m_1^2+m_2^2)^2)R_{22}R_{21}-32\,W^2(m_1^2R_{11}R_{22}+m_2^2R_{12}R_{21})}{\Delta_3\,\Delta_5} + \\
& \frac{32\,(\tilde{u}_1^2+\tilde{s}\,\tilde{s}_1-2\,(m_1^2+m_2^2)^2)R_{11}R_{22}-32\,W^2(m_1^2R_{21}R_{22}+m_2^2R_{11}R_{12})}{\Delta_3\,\Delta_6} + \\
& \frac{32\,(\tilde{u}_2^2+\tilde{s}\,\tilde{s}_1-2\,(m_1^2+m_2^2)^2)R_{12}R_{21}-32\,W^2(m_1^2R_{11}R_{12}+m_2^2R_{21}R_{22})}{\Delta_4\,\Delta_5} + \\
& \frac{32\,(\tilde{s}_1^2+\tilde{u}_1\tilde{u}_2-2\,(m_1^2+m_2^2)^2)R_{11}R_{12}-32\,W^2(m_1^2R_{12}R_{21}+m_2^2R_{11}R_{22})}{\Delta_4\,\Delta_6} + \\
& 16\,W^2\{(R_{11}+R_{12})^2+(R_{12}-R_{21})^2\}[\frac{\tilde{s}}{\Delta_3\Delta_5}-\frac{\tilde{u}_1}{\Delta_3\Delta_6}-\frac{\tilde{u}_2}{\Delta_4\Delta_5}+\frac{\tilde{s}_1}{\Delta_4\Delta_6}] - \\
& 32\,\frac{\tilde{s}\,R_{21}(R_{11}+R_{12})-\tilde{u}_2R_{21}(R_{11}-R_{22})}{\Delta_5} - 32\,\frac{\tilde{s}\,R_{22}(R_{11}+R_{12})+\tilde{u}_1R_{22}(R_{11}-R_{22})}{\Delta_3} - \\
& 32\,\frac{\tilde{s}_1R_{12}(R_{21}+R_{22})+\tilde{u}_2R_{12}(R_{21}-R_{12})}{\Delta_4} - 32\,\frac{\tilde{s}_1R_{11}(R_{21}+R_{22})-\tilde{u}_1R_{11}(R_{21}-R_{12})}{\Delta_6} + \\
& 8\,W^2(\tilde{s}^2+\tilde{u}_1^2+\tilde{u}_2^2+\tilde{s}_1^2)[\frac{\tilde{s}}{\Delta_3\Delta_5}-\frac{\tilde{u}_1}{\Delta_3\Delta_6}-\frac{\tilde{u}_2}{\Delta_4\Delta_5}+\frac{\tilde{s}_1}{\Delta_4\Delta_6}] + \\
& 4\,(4\,m_3^2-W^2)\,((s-s_1)^2-(u_1-u_2)^2)[\frac{t_2}{\Delta_3\Delta_4}+\frac{t_1}{\Delta_5\Delta_6}] - \\
& 8\,(4\,m_3^2+W^2)\,W^2t_1t_2((s-s_1)^2-(u_1-u_2)^2)\,/\,(\Delta_3\Delta_4\Delta_5\Delta_6) + \\
& 16\,W^2(m_1^2+m_2^2)(t_1+t_2+W^2)[\frac{\tilde{s}}{\Delta_3\Delta_5}-\frac{\tilde{u}_1}{\Delta_3\Delta_6}-\frac{\tilde{u}_2}{\Delta_4\Delta_5}+\frac{\tilde{s}_1}{\Delta_4\Delta_6}] - \\
& 32\,m_1^2W^2(s-u_1)\,/\,\Delta_3 - 32\,m_2^2W^2(s-u_2)\,/\,\Delta_5 - \\
& 32\,m_1^2W^2(s_1-u_2)\,/\,\Delta_4 - 32\,m_2^2W^2(s_1-u_1)\,/\,\Delta_6 +
\end{aligned}
$$

$$4\,(4\,m_3^2 - W^2)\{W^2(s_1 - s) + (t_1 - t_2)(u_1 - u_2)\}\frac{\tilde{s}}{\Delta_3\Delta_5} -$$

$$4\,(4\,m_3^2 - W^2)\{W^2(u_2 - u_1) + (t_1 - t_2)(s - s_1)\}\frac{\tilde{u}_1}{\Delta_3\Delta_6} -$$

$$4\,(4\,m_3^2 - W^2)\{W^2(u_1 - u_2) + (t_1 - t_2)(s_1 - s)\}\frac{\tilde{u}_2}{\Delta_4\Delta_5} +$$

$$4\,(4\,m_3^2 - W^2)\{W^2(s - s_1) + (t_1 - t_2)(u_2 - u_1)\}\frac{\tilde{s}_1}{\Delta_4\Delta_6} \quad \}$$

$$s = (p_+ + p_-)^2,\ u_1 = (p_- - q_+)^2,\ s_1 = (q_+ + q_-)^2,\ u_2 = (p_+ - q_-)^2,$$

$$R_{11} = \varepsilon\cdot p_+ ,\ R_{12} = \varepsilon\cdot p_- ,\ R_{21} = \varepsilon\cdot q_+ ,\ R_{22} = \varepsilon\cdot q_- ,\ \varepsilon = k_+ - k_-,$$

$$\Delta_3 = \tilde{s} + \tilde{u}_1 + t_2 ,\ \Delta_4 = \tilde{s}_1 + \tilde{u}_2 + t_2 ,\ \Delta_5 = \tilde{s} + \tilde{u}_2 + t_1 ,\ \Delta_6 = \tilde{s}_1 + \tilde{u}_1 + t_1 ,$$

$$\tilde{A} = A - m_1^2 - m_2^2 ,\ \tilde{\tilde{A}} = \tilde{A} - m_1^2 - m_2^2 ,\ A = s,\ s_1,\ u_1,\ u_2. \qquad (3.27)$$

The interference between S_{aq} and S_{ak} can again be found by interchanging the momenta. It equals :

$$I\,(-k_+, k_-, -q_-, q_+, -p_+, -p_-). \qquad (3.28)$$

Notice that these changes can be easily implemented in a computer program. Thus using eqs. (3.26), (3.27), (3.28) and table 2, we can calculate the exact cross section for each of the four subgroups, as soon as the particle momenta are specified.

4. The multiperipheral subgenerator

In this and the next three sections we shall discuss the subgenerators for the process :

$$e^+(p_+)\ e^-(p_-) \to e^+(q_+)\ e^-(q_-)\ \mu^+(k_+)\ \mu^-(k_-) \qquad (3.29)$$

To this end we specify for each subgroup of Feynman diagrams a set of integration variables and a suitable approximation for the exact matrix element squared. The remaining features of the approximations used will only be treated in so far as they are thought to be of relevance for a better understanding. For computational details we refer to reference [9]. We first consider the multiperipheral subgroup. The corresponding exact differential cross section reads :

$$d\sigma_m = \frac{\alpha^4}{256\,\pi^4 E_b^2}\,\delta\,(4 - 4x - 4y - W^2 + 2m_e^2 + 2xy - 2|\vec{x}|\,|\vec{y}|\cos\tilde{\Theta})$$
$$|M_m|^2 (1 - \frac{4m_\mu^2}{W^2})^{\frac{1}{2}}\, d\vec{\Omega}_\mu \frac{d^3\vec{x}}{x}\frac{d^3\vec{y}}{y}\, dW^2 \,. \qquad (3.30)$$

Here we defined :

$x = q_-^\circ$, $\vec{x} = \vec{q}_-$, $y = q_+^\circ$, $\vec{y} = \vec{q}_+$, $\cos\tilde{\Theta} = -c_+c_- - s_+s_-\cos\tilde{\phi}$,
$c_\pm = \cos\Theta_\pm$, $s_\pm = \sin\Theta_\pm$, $\Theta_\pm$ is the angle between $\vec{p}_\pm$ and $\vec{q}_\pm$,
$\tilde{\phi} = \phi_+ - \phi_- + \pi$, $\phi_\pm$ is the azimuthal angle of $\vec{q}_\pm$,
$d\vec{\Omega}_+ = dc_+ d\tilde{\phi}$, $d\vec{\Omega}_- = dc_- d\phi_-$, $d\vec{\Omega}_\mu = d\cos\Theta_\mu\, d\phi_\mu$, Θ_μ is the angle between
$\vec{k}_-$ and $\vec{p}_- - \vec{q}_-$, ϕ_μ the azimuthal angle in the CM system of the muons.

In the $ee\mu\mu$ case $W^2_{min} \geq 4m_\mu^2$ and we can safely neglect m_e in the kinematics. Solving the argument of the δ function we find a one-to-one relation between x and y. However, since we want our calculations to be valid also for the eeee case (when $W^2_{min} \geq 4m_e^2$) it is no longer obvious that m_e can be neglected. We therefore treat the kinematics exactly and find the following result after solving the argument of the δ function :

$$y_\pm = \frac{(2-x)(4 - 4x + 2m_e^2 - W^2) \pm |\vec{x}|\cos\tilde{\Theta}\,\tilde{\Delta}}{2\,[\,(2-x)^2 - |\vec{x}|^2\cos^2\tilde{\Theta}\,]}\,,$$
$$\tilde{\Delta} = [\,(4 - 4x + 2m_e^2 - W^2)^2 - 4(2-x)^2 m_e^2 + 4|\vec{x}|^2 m_e^2\cos^2\tilde{\Theta}\,]^{\frac{1}{2}}. \qquad (3.31)$$

We resolve the sign ambiguity by dividing the phase-space into two parts. In part 1 we have :

$$y = y_1 = y_- \,, \quad x_{min} = m_e \,, \quad x_{max} = 1 - \tfrac{1}{2}m_e W - \tfrac{1}{2}W^2 \,,$$

if $m_e \leq x \leq x'$ then $-1 \leq \cos\tilde{\Theta} \leq +1$,

if $x' \leq x \leq x_{max}$ then $-1 \leq \cos\tilde{\Theta} \leq -c_a$,

$$x' = \frac{(4 - 4m_e + 2m_e^2 - W^2)}{4 - 2m_e}\,, \quad c_a = \Big[\frac{4(2-x)^2 m_e^2 - (4 - 4x + 2m_e^2 - W^2)^2}{4|\vec{x}|^2 m_e^2}\Big]^{\frac{1}{2}},$$

whereas in part 2 :

$$y = y_2 = y_+ \; , \quad x_{min} = x' \; , \quad x_{max} = 1 - \tfrac{1}{2} m_e W - \tfrac{1}{4} W^2 ,$$

$$-1 \leq \cos\tilde{\Theta} \leq - c_a \; . \tag{3.32}$$

We see that the scattered electron and positron are forced to be back to back when x approaches its maximum. This feature only occurs when we treat the kinematics exactly. If we had neglected m_e the maximum of x would correspond to the minimum of y, that is, the positron would have zero momentum. We now write $d\sigma_m$ as the sum of the differential cross sections in part 1 and 2 :

$$d\sigma_m = d\sigma_{m_1} + d\sigma_{m_2} \; ,$$

$$d\sigma_{m_1} = \frac{\alpha^4}{256\,\pi^4 E_b^2} \left| M_m \right|^2 \frac{\left| \vec{x} \right| \left| \vec{y}_i \right|}{\left| 4 - 2x + 2 \left| \vec{x} \right| y_1 \cos\tilde{\Theta} / \left| \vec{y}_i \right| \right|} \left(1 - \frac{4 m_\mu^2}{W^2}\right)^{\frac{1}{2}}$$

$$dW^2 dx \, d\vec{\Omega}_+ d\vec{\Omega}_- d\vec{\Omega}_\mu \; . \tag{3.33}$$

Now we must construct a suitable approximation for $\left| M_m \right|^2$. It turns out that $\left| M_m \right|^2$ can best be described by an approximation proportional to :

$$\frac{1}{t_1 t_2 \Delta_1 \Delta_2} \; . \tag{3.34}$$

At first sight it might look strange that the $1 / (t_1 t_2)$ is not squared in the approximation, whereas it is squared in eq. (3.26). This seeming paradox is resolved, if we remember the discussion about the numerical stability in the previous section. There we showed that whenever t_1 or t_2 becomes of order m_e^2 also Π_{12} is of order m_e^2. As a consequence the square of t_1 and t_2 is effectively cancelled. Moreover choosing this approximation we can easily verify that the approximate total cross section increases logarithmically with the beam energy. Since we require the chosen approximation to be analytically integrable over phase-space additional weight factors have to be determined. These factors neglect the functional behaviour which might spoil the integrability and are given explicitly in ref. [9]. Denoting the product of the weight factors for phase-space part i by V_{mi}, we write the approximate differential cross section as follows :

$$d\tilde{\sigma}_m = d\tilde{\sigma}_{m_1} + d\tilde{\sigma}_{m_2} \; ,$$

$$d\tilde{\sigma}_{m_i} = \frac{\alpha^4}{256\,\pi^4 E_b^2} \frac{512\,|\vec{x}|\,|\vec{y}_i|}{t_1 t_2 \Delta_1 \Delta_2 V_{mi} |4 - 2x + 2|\vec{x}|\,y_i \cos\tilde{\Theta} / |\vec{y}_i|\,|} \left(1 - \frac{4m_\mu^2}{W^2}\right)^{\frac{1}{2}}$$
$$d\vec{\Omega}_\mu d\vec{\Omega}_- d\vec{\Omega}_+ dx\, dW^2. \qquad (3.35)$$

We generate the events using again the procedure described in eq. (2.10). In this case N equals 2 because we have divided the exact differential cross section in two parts according to eq. (3.33). Finally, we want to remark that, when the condition on $\cos\tilde{\Theta}$ (eq. 3.32) is not satisfied, the weight of the generated event is set equal to 0. This condition reduces the efficiency of the program very little since it has only to be applied to events with $x > x'$.

5. The bremsstrahlung subgenerator

The bremsstrahlung subgroup consists of two gauge invariant subsets S_{be} and S_{bp}. The corresponding exact differential cross section reads :

$$d\sigma_b = \frac{\alpha^4}{128\,\pi^4 E_b^2} |M_b|^2\, \delta^4(p_+ + p_- - q_+ - q_- - k_+ - k_-) \frac{d^3\vec{q}_+}{q_+^\circ} \frac{d^3\vec{q}_-}{q_-^\circ} \frac{d^3\vec{k}_+}{k_+^\circ} \frac{d^3\vec{k}_-}{k_-^\circ},$$
$$|M_b|^2 = |M_{be}|^2 + |M_{bp}|^2 + I\,(p_-, q_-, p_+, q_+, k_-, k_+)\,. \qquad (3.36)$$

We now write the approximate differential cross section corresponding to the bremsstrahlung group as a sum of approximations for the two subsets. Consequently the interference between the two subsets is dealt with by a weight assignment. Event distributions according to the total approximation can again be obtained by the use of the superposition principle.

We start with considering the differential cross section corresponding to subset S_{be} :

$$d\sigma_{b_e} = \frac{\alpha^4}{256\,\pi^4 E_b^2}\, \delta\,(4 - 4y - 4k^\circ + W^2 + 2yk^\circ - 2|\vec{y}|\,|\vec{k}|\cos\tilde{\Theta})$$
$$|M_{be}|^2\, (1 - \frac{4m_\mu^2}{W^2})^{\frac{1}{2}}\, d\vec{\Omega}_\mu \frac{d^3\vec{y}}{y} \frac{d^3\vec{k}}{k^\circ} dW^2. \qquad (3.37)$$

Here we defined :

$$k = k_+ + k_-\,,\quad \cos\tilde{\Theta} = -c_k c_+ + s_k s_+ \cos\tilde{\phi}\,,\quad \tilde{\phi} = \phi_+ - \phi_k,$$

$c_k = \cos\Theta_k$, $s_k = \sin\Theta_k$, $d\vec{\Omega}_k = dc_k d\phi_k$, Θ_k is the angle between $\vec{p}_-$ and $\vec{k}$,
$c_+ = \cos\Theta_+$, $s_+ = \sin\Theta_+$, $d\vec{\Omega}_+ = dc_+ d\tilde{\phi}$, Θ_+ is the angle between $\vec{p}_+$ and $\vec{q}_+$,
ϕ_k and ϕ_+ are the azimuthal angles of respectively $\vec{k}$ and $\vec{q}_+$.

In order to treat the kinematics exactly we now proceed in the same way as in sect. 4 , that is, we divide the phase-space into two parts and write the differential cross section as a sum :

$$y_{\pm} = \frac{2\,(2 - k^{\circ})\,u \pm |\vec{k}|\cos\tilde{\Theta}\,\tilde{\Delta}}{4\,u + |\vec{k}|^2(1 - \cos^2\tilde{\Theta})} \quad , \quad u = 1 - k^{\circ} + \tfrac{1}{4} W^2,$$

$$\tilde{\Delta} = \left(4\,u^2 + m_e^2\,|\vec{k}|^2\cos^2\tilde{\Theta} - m_e^2(2 - k^{\circ})^2\right)^{\frac{1}{2}},$$

In part 1 we have :

$$y = y_1 = y_- \ , \ u_{min} = m_e^2 \ , \ u_{max} = (1 - \tfrac{1}{2} W)^2,$$

$$\text{if} \quad u_{min} \leqslant u \leqslant u' \quad \text{then} \quad -1 \leqslant \cos\tilde{\Theta} \leqslant -c'_a \ ,$$

$$\text{if} \quad u' < u \leqslant u_{max} \quad \text{then} \quad -1 \leqslant \cos\tilde{\Theta} \leqslant +1 \ ,$$

$$u' = \frac{m_e(1 - \frac{1}{4} W^2)}{2 - m_e} \quad , \quad c'_a = \left(\frac{(2 - k^{\circ})^2 m_e^2 - 4\,u^2}{m_e^2\,|\vec{k}|^2}\right)^{\frac{1}{2}} \ ,$$

whereas in part 2 :

$$y = y_2 = y_+ \ , \ u_{min} = m_e^2 \ , \ u_{max} = u' \ , \ -1 \leqslant \cos\tilde{\Theta} \leqslant -c'_a \ . \qquad (3.38)$$

$$d\sigma_{be} = d\sigma_{be_1} + d\sigma_{be_2},$$

$$d\sigma_{be_i} = \frac{\alpha^4}{256\,\pi^4 E_b^2}\,|M_{be}|^2\,\frac{|\vec{x}|\,|\vec{y}_i|}{|4 - 2x + 2|\vec{x}|\,y_i\cos\tilde{\Theta} / |\vec{y}_i||}\left(1 - \frac{4\,m_\mu^2}{W^2}\right)^{\frac{1}{2}}$$
$$d\vec{\Omega}_\mu\, d\vec{\Omega}_+\, d\vec{\Omega}_k\, dk^{\circ}\, dW^2. \qquad (3.39)$$

Just like in the multiperipheral case we choose the approximation of $|M_{be}|^2$ to be proportional to the product of the four propagators which occur in subset S_{be}. The remaining approximations which are needed to integrate t approximate differential cross section analytically, yield for phase-space part i a weight which we write again symbolically as V_{bi}. Consequently the

approximate differential cross section used, equals :

$$d\tilde{\sigma}_{be} = d\tilde{\sigma}_{be_1} + d\tilde{\sigma}_{be_2} ,$$

$$d\tilde{\sigma}_{be_i} = \frac{\alpha^4}{256\,\pi^4 E_b^2} \frac{512\,|\vec{k}|\,|\vec{y}_i|}{W^2 t_2 \Delta_3 \Delta_4 \tilde{V}_{bi} |4 - 2k^o + 2|\vec{k}|\, y_i \cos\tilde{\Theta} / |\vec{y}_1||} \left(1 - \frac{4m_\mu^2}{W^2}\right)^{\frac{1}{2}}$$
$$d\vec{\Omega}_\mu d\vec{\Omega}_+ d\vec{\Omega}_k dk^o dW^2 . \qquad (3.40)$$

If we do not apply cuts that distinguish the electron from the positron, both particles play symmetric roles. Therefore we choose the approximation for subset S_{bp} identical to the one derived above for S_{be} , only with the roles of the electron and the positron interchanged. Thus the approximate differential cross section corresponding to S_{bp} reads :

$$d\tilde{\sigma}_{bp} = d\tilde{\sigma}_{bp_1} + d\tilde{\sigma}_{bp_2} ,$$

$$d\tilde{\sigma}_{bp_i} = \frac{\alpha^4}{256\,\pi^4 E_b^2} \frac{512\,|\vec{k}|\,|\vec{x}_i|}{W^2 t_1 \Delta_5 \Delta_6 \tilde{V}_{bi} |4 - 2k^o + 2|\vec{k}|\, x_i \cos\Theta' / |\vec{x}_1||} \left(1 - \frac{4m_\mu^2}{W^2}\right)^{\frac{1}{2}}$$
$$d\vec{\Omega}_\mu d\vec{\Omega}_- d\vec{\Omega}_k dk^o dW^2 . \qquad (3.41)$$

Here Θ' is the angle between $\vec{k}$ and $\vec{q}_-$, x_i is defined in a way completely similar to the y_i definition in eq. (3.38). As a consequence there are now two independent divisions of phase-space into two parts : one division is needed to distinguish y_1 from y_2, the other is needed to define x_1 and x_2. The $\tilde{V}_{bi}$ weight can be obtained from the corresponding W_i weight by changing : $\vec{q}_- \to \vec{q}_+$, $q_-^o \to q_+^o$, $\vec{k} \to -\vec{k}$. The complete approximate differential cross section corresponding to the bremsstrahlung subgroup now equals :

$$d\tilde{\sigma}_b = d\tilde{\sigma}_{be} + d\tilde{\sigma}_{bp} . \qquad (3.42)$$

Notice that we can generate events according to $d\tilde{\sigma}_b$ in the following way. We first generate events according to $d\tilde{\sigma}_{be}$. Next we apply to 50 % of the generated events the following symmetrization procedure : $\vec{q}_+ \to -\vec{q}_-$, $q_+^o \to q_-^o$, $\vec{k}_+ \to -\vec{k}_+$, $\vec{k}_- \to -\vec{k}_-$. This observation simplifies the structure of the subgenerator considerably.

6. The conversion subgenerator

This subgenerator is most easily designed because only two Feynman diagrams have to be taken into account and no phase-space division is necessary. The exact differential cross section reads :

$$d\sigma_c = \frac{\alpha^4}{4096\,\pi^4 E_b^2} |M_c|^2 \left((1 - \frac{4m_e^2}{s_1})(1 - \frac{4m_\mu^2}{W^2})\right)^{\frac{1}{2}} |\vec{k}|\, d\vec{\Omega}_e d\vec{\Omega}_\mu d\vec{\Omega}_k ds_1 dW^2,$$

$$k^\circ = \tfrac{1}{2}(4 + W^2 - s_1)\ ,\ |\vec{k}| = \tfrac{1}{2}\lambda^{\frac{1}{2}}(4, W^2, s_1)\ ,\ \lambda(x,y,z) = (x - y - z)^2 - 4yz\ ,$$

$d\vec{\Omega}_e$: the angles of $\vec{q}_-$ in the CM frame of $q = q_+ + q_-$, $s_1 = q^2$. (3.43)

As usual we choose for $|M_c|^2$ an approximation proportional to the product of the four contributing propagators. Next we can integrate over all angles. The remaining integrations over s_1 and W^2 are performed after one more approximation which yields a weight V_c. Thus the used approximation reads :

$$d\tilde{\sigma}_c = \frac{\alpha^4}{4096\,\pi^4 E_b^2} \frac{32}{W^2 s_1 \Delta_7 \Delta_8 V_c} \left((1 - \frac{4m_e^2}{s_1})(1 - \frac{4m_\mu^2}{W^2})\right)^{\frac{1}{2}} |\vec{k}|\, d\vec{\Omega}_e d\vec{\Omega}_\mu d\vec{\Omega}_k ds_1 dW^2,$$

$$\Delta_7 = (p_+ - q_+ - q_-)^2 - m_e^2\ ,\ \Delta_8 = (p_+ - k_+ - k_-)^2 - m_e^2. \qquad (3.44)$$

7. The annihilation subgenerator

The exact differential cross section corresponding to the annihilation subgroup reads :

$$d\sigma_a = \frac{\alpha^4}{128\,\pi^4 E_b^2} |M_a|^2\, \delta^4(p_+ + p_- - q_+ - q_- - k_+ - k_-) \frac{d^3\vec{q}_+}{q_+^\circ} \frac{d^3\vec{q}_-}{q_-^\circ} \frac{d^3\vec{k}_+}{k_+^\circ} \frac{d^3\vec{k}_-}{k_-^\circ},$$

$$|M_a|^2 = |M_{aq}|^2 + |M_{ak}|^2 + I(-k_+, k_-, -q_-, q_+, -p_+, -p_-)\ . \qquad (3.45)$$

We now follow the same procedure as in sect. 5, that is, for both subset S_{aq} and S_{ak} we construct a separate but similar approximate differential cross section. To this end we first consider S_{aq} and write its differential cross section as follows :

$$d\sigma_{ak} = \frac{\alpha^4}{512\,\pi^4 E_b^2} \left|M_{ak}\right|^2 \left(1 - \frac{4\,m_\mu^2}{W^2}\right)^{\frac{1}{2}} d\vec{\Omega}_\mu d\vec{\Omega}_- d\phi_+ dy\, dx\, dW^2. \qquad (3.46)$$

Notice that, because of the elimination of $\cos\Theta_+$ no phase-space division is needed. The eliminated $\cos\Theta_+$ equals :

$$\cos\Theta_+ = \frac{4 - 4\,x - 4\,y + 2\,m_e^2 - W^2 + 2\,x\,y}{2\,|\vec{x}|\,|\vec{y}|}\,. \qquad (3.47)$$

Proceeding in the same way as in the previous three sections we write the approximation as follows :

$$d\tilde{\sigma}_{ak} = \frac{\alpha^4}{512\,\pi^4 E_b^2} \frac{32}{W^2 s\,\Delta_{11}\Delta_{12} V_a} \left(1 - \frac{4\,m_\mu^2}{W^2}\right)^{\frac{1}{2}} d\vec{\Omega}_\mu d\vec{\Omega}_- d\phi_+ dy\, dx\, dW^2,$$

$$\Delta_{11} = (p_+ + p_- - q_-)^2 - m_e^2\,, \quad \Delta_{12} = (p_+ + p_- - q_+)^2 - m_e^2. \qquad (3.48)$$

Here V_a stands for the weight which corresponds to the remaining approximations needed. The approximation for subset S_{aq} is obtained by interchanging the four-momenta in the following way : $q_+ \leftrightarrow k_+$, $q_- \leftrightarrow k_-$.

$$d\tilde{\sigma}_{aq} = \frac{\alpha^4}{512\,\pi^4 E_b^2} \frac{32}{s_1 s\,\Delta_9\Delta_{10}\tilde{V}_a} \left(1 - \frac{4\,m_e^2}{s_1}\right)^{\frac{1}{2}} d\vec{\Omega}_e d\vec{\Omega}_\mu d\phi_\mu d\phi_+ dk_+^\circ dk_-^\circ ds_1\,,$$

$$\Delta_9 = (p_+ + p_- - k_-)^2 - m_\mu^2\,, \quad \Delta_{10} = (p_+ + p_- - k_+)^2 - m_\mu^2\,. \qquad (3.49)$$

The complete approximation for the annihilation subgroup now equals :

$$d\tilde{\sigma}_a = d\tilde{\sigma}_{ak} + d\tilde{\sigma}_{aq}. \qquad (3.50)$$

Events are generated according to this distribution by the use of the superposition principle. Since the integration variables used in $d\tilde{\sigma}_{ak}$ and $d\tilde{\sigma}_{aq}$ have no variable in common, it is no longer possible to apply a cut to the events by a restriction of the boundaries of the corresponding integration variable. Instead we must first generate the events in the complete phase-space. Subsequently we may impose cuts by throwing away those events (that is, putting their weight equal to 0) that do not satisfy these cuts.

8. The complete lowest order cross section

In the preceding sections we discussed the four subgenerators. Now we shall show how the exact cross section corresponding to all Feynman graphs contributing in lowest order can be calculated and which weights have to be assigned to the events generated by the four subgenerators. The exact differential cross section reads :

$$d\sigma = \frac{\alpha^4}{128\,\pi^4 E_b^2} |M|^2\, \delta^4(p_+ + p_- - q_+ - q_- - k_+ - k_-)\, \frac{d^3\vec{q}_+ d^3\vec{q}_- d^3\vec{k}_+ d^3\vec{k}_-}{q_+^o\, q_-^o\, k_+^o\, k_-^o} \,. \quad (3.51)$$

Here $|M|^2$ stands for the complete matrix element squared which was calculated in sect. 2. The exact cross section can now be obtained by the use of :

$$\sigma = \sum_{i\,=\,m,b,c,a} \frac{N_i}{N} \left\langle \frac{d\sigma}{d\sigma'} \right\rangle_{\alpha_i \beta_i d\tilde{\sigma}_i} \left\langle \frac{d\sigma_i}{\beta_i d\tilde{\sigma}_i} \right\rangle_{\tilde{\sigma}} ,$$

$$d\sigma' = \sum_{i\,=\,m,b,c,a} \alpha_i d\sigma_i \quad , \quad \tilde{\sigma} = \sum_{i\,=\,m,b,c,a} \alpha_i \beta_i \tilde{\sigma}_i \quad ,$$

$$\frac{N_i}{N} = \frac{\alpha_i \beta_i \tilde{\sigma}_i}{\tilde{\sigma}} \quad , \quad \tilde{\sigma}_i = \int d\tilde{\sigma}_i \;\; (i = m,b,c,a) \,. \quad (3.52)$$

Alternatively, one may use :

$$\sigma = \left\langle \frac{d\sigma}{d\sigma'} \right\rangle_{d\sigma'} \sigma' \quad , \quad \sigma' = \sum_{i\,=\,m,b,c,a} \alpha_i \sigma_i \quad ,$$

$$\sigma_i = \int d\sigma_i \quad (i = m,b,c,a) \quad (3.53)$$

$$\sigma' = \sum_{i\,=\,m,b,c,a} \frac{N_i}{N} \left\langle \frac{d\sigma_i}{\beta_i d\tilde{\sigma}_i} \right\rangle_{\alpha_i \beta_i d\tilde{\sigma}_i} \tilde{\sigma} \,. \quad (3.54)$$

α_i and β_i ($i = m, b, c, a$) are arbitrary numbers (α_i not all equal to 0, $\beta_i \neq 0$).

Just like in chapter II the bracket notation $\langle f(x) \rangle_{g(x)}$ stands for the average of $f(x)$ calculated with events x distributed according to $g(x)$. In principle we obtain the cross section by calculating the four averages in eqs.

(3.52) and (3.54) independently. However since we want not only to calculate the cross section but also produce unweighted events, that is, events distributed according to $d\sigma$, we have to call on each subgenerator with label i (i = m,b,c or a) with a probability equal to $\alpha_i \beta_i \tilde{\sigma}_i / \tilde{\sigma}$. Thus we generate events according to $\Sigma \alpha_j \beta_j d\tilde{\sigma}_j$ (the summation index j runs over the labels of the four subgenerators) and N_i can be interpreted as the average number of events generated by subgenerator i. As a consequence, when using eq. (3.52), we can assign to each event generated by subgenerator with the label i the weight :

$$\frac{d\sigma}{d\sigma'} \frac{d\sigma_i}{\beta_i d\tilde{\sigma}_i} .$$

Calculation of the average of this weight for all events generated, yields after multiplication with $\tilde{\sigma}$ the exact cross section σ . Unweighted events are produced after the application of a rejection algorithm.

When eq. (3.54) is used we first generate events according to $d\sigma'$. To this end we assign to the events generated by the subgenerator with label i the weight $d\sigma_i / (\beta_i d\tilde{\sigma}_i)$ and apply a rejection algorithm. Multiplying the average of the weights of all events with $\tilde{\sigma}$, we find the cross section σ'. We proceed with the events that survive the rejection algorithm. These events are assigned a weight equal to $d\sigma / d\sigma'$ which takes into account the interferences between the various groups of Feynman graphs. The cross section σ is given by eq. (3.53). Finally, unweighted events are obtained by the approximation of yet another rejection algorithm.

When we do not apply severe cuts to our data and can afford to throw some events away in the middle of the calculation, it is often worthwhile using the second method because the calculation of the second weight (in eq. (3.53)) takes a considerable amount of computing time. However, when a lot of cuts are imposed, we loose to much statistical accuracy this way and should therefore rely on the first method.

The arbitrary parameters α_i and β_i enable us to tune the 'strengths' of the four subgenerators in order to obtain the best possible efficiency of the event generator. For example, if we suspect that the cuts favor the annihilation group and that the other diagrams can be treated as corrections, only the annihilation subgenerator can be used by the specification $\alpha_m = \alpha_b = \alpha_c = 0$. The effect of the other groups is accounted for by their presence in the event weight. Of course, as the contributions of the other diagrams grow

bigger, the fluctuations in the weight of the events will increase accordingly.

Until now we considered the process $e^+e^- \to e^+e^-\mu^+\mu^-$. When we simulate $e^+e^- \to e^+e^+e^-e^-$ or $e^+e^- \to \mu^+\mu^+\mu^-\mu^-$, we apply a symmetrization procedure, as was already announced in sect. 3. The cross section is now calculated in the following way :

1) Replace in eqs. (3.54-56) the exact differential cross section corresponding to each group by the sum of exact differential cross sections corresponding to the contributing subgroups.
2) Multiply the approximate total cross section of each group with the number of contributing subgroups and insert a factor $\frac{1}{4}$ to take into account the indistinguishability of the final state particle.
3) Apply the following symmetrization procedure to the generated events :

$$0 \leq \eta < \frac{1}{4} : q_+ \to k_+ \ , \quad \frac{1}{4} \leq \eta < \frac{1}{2} : q_+ \to k_+ \ , \ q_- \to k_- \ ,$$

$$\frac{1}{2} \leq \eta < \frac{3}{4} : q_- \to k_- \ , \quad \frac{3}{4} \leq \eta < 1 : \text{no interchange.}$$

References

1. M. Pohl, Proceedings of the 5th Intern. Workshop on Photon-Photon Collisions, Aachen, ed. Ch. Berger, Lectures Notes in Physics Vol. 191, Springer Verlag (1983).
2. CELLO Coll., H.-J. Behrend et al., DESY report 103 (1984).
3. CELLO Coll., H.-J. Behrend et al., Phys. Lett. 141B (1984) 145.
4. S. Yamada private communication.
5. R. Kleiss, Nucl. Phys. B241 (1984) 61.
6. R. Bhattacharya, J. Smith and G. Grammer Jr., Phys. Rev. D15 (1977) 3267.
7. F. Gutbrod and Z. Rek, Z. Physik C 1 (1979) 171.
8. A. C. Hearn, REDUCE 2, User's manual, Univ. of Utah (1973).
9. F.A. Berends, P.H. Daverveldt and R. Kleiss, Program Write-Up (submitted to Comp. Phys. Comm.)

CHAPTER IV

RADIATIVE CORRECTIONS

1. Introduction

In the previous chapter we considered all Feynman diagrams contributing in lowest order. Thus we calculated corrections to the multiperipheral treatment of two-photon processes, as described in chapter II. In this chapter we shall continue our study of corrections to the multiperipheral treatment and calculate the so-called radiative corrections to the two multiperipheral diagrams which describe in lowest order the process :

$$e^+(p_+)\ e^-(p_-) \to e^+(q_+)\ e^-(q_-)\ \mu^+(k_+)\ \mu^-(k_-)\ . \qquad (4.1)$$

This involves not only the $ee\mu\mu$ state but also the reaction :

$$e^+(p_+)\ e^-(p_-) \to e^+(q_+)\ e^-(q_-)\ \mu^+(k_+)\ \mu^-(k_-)\ \gamma\ (k)\ . \qquad (4.2)$$

Since these corrections involve an extra power of α, but usually no large logarithms such as $\ln(s / m_e^2)$, their effect on the total cross section is expected to be on the percent level. However, the corrections may increase under stricter cuts (e.g. in the single- or double-tagging case). Several such calculations have already been made. In refs. [1,2] the corrections to the process (4.1), as given by the Feynman diagrams of fig. 8^a-8^f were calculated in the Weizsäcker-Williams approximation. Secondly, some calculations have been performed for the case where in eqs. (4.1) and (4.2) the $\mu\mu$ system is replaced by a (pseudo) scalar particle, such as in $e^+e^- \to e^+e^-\pi^0$, $e^+e^- \to e^+e^-\eta'$ [3,4]. These results are not suited to describe the corrections to (4.1) because the $\mu\mu$ system has more degrees of freedom. Moreover these calculations cannot be translated easily into an event generator.

In this chapter we present a calculation of the process (4.1) and (4.2) to order α^5. The corrections we take into account are those of figs. 8^a-8^f. Of course many other corrections can play a role in this order, such as those given by diagrams like the ones in fig. 9. We leave them out of consideration. The diagrams with five-point functions have recently been shown to contribute very little to the correction [5,6]. As for the diagrams with three vertices on the muon line, there have not been given arguments why their contribution should be small. However since these diagrams give the muons in a different C-conjugation state than those of fig. 8, their interference will vanish in any

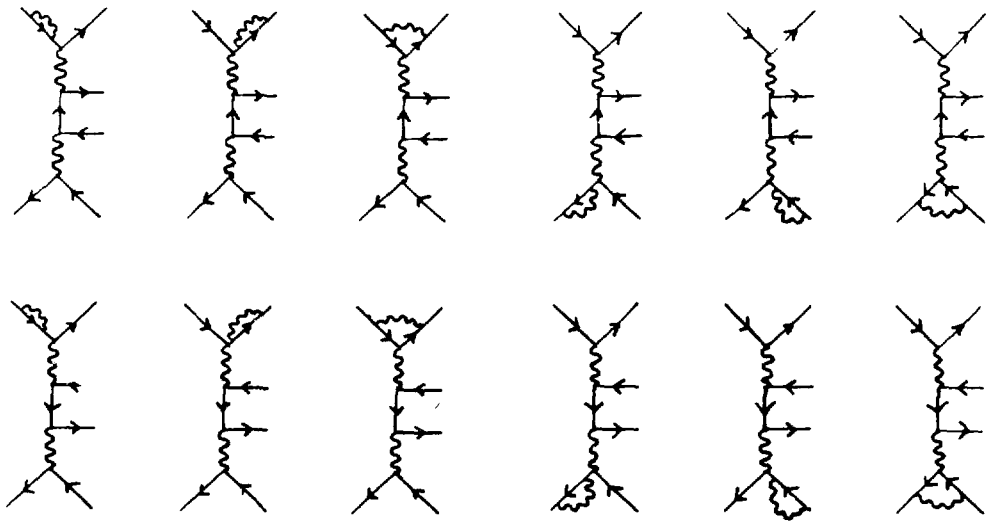

fig. 8^a

fig. 8^d

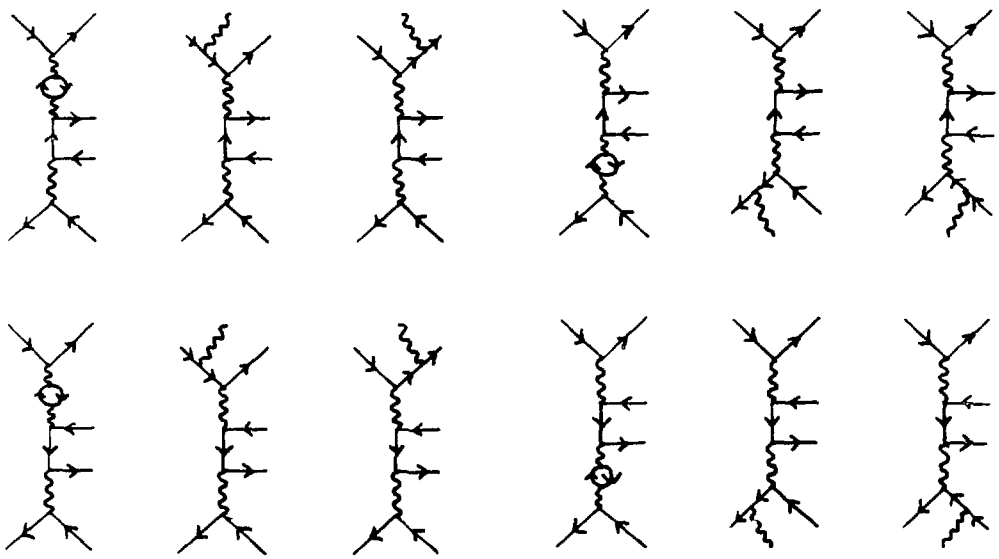

fig. 8^b

fig. 8^c

fig. 8^e

fig. 8^f

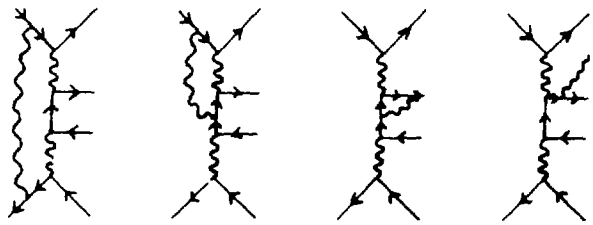

fig. 9

quantity that is defined in a C-symmetric way, such as the total cross section. Graphs with four vertices on the muon lines have been calculated - ref.[7] for the case of QCD.

The final goal of the calculation is not exclusively to provide numbers for total or differential cross sections, but rather to obtain algorithms for a simultaneous Monte Carlo simulation of the processes (4.1) and (4.2), similar to those described in refs. [8,9]. This poses some restrictions : in particular the cross section must be positive at every point in phase-space, and therefore one has to be very cautious not to get infrared divergent cancellations that give a finite but negative result for a cross section with very soft photon emission.

The outline of this chapter is as follows. In sect.2 we discuss the cross section for the process (4.1) and the corrections to it from figs. 8^a,8^b, 8^d,8^e. These are infrared divergent, and must be compensated by contributions from the bremsstrahlung (figs. 8^c,8^f) where the bremsstrahlung photon becomes very soft. In sect.3 we discuss the hard bremsstrahlung contribution. Special attention is given to the distinction between hard and soft bremsstrahlung, which turns out to be more complicated than in one-photon processes due to the multiperipheral character of the scattering. Finally, in sect. 4 we describe the radiative event generator.

2. Soft corrections

In this section we shall consider the virtual and soft photon corrections corresponding to the Feynman diagrams drawn in fig. 8^a-9^f. Since under phase-space cuts which are symmetrical with respect to e^+,e^- the contribution of the

graphs 8^d-8^f equals the contribution of graphs 8^a-8^c we only have to calculate the corrections to the electron vertex. We therefore only consider graphs 8^a-8^c. Then, the total correction to the cross section is obtained by multiplying this correction by 2. Also in the Monte Carlo simulation program events generated according to graphs 8^a-8^c will have to be symmetrized by interchanging $e^+ \leftrightarrow e^-$ in 50% of all the generated events, that is, changing the four-momenta in the following way : $\vec{p}_+ \to -\vec{p}_-$, $\vec{q}_+ \to -\vec{q}_-$, $q_+^o \leftrightarrow q_-^o$, $\vec{k}_+ \to -\vec{k}_+$, $\vec{k}_- \to -\vec{k}_-$, $\vec{k} \to -\vec{k}$.

As we have seen in sect. 3 of the previous chapter the lowest order multiperipheral differential cross section for process (4.1) is given by the following expression :

$$d\sigma = \frac{\alpha^4}{128\,\pi^4 E_b^2} L_0^{\mu\nu}(p_-,q_-)\, H_{\mu\nu}(p_+,q_+,k_+,k_-)$$
$$\delta^4(p_+ + p_- - q_+ - q_- - k_+ - k_-)\ \frac{d^3\vec{q}_+}{q_+^o}\frac{d^3\vec{q}_-}{q_-^o}\frac{d^3\vec{k}_+}{k_+^o}\frac{d^3\vec{k}_-}{k_-^o} \qquad (4.3)$$

Performing the contractions over μ and ν, we find the multiperipheral matrix element squared as it is written in eq. (3.26). Since the radiative corrections we are about to discuss, corresponding to graphs 8^a-8^c, will only enter in the expression for $L_0^{\mu\nu}$, it is convenient to keep $L_0^{\mu\nu}$ apart from $H_{\mu\nu}$. Therefore we list separately the contractions between $\varepsilon_1^\mu \varepsilon_1^\nu$ and $H_{\mu\nu}$ and the contractions between $g^{\mu\nu}$ and $H_{\mu\nu}$ in appendix F.

We shall now consider the various radiative corrections to the electron vertex. First of all we consider the vertex corrections and the electron self-energy resulting from the Feynman diagrams drawn in fig. 8^a. Omitting terms proportional to Q^μ because of current conservation, that is $Q^\mu H_{\mu\nu} = 0$, we write the modified $L_0^{\mu\nu}$ as follows :

$$L_{vc}^{\mu\nu} = (\tfrac{1}{2} + 2\,\mathrm{Re}\,F_1)\, L_0^{\mu\nu} + 2\,\mathrm{Re}\,F_2\, Q^2 g^{\mu\nu} \quad *, \qquad (4.4)$$

$$\mathrm{Re}\,F_1 = -\frac{\alpha}{\pi}\Big\{ 1 + \frac{1+2a^2}{4a}\ln\Big(\frac{a-1}{a+1}\Big) + \frac{1+a^2}{2a}\Big[-\mathrm{Li}_2\Big(\frac{1-a}{1+a}\Big) + \tfrac{1}{4}\ln^2\Big(\frac{a-1}{a+1}\Big) - \ln\Big(\frac{a-1}{a+1}\Big)\ln\Big(\frac{2a}{a+1}\Big) - \frac{\pi^2}{12}\Big] + \ln\Big(\frac{\lambda}{m_e}\Big)\Big(1 + \frac{1+a^2}{2a}\ln\Big(\frac{a-1}{a+1}\Big)\Big)\Big\},$$

* We would like to point out that the factor $\frac{1}{2}$ is necessitated by the symmetrization procedure used in our approach.

$$\text{Re } F_2 = \frac{\alpha}{\pi} \frac{1-a^2}{4a} \ln\left(\frac{a-1}{a+1}\right) ,$$

$$a = \left(1 - \frac{4\pi^2}{Q^2} \right)^{\frac{1}{2}} , \quad Q^\mu = p_-^\mu - q_-^\mu , \quad Li_2(x) = - \int_0^x \frac{\ln(1-t)}{t} dt . \qquad (4.5)$$

Here a small fictitious photon mass, λ , has been introduced to regulate the infrared divergence. These formulae are already well known in the literature [e.g. 10]. The infrared divergence occurring in Re F_1 will be cancelled according to the Bloch-Nordsieck theorem [11,12] by a similar divergence resulting from soft photon emission. The corresponding bremsstrahlung graphs are depicted in fig. 8c. Now for soft photons i.e. photons with sufficiently small energy the electron tensor $L_{sb}^{\mu\nu}$ again factorizes into the lowest order tensor $L_0^{\mu\nu}$ and an infrared divergent part :

$$L_{sb}^{\mu\nu} = - \frac{\alpha}{4\pi^2} \int_{k^o < k_s} \left(\frac{m_e^2}{p_-.k^2} + \frac{m_e^2}{q_-.k^2} - \frac{2\, p_-.q_-}{p_-.k\; q_-.k} \right) \frac{d^3\vec{k}}{k^o} L_0^{\mu\nu} . \qquad (4.6)$$

Performing the integration over the momentum of the soft photon which is not detected in the final state, we find the following result [13] :

$$L_{sb}^{\mu\nu} = \delta_s \, L_0^{\mu\nu} ,$$

$$\delta_s = \frac{\alpha}{\pi} \left\{ -2 \ln\left(\frac{2k_s}{\lambda}\right) \left(1 + \frac{a^2+1}{2a} \ln\left(\frac{a-1}{a+1}\right)\right) + \right.$$

$$\frac{1}{2} \left(\frac{p_-^o}{|\vec{p}_-|} \ln\left(\frac{p_-^o + |\vec{p}_-|}{p_-^o - |\vec{p}_-|}\right) + \frac{q_-^o}{|\vec{q}_-|} \ln\left(\frac{q_-^o + |\vec{q}_-|}{q_-^o - |\vec{q}_-|}\right) \right) -$$

$$\frac{1}{2} \frac{a^2+1}{a} \left[\frac{1}{2} \ln^2\left(\frac{u^o - |\vec{u}|}{u^o + |\vec{u}|}\right) + Li_2\left(\frac{v + u^o - |\vec{u}|}{v}\right) + \right.$$

$$\left. \left. Li_2\left(\frac{v + u^o + |\vec{u}|}{v}\right) \right]_{u=q_-}^{u=\gamma p_-} \right\} ,$$

$$\gamma = \frac{a-1}{a+1} \quad , \quad v = - \frac{(\gamma^2 - 1)\, m_e^2}{2\,(\gamma p_-^o - q_-^o)} . \qquad (4.7)$$

We notice that the sum of $L_{vc}^{\mu\nu}$ and $L_{sb}^{\mu\nu}$ is indeed finite. The last virtual correction we take into account is the vacuum polarization which modifies the photon propagator.

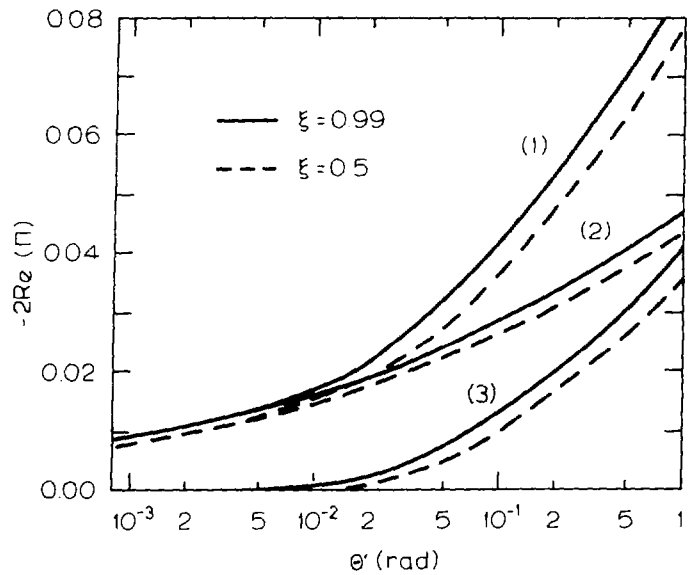

fig. 10

Vacuum polarization correction as a function of the scattering angle of the electron Θ' ($\xi = q^0/p^0$).

(1) Sum of leptonic and hadronic vacuum polarizations.

(2) Leptonic vacuum polarization.

(3) Hadronic vacuum polarization.

The corresponding Feynman diagram is drawn in fig. 8[b]. The effect of this diagram is the following change in $L_0^{\mu\nu}$:

$$L_{vp}^{\mu\nu} = -2\ \mathrm{Re}\ (\Pi)\ L_0^{\mu\nu},$$

$$\mathrm{Re}(\Pi) = \sum_{i=e,\mu,\tau} \frac{\alpha}{\pi}\left\{ \frac{8}{9} - \frac{1}{3}a_i^2 + a_i\left(\frac{1}{2} - \frac{1}{6}a_i^2\right) \ln\left(\frac{a_i - 1}{a_i + 1}\right) \right\} +$$

$$\frac{\alpha}{3\pi} P \int_{4m_\pi^2}^{\infty} R(s')\left(\frac{1}{s'-s} - \frac{1}{s'}\right) ds',$$

$$a_i = \left(1 - \frac{4m_i^2}{Q^2}\right)^{\frac{1}{2}}. \qquad (4.8)$$

Here we calculated the hadronic part of Π from the energy-dependence of R by

means of a dispersion principle value integral [14,15].* In fig. 10 the dependence of $-2\ \mathrm{Re}\ (\Pi)$ on the energy of the scattered beam particle $\xi = q_-^o / p_-^o$ and its scattering angle Θ' is depicted at a fixed beam energy of 20 GeV. Combining now all the corrections we find the following result for the soft differential cross section :

$$d\sigma = \frac{\alpha^4}{128\,\pi^4 E_b^2} L_s^{\mu\nu}(p_-,q_-)\ H_{\mu\nu}(p_+,q_+,k_+,k_-)$$
$$\delta^4(p_+ + p_- - q_+ - q_- - k_+ - k_-)\ \frac{d^3\vec{q}_+}{q_+^o}\ \frac{d^3\vec{q}_-}{q_-^o}\ \frac{d^3\vec{k}_+}{k_+^o}\ \frac{d^3\vec{k}_-}{k_-^o}\ ,$$

$$L_s^{\mu\nu} = (\tfrac{1}{2} + 2\ \mathrm{Re}\ F_1 + \delta_s - 2\ \mathrm{Re}\ \Pi)\ L_0^{\mu\nu} + 2\ \mathrm{Re}\ F_2\ Q^2 g^{\mu\nu}. \qquad (4.9)$$

3. Hard bremsstrahlung

In this section we consider hard bremsstrahlung. In this case the emitted photon is so energetic that in principle it can be detected. The differential cross section for process (4.2) is described by the Feynman diagrams of fig. 8c and can be written as follows :

$$d\sigma = \frac{\alpha^5}{512\,\pi^6 E_b^2} L_{hb}^{\mu\nu}(p_-,q_-,k)\ H_{\mu\nu}(p_+,q_+,k_+,k_-)$$
$$\delta^4(p_+ + p_- - q_+ - q_- - k_+ - k_- - k)\ \frac{d^3\vec{q}_+}{q_+^o}\ \frac{d^3\vec{q}_-}{q_-^o}\ \frac{d^3\vec{k}_+}{k_+^o}\ \frac{d^3\vec{k}_-}{k_-^o}\ \frac{d^3\vec{k}}{k^o}\ . \qquad (4.10)$$

Here $L_{hb}^{\mu\nu}$ stands for the electron tensor now modified by the bremsstrahlung. Calculation of $L_{hb}^{\mu\nu}$ using current conservation yields :

$$L_{hb}^{\mu\nu} = - c_1 \tilde{p}_-^{\mu}\tilde{p}_-^{\nu} - c_2 \tilde{q}_-^{\mu}\tilde{q}_-^{\nu} - c_3 \tilde{k}^{\mu}\tilde{k}^{\nu} - c_4 g^{\mu\nu} Q^2,$$

$$c_1 = \frac{4\,m_e^2}{q_-.k^2} + \frac{2\,Q^2 - 4\,m_e^2}{p_-.k\ q_-.k}\ ,\quad c_2 = \frac{4\,m_e^2}{p_-.k^2} + \frac{2\,Q^2 - 4\,m_e^2}{p_-.k\ q_-.k}\ ,\quad c_3 = \frac{4\,m_e^2}{p_-.k\ q_-.k}\ ,$$

$$c_4 = \{4\,m_e^2[\,Q^2 - 2\,m_e^2 - 2\,q_-.k + 2\,p_-.k\,] - Q^2[\,4\,m_e^2 - Q^2 + 2\,q_-.k - 2\,p_-.k\,] +$$

* It turns out to be simplest to calculate a table of the vacuum polarization only once for a q^2 range, and then use numerical interpolation or a simple parametrization of this table in the program.

$$2\,(p_-.k^2 + q_-.k^2) + 2\,m_e^2\Big[\,4\,m_e^2 - Q^2 + 2\,q_-.k - 2\,p_-.k - \frac{4\,p_-.k\;q_-.k}{Q^2}\Big]$$

$$+\frac{m_e^2(\,2\,q_-.k - Q^2)^2}{Q^4\,q_-.k^2} + \frac{m_e^2(\,2\,p_-.k + Q^2)^2}{Q^4\,p_-.k^2}\,, \qquad (4.$$

$$\tilde{p}_-^\mu = p_-^\mu - \frac{p_-.Q}{Q^2}\,Q^\mu\,,\quad \tilde{q}_-^\mu = q_-^\mu - \frac{q_-.Q}{Q^2}\,Q^\mu\,,\quad \tilde{k}^\mu = k^\mu - \frac{k.Q}{Q^2}\,Q^\mu\,,\quad Q^2 = (p_- - q_- - k)^2.$$

The complete matrix element squared can now be obtained in a straightforward way using the formulae in appendix F. Notice that the coefficients c_1, c_2, c_3 and c_4 are numerically stable : if the emitted photon is collinear with $\vec{p}_-$ and $\vec{q}_-$ so that $p_-.k$ and $q_-.k$ are $O(m_e^2)$ then also Q^2 is $O(m_e^2)$. The contractions of $\tilde{p}_-^\mu\tilde{p}_-^\nu$, $\tilde{q}_-^\mu\tilde{q}_-^\nu$ and $\tilde{k}^\mu\tilde{k}^\nu$ with $H_{\mu\nu}$ can be made stable in the same way as we ensured stability of the lowest order matrix element squared (see sect. 3 of chapter III). Because the contractions are performed with the complete $H_{\mu\nu}$ tensor we are allowed to choose for each $\tilde{p}_-$, $\tilde{q}_-$ and $\tilde{k}$ a separate z-parameter. Consequently each of these contractions can be made numerically stable without destroying the numerical stability of the other two contractions.

Because we have to separate the soft photon emission (which we defined up to now as radiation of photons with energy smaller than k_s), the most natural way to proceed would be to rewrite the five-particle kinematics in such a way that the energy of the photon occurred explicitly. However looking at eq. (4.10) one sees that it is much more advantageous to express the kinematics in terms of the angles of the photon, in the CM frame of the scattered electron and the photon, and the invariant mass squared of this pair. Thereby we obtain an expression for the differential cross section which shows a great similarity to the expression for the lowest order multiperipheral differential cross section (eq. (4.3)) :

$$d\sigma = \frac{\alpha^5}{2048\,\pi^6 E_b^2}\,L_{hb}^{\rho\sigma}(p_-,q_-,k)\;H_{\rho\sigma}(p_+,q_+,k_+,k_-)$$

$$\delta^4(p_+ + p_- - q_+ - P - k_+ - k_-)\;\frac{\mu^2 - m_e^2}{\mu^2}\,d\vec{\Omega}_\gamma\,\frac{d^3\vec{P}}{P^o}\,\frac{d^3\vec{q}_+}{q_+^o}\,\frac{d^3\vec{k}_+}{k_+^o}\,\frac{d^3\vec{k}_-}{k_-^o}\,d\mu^2,$$

$$P^\mu = q_-^\mu + k^\mu\,,\quad \mu^2 = P^2. \qquad (4.12)$$

This similarity will be exploited in the Monte Carlo event generator. After having generated the μ variable a four-particle final state is generated in a similar way as in the multiperipheral subgenerator, except for one difference :

one of the final state four-momenta has a variable mass μ . The photon four-momentum is generated in the frame where $\vec{P} = \vec{0}$ and then boosted back to the laboratory system.

However this scheme has also a clear disadvantage. The photon energy is no longer an integration variable but can only be calculated after having performed the boost to the laboratory system. Of course this can be remedied by using a new definition for soft photons, namely a definition based upon the mass μ instead of the photon energy. Then soft photons are defined as having a μ value smaller than an arbitrary number μ_o . If we examine the three-momentum space in the laboratory frame we see that the three-momenta of the soft photons now fill up an ellipsoid which peaks strongly in the $\vec{q}_-$ direction. Using the previous definition of soft photons they would of course lie within a sphere with radius k_s. It is worthwhile noticing the big difference in magnitude (at fixed μ) between the photon energies corresponding to parallel and anti-parallel photon three-momenta with respect to $\vec{q}_-$:

$$k^o_{parallel} = \frac{\mu^2 - m_e^2}{2\,(q_-^o - |\vec{q}_-|)} = \frac{\mu^2 - m_e^2}{2\,m_e^2}\,(q_-^o + |\vec{q}_-|) \approx \frac{\mu^2 - m_e^2}{m_e^2}\,q_-^o \,,$$

$$k^o_{antiparallel} = \frac{\mu^2 - m_e^2}{2\,(q_-^o + |\vec{q}_-|)} \,. \qquad (4.13)$$

The choice of μ_o is restricted by the condition that, when $\mu < \mu_o$, k^o should not exceed a value of, say, 1% of the beam energy in order to be still considered as soft. We denote the value of this boundary by k'. Using the above-mentioned k' we are allowed to use the soft photon approximation

$$L^{\mu\nu}_{sb} = -\frac{\alpha}{4\pi^2} \int_{\mu<\mu_o} \left(\frac{m_e^2}{p_-.k^2} + \frac{m_e^2}{q_-.k^2} - \frac{2\,p_-.q_-}{p_-.k\;q_-.k}\right) \frac{d^3\vec{k}}{k^o}\; L_0^{\mu\nu}, \qquad (4.14)$$

within the ellipsoid. Moreover we ensure that photons with an energy $k^o > k'$ will be hard ones and thus explicitly generated in the Monte Carlo program. This choice for k' implies that μ_o will be $O(m_e)$. Consequently the ellipsoid which surrounds the soft photon space is very thin indeed.

The integration over soft photon phase-space ($\mu<\mu_o$) is performed most easily in the rest frame of the scattered electron. It yields :

$$L_{sb}^{\mu\nu} = \frac{\alpha}{\pi}\Big\{ \ln\Big(\frac{\mu_o^2 - m_e^2}{m_e\lambda}\Big)\Big(-2 + \frac{p_-^o}{|\vec{p}_-|}\ln\Big(\frac{p_-^o + |\vec{p}_-|}{p_-^o - |\vec{p}_-|}\Big)\Big) + 1 +$$

$$\frac{p_-^o}{|\vec{p}_-|}\Big[\tfrac{1}{2}\ln\Big(\frac{p_-^o + |\vec{p}_-|}{p_-^o - |\vec{p}_-|}\Big) - \tfrac{1}{2}\ln\Big(\frac{p_-^o + |\vec{p}_-|}{p_-^o - |\vec{p}_-|}\Big)\ln\Big(\frac{4\, p_-^o p_-^o}{m_e^2}\Big) + \frac{\pi^2}{12} -$$

$$-\tfrac{1}{2}\ln\Big(\frac{p_-^o - |\vec{p}_-|}{2\, p_-^o}\Big)\ln\Big(\frac{p_-^o + |\vec{p}_-|}{2\, p_-^o}\Big) - Li_2\Big(\frac{p_-^o - |\vec{p}_-|}{2\, p_-^o}\Big) -$$

$$Li_2\Big(\frac{|\vec{p}_-|}{p_-^o}\Big) + Li_2\Big(-\frac{|\vec{p}_-|}{p_-^o}\Big)\Big]\Big\} L_0^{\mu\nu}. \qquad (4.15)$$

Summing $L_{sb}^{\mu\nu}$ and $L_{vc}^{\mu\nu}$, the infrared divergence drops out as usual. However if we now calculate the cross section corresponding to soft photon radiation it turns out to be negative. This is not a problem if we are only interested in the total cross section corresponding to soft- and hard bremsstrahlung but must be avoided by all means when we want to use the Monte Carlo program as an event generator because negative cross sections lack a statistical interpretation. The fact that the resulting soft photon cross section is negative can be understood in the following way. First of all we have seen that the soft photon phase-space is very small. Consequently its contribution is not large enough to result into a finite positive cross section after the summation with the virtual cross section. Moreover, looking at the integrand of $L_{sb}^{\mu\nu}$ we notice that the main contribution to it comes from photons going either parallel to $\vec{q}_-$ or to $\vec{p}_-$. Since photons going parallel to $\vec{p}_-$ will only lie within the ellipsoid as long as $\vec{p}_-$ is parallel to $\vec{q}_-$ the contribution of the photons going parallel to $\vec{p}_-$ will often be counted as hard photon radiation in our procedure and thus not help to cancel the negative virtual cross section. In order to obtain a positive soft photon cross section we should therefore enlarge the soft photon phase-space. Tuning μ_o towards bigger values will not be helpful because then we should count very energetic photons going parallel to the scattered electron as soft ones which is not acceptable. A far better way to achieve our goal is to change again our concept of soft photons. We now make the following distinction between hard and soft photons :

soft photons : $k^o < k_s$ or $\mu < \mu_o$

hard photons : $k^o > k_s$ and $\mu > \mu_o$ (4.16)

where k_s and μ_o are in principle arbitrary parameters.

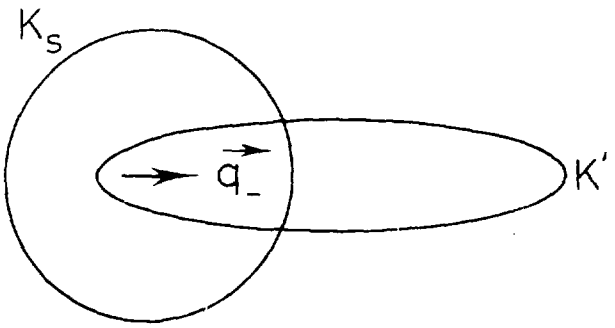

Fig. 11

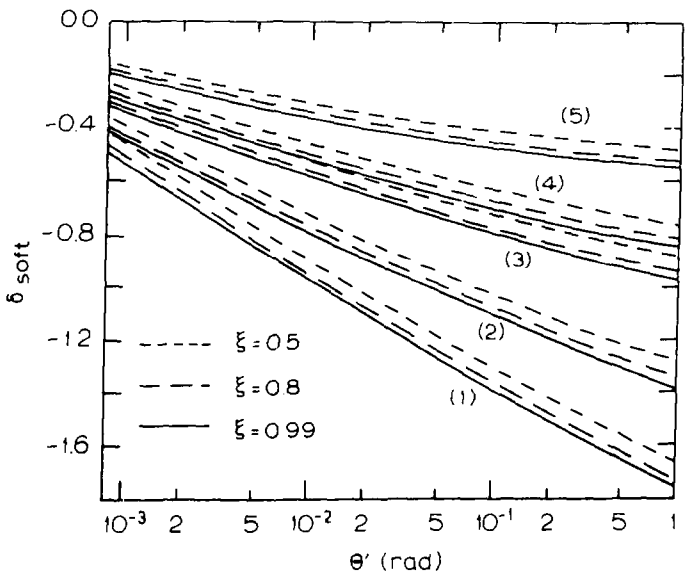

Fig. 12

Total soft correction as a function of the scattering angle of the electron Θ' at various values for ξ and k_s :
(1) $k_s = 0.00001\ E_b$; (2) $k_s = 0.0001\ E_b$; (3) $k_s = 0.001\ E_b$;
(4) $k_s = 0.002\ E_b$; (5) $k_s = 0.01\ E_b$.

So in the three-momentum space of the photon the soft photon phase-space is bounded by a sphere of radius k_s and an ellipsoid corresponding to $\mu = \mu_o$. (fig. 11) The value of μ_o is again chosen such that the maximum energy of soft photons is k'. The soft cross section can now be made positive by a suitable choice for k_s . Notice that only the condition on μ can be handled directly during the hard photon generation because μ is an integration variable. The energy condition $k^o > k_s$ must be put in by hand, that is we have to throw away those generated hard photon events that do not fulfil this condition. This shows that k_s has to be optimized in such a way that, on the one hand, it is large enough to ensure a positive soft photon cross section, but on the other hand small enough in order not to loose too much efficiency by having to throw away a lot of the generated hard photon events. In practice $0.1\ k' < k_s < k'$ works fine. In fig.12 the soft photon correction $2\,(2\ \mathrm{Re}\ F_1 + \delta_{s_1} + \delta_{s_2} - 2\ \mathrm{Re}\ \Pi)$ is depicted as a function of the angle θ' between $\vec{p}_-$ and $\vec{q}_-$ at various values for $\xi = q_-^o / p_-^o$ and k_s (E_b = 20 GeV).

Because of this new definition of soft photons the expression for $L_{sb}^{\mu\nu}$ (eq. 4.6) is modified in the following way :

$$L_{sb}^{\mu\nu} = (\delta_{s_1} + \delta_{s_2})\, L_0^{\mu\nu}$$

$$\delta_{s_1} = -\frac{\alpha}{4\pi^2} \int_{k^o < k_s} \left(\frac{m_e^2}{p_-.k^2} + \frac{m_e^2}{q_-.k^2} - \frac{2\, p_-.q_-}{p_-.k\ q_-.k}\right) \frac{d^3\vec{k}}{k^o} ,$$

$$\delta_{s_2} = -\frac{\alpha}{4\pi^2} \int_{k^o > k_s,\ \mu < \mu_o} \left(\frac{m_e^2}{p_-.k^2} + \frac{m_e^2}{q_-.k^2} - \frac{2\, p_-.q_-}{p_-.k\ q_-.k}\right) \frac{d^3\vec{k}}{k^o} . \qquad (4.17)$$

The first term has already been calculated in sect. 2 (eq. (4.7)). The second term can be obtained by performing first the k^o integration between the boundaries

$$k_s \quad \text{and} \quad k^o_{max}(\cos\theta) = \frac{\mu_o^2 - m_e^2}{2\,(q_-^o - |\vec{q}_-|\cos\theta)} . \qquad (4.18)$$

The angle θ is the angle between $\vec{k}$ and $\vec{q}_-$ in the laboratory system. Next the integration over $\cos\theta$ is performed between the boundaries :

$$A = \max\left(-1, \frac{q_-^o}{|\vec{q}_-|} - \frac{\mu_o^2 - m_e^2}{2\,|\vec{q}_-|\,k_s}\right) \quad \text{and} \quad 1 . \qquad (4.19)$$

Because the infrared divergence is contained within the k_s sphere we may put the photon mass λ equal to 0 during this integration. The complicated calculation results in the following expression :

$$\delta_{s_2} = \frac{\alpha}{2\pi}\left\{ \ln\left(\frac{\mu_o^2 - m_e^2}{2\,|\vec{q}_-|\,k_s}\right)\left[e-1+2(e^2-1)\left(\frac{c\eta_o - e(1-c^2)}{\eta_o^2+\nu}\right)\right] - \right.$$

$$(1-A)\,\frac{e'+1}{e'-A} + \frac{2(ee'-c)}{\Delta}\,\ln\left(\frac{(\Delta+\eta_1-b)^2(\Delta-\eta_o+b)^2}{4\eta_o\eta_1(e'-1)(e'-A)}\right)\Big] -$$

$$(e-1)\,\ln(e'-1) + (e^2-1)\left(\frac{2e(1-c^2)-2\eta_o c}{\eta_o^2+\nu}\right)\ln(e'-A) -$$

$$2e\,\ln\left(\frac{\eta_1}{\eta_o}\right) + (e^2-1)\frac{(e-e'c-c\Delta)}{\Delta(\Delta+b)}\,\ln\left(\frac{2\eta_1(e'-1)}{(\Delta-b+\eta_1)(\Delta+b-\eta_o)}\right) +$$

$$(e^2-1)\frac{(e-e'c+c\Delta)}{\Delta(\Delta-b)}\,\ln\left(\frac{(\Delta-b+\eta_1)(\Delta+b-\eta_o)}{2\eta_o(e'-A)}\right) + (1-A)\frac{(e'+1)}{(e'-A)} -$$

$$\frac{e'^2-1}{e'-A}\,\ln(e'-A) + (e'+1)\,\ln(e'-1) -$$

$$\frac{2(ee'-c)}{\Delta}\left[-\ln^2\left(\frac{\Delta-b+\eta_1}{2(e'-1)}\right) + \tfrac{1}{2}\ln^2\left(2(e'-1)\right) + \ln^2\eta_1 + \right.$$

$$\ln^2\left(\frac{\Delta+b-\eta_o}{\eta_o}\right) - \tfrac{1}{2}\ln^2\left(2(e'-A)\right) - \ln^2\eta_o -$$

$$\ln(\Delta+b)\,\ln\left(\frac{\eta_1}{\eta_o}\right) - \ln\left(\frac{2\eta_1(e'-1)}{(\Delta-b+\eta_1)(\Delta+b-\eta_o)}\right)\ln(4\Delta^2) +$$

$$Li_2\left(\frac{-\nu}{\eta_1(\Delta+b)}\right) - Li_2\left(\frac{-\nu}{\eta_o(\Delta+b)}\right) + Li_2\left(\frac{\eta_1}{\Delta+b}\right) -$$

$$Li_2\left(\frac{\eta_o}{\Delta+b}\right) + 2Li_2\left(\frac{(e'-1)\eta_1}{\Delta(\Delta-b+\eta_1)}\right) - 2Li_2\left(\frac{\Delta+b-\eta_o}{2\Delta}\right) -$$

$$\ln 2 \ln\left(\frac{(\Delta+\eta_1-b)^2(\Delta-\eta_0+b)^2}{4\eta_0\eta_1(e'-1)(e'-A)}\right)] \} , \qquad (4.20)$$

$$e = \frac{p_-^0}{|\vec{p}_-|} , \quad e' = \frac{q_-^0}{|\vec{q}_-|} , \quad c = \cos\theta' ,$$

$$\Delta = \left((ee'-c)^2-(e^2-1)(e'^2-1)\right)^{\frac{1}{2}} , \quad b = e'-ec , \quad \nu = (e^2-1)(1-c^2) ,$$

$$\eta_0 = A-ec+\left((A-e)^2+(2eA-1-c)(1-c)\right)^{\frac{1}{2}} \text{ and } \eta_1 = (e+1)(1-c) . \qquad (4.21)$$

4. The radiative generator

Before closing the discussion of the radiative corrections we want to make a few remarks on the event generator which simulates simultaneously the processes in eqs. (4.1) and (4.2). By now it will no longer be surprising to the reader that events are generated by the use of the superposition principle (see chapter II, sect. 5). In the radiative Monte Carlo program it is first decided at random whether a soft (eq. (4.1)) or a hard (eq. (4.2)) event will be generated. Again the probability for a soft or a hard event to be generated is proportional to the approximate total cross sections corresponding to respectively soft and hard photon radiation. In the former case the event generation takes place in a way similar to the generation of multiperipheral events (see chapter III, sect. 4). The soft radiative corrections enter only in the weights, not in the algorithms. Also the hard photon generation resembles in many respects the multiperipheral subgenerator, as was already mentioned in sect. 3. However, since now it concerns a five-particle final state, three more variables have to be generated namely μ, $\cos\tilde{\theta}$ and $\tilde{\phi}$, where $\tilde{\theta}$ and $\tilde{\phi}$ denote respectively the polar and azimuthal angle of $\vec{k}$ in the CM system of the photon and scattered electron (with the pole axis along the $\vec{p}_-$ direction). Because the dominant contribution in eq. (4.10) originates from terms proportional to $1 / (p_-.k\ q_-.k)$ in eq. (4.11), we expect that algorithms which generate $\tilde{\phi}$ randomly and uniformly in the interval $[0, 2\pi]$ and μ^2 and $\cos\tilde{\theta}$ according to respectively $1 / (\mu^2 - m_e^2)$ and $1 / (p_-^0 - |\vec{p}_-|\cos\tilde{\theta})$ (p_- in the frame where $\vec{P} = \vec{0}$) will result into an acceptable weight distribution.

Since the four-momenta of the photon and the scattered electron are generated in their CM system, it is impossible to control the scattering angle

of the electron in the laboratory frame directly, that is, to make sure that this angle is within a particular angular range. Consequently cuts on this angle can only be dealt with by the application of a rejection algorithm. Therefore the radiative Monte Carlo program runs most efficiently when no-tagging conditions are applied. Detailed information on this generator can be found in ref. [16].

References

1. M. Defrise, S. Ong, J. Silva and C. Carimalo, Phys. Rev. D23 (1981) 663.
2. S. Ong, C. Carimalo and P. Kessler, Phys. Lett. 142B (1984) 429.
3. M. Defrise, Z. Physik C 9 (1981) 41.
4. W.L. van Neerven and J.A.M. Vermaseren, Nucl. Phys. B238 (1984) 73.
5. W.L. van Neerven and J.A.M. Vermaseren, Phys .Lett. 137B (1984) 241.
6. W.L. van Neerven and J.A.M. Vermaseren, NIKHEF Amsterdam preprint (84-2).
7. F.A. Berends, Z. Kunszt and R. Gastmans, Nucl. Phys. B182 (1981) 397.
8. F.A. Berends and R. Kleiss, Nucl. Phys. B177 (1981) 237; Nucl. Phys. B178 (1981) 141; Nucl. Phys. B228 (1983) 537.
9. F.A. Berends, R. Kleiss and S. Jadach, Nucl. Phys. B202 (1982) 63; Comp. Phys. Comm. 29 (1983) 183.
10. F.A. Berends and R. Gastmans in "Electromagnetic Interactions of Hadrons" Vol. 2, eds. A. Donnachie and G. Shaw (Plenum 1978).
11. F. Bloch and A. Nordsieck, Phys. Rev. 52 (1937) 54.
12. D.R. Yennie, S.C. Frautschi and H. Suura, Ann. Phys. 13 (1961) 379.
13. G. 't Hooft and M. Veltman, Nucl. Phys. B153 (1979) 365.
14. F.A. Berends and G. Komen, Phys. Lett. 63B (1976) 432.
15. H. Burkhardt, TASSO note no. 192 (1981) unpublished.
16. F.A. Berends, P.H. Daverveldt and R. Kleiss, Program Write-Up (submitted to Comp. Phys. Comm.).

CHAPTER V

RESULTS

1. Introduction

In this last chapter we present some results which were obtained by the use of the described event generators. Moreover we compare them to the experimental data, whenever available. The Monte Carlo predictions which we shall deal with in the subsequent sections concern total and differential cross sections and charge asymmetries.

Here a few remarks are in order. First of all, it goes without saying that the presented results depend heavily on the chosen cuts. When specifying these cuts we are guided by two considerations. Firstly, the cuts must be experimentally feasible. Secondly we want to impose cuts which favor in some sense those kinematical regions where the corrections due to non-multiperipheral diagrams or to radiation are expected to be large. The case when no cuts at all are applied is also included because it is, although experimentally irrelevant, still of theoretical interest. The second remark concerns the way the results have been obtained. We have acquired most of them using weighted events. It has been sufficient to use only weighted events because we confine ourselves to the study of cross sections and related topics and do not intend to perform detector simulations which indeed require unweighted events. Although all results which will be presented could equally well be obtained by the use of unweighted events, we choose to use weighted ones in view of the computing time needed. Finally we want to remark that we do not include results for final states with a quark pair. The reason for this omission is that we only want to present results for processes which are completely described by the event generators described in this thesis. In order to make sensible comparisons between theory and experiments for processes involving quarks, we must use a Monte Carlo event generator which not only generates final states with a quark pair in a way as is described above but also describes the fragmentation of the quarks into jets. This topic is outside the scope of this work.

The rest of this chapter is organized as follows. In sect. 2 total and visible cross sections are presented for four-lepton production processes. In

sect. 3 we consider the process $e^+e^- \to e^+e^-\mu^+\mu^-$ in the single-tagging case and discuss the muon charge asymmetry and the differential cross section with respect to the Bjorken scaling variable. Next in sect. 4 results concerning the radiative corrections to this same process are given with both no-tagging and single-tagging cuts. Finally, in sect. 5 we present an outlook.

2. Total and visible cross sections for four-lepton final states

In this section we calculate cross sections for e^+e^- scattering into four-lepton final states. Moreover, we give exclusive cross sections for all cases where one or more lepton track is at large angles with respect to the beams. The calculations are performed by the use of the event generators described in chapter III and appendices D and E.

In table 3 the total cross sections for the production of $e^+e^+e^-e^-$, $e^+e^-\mu^+\mu^-$, $\mu^+\mu^+\mu^-\mu^-$ and $\mu^+\mu^-\tau^+\tau^-$ final states are listed for beam energies ranging from 10 GeV to 50 GeV. The table is divided into three parts. In the first part all lowest order QED diagrams are calculated. In the second only the multiperipheral ones are taken into account. In the third the lowest order cross section as predicted by the electro-weak theory is calculated. The total cross section for $e^+e^+e^-e^-$ (and to a lesser extent for $e^+e^-\mu^+\mu^-$) is very large, due to the fact that these final states are predominantly produced by multiperipheral scattering. This implies that the vast majority of the $e^+e^+e^-e^-$ events will be invisible, all the particles being produced at very small angles with respect to the beams.

In order to obtain cross sections for those final states that may be experimentally accessible we proceed as follows. For every Monte Carlo event we determine the number of tracks coming out at an angle (with respect to the e^+e^- beams) larger than some Θ_o, which for actual experiments is usually 20 to 30 degrees. This procedure, which is trivial once an event generator has been constructed, then gives us the 'visible' cross sections for 1,2,3 or 4 tracks. For the case of $e^+e^+e^-e^-$ production we also apply a cut of 1 GeV on the invariant masses of every outgoing e^+e^- combination. This considerably improves the efficiency of the program. A systematic error is now made by rejecting events where one e^+e^- pair with a mass of less than 1 GeV is produced, with one or both tracks at less than Θ_o from the beams. We estimate that this error is less than 1 % of the 2-track visible cross section for

Table 3

final state	beam energy (GeV) 10	17.5	25	50
	contribution of all lowest order QED diagrams in nanobarns			
eeee	$0.920\ 10^{7}$	$1.070\ 10^{7}$	$1.233\ 10^{7}$	$1.459\ 10^{7}$
	$\pm\ 0.011\ 10^{7}$	$\pm\ 0.015\ 10^{7}$	$\pm\ 0.018\ 10^{7}$	$\pm\ 0.025\ 10^{7}$
eeμμ	98.9	131.4	154.0	205.9
	$\pm$ 0.6	$\pm$ 2.2	$\pm$ 0.9	$\pm$ 1.2
μμμμ	$162.2\ 10^{-6}$	$77.3\ 10^{-6}$	$48.7\ 10^{-6}$	$18.06\ 10^{-6}$
	$\pm\ 1.5\ 10^{-6}$	$\pm\ 1.6\ 10^{-6}$	$\pm\ 0.4\ 10^{-6}$	$\pm\ 0.16\ 10^{-6}$
μμττ	$96.8\ 10^{-6}$	$55.2\ 10^{-6}$	$36.7\ 10^{-6}$	$15.87\ 10^{-6}$
	$\pm\ 1.0\ 10^{-6}$	$\pm\ 1.0\ 10^{-6}$	$\pm\ 0.4\ 10^{-6}$	$\pm\ 0.14\ 10^{-6}$
	contribution of the multiperipheral diagrams only			
eeee	$0.920\ 10^{7}$	$1.070\ 10^{7}$	$1.229\ 10^{7}$	$1.459\ 10^{7}$
	$\pm\ 0.010\ 10^{7}$	$\pm\ 0.013\ 10^{7}$	$\pm\ 0.016\ 10^{7}$	$\pm\ 0.025\ 10^{7}$
eeμμ	97.2	129.6	152.1	203.8
	$\pm$ 0.5	$\pm$ 2.1	$\pm$ 0.8	$\pm$ 1.1
	contribution of all lowest order electroweak diagrams			
μμμμ	$159.\ 10^{-6}$	$77.9\ 10^{-6}$	$50.8\ 10^{-6}$	$84.1\ 10^{-6}$
	$\pm\ 6.\ 10^{-6}$	$\pm\ 2.9\ 10^{-6}$	$\pm\ 1.9\ 10^{-6}$	$\pm\ 4.1\ 10^{-6}$
μμττ	$96.9\ 10^{-6}$	$56.6\ 10^{-6}$	$39.6\ 10^{-6}$	$88.3\ 10^{-6}$
	$\pm\ 3.4\ 10^{-6}$	$\pm\ 2.0\ 10^{-6}$	$\pm\ 1.5\ 10^{-6}$	$\pm\ 3.9\ 10^{-6}$

Table 4

tracks visible	multiperipheral cross section (nb)		QED cross section (nb)		electroweak cross section (nb)	
	$e^+e^- \to e^+e^+e^-e^-$					
ee	1.51 ± 0.06		1.47 ± 0.03		1.66 ± 0.13	
eee	2.1 ± 0.4	10^{-3}	2.6 ± 0.2	10^{-3}	2.0 ± 0.6	10^{-3}
eeee	2.50 ± 0.02	10^{-5}	1.32 ± 0.02	10^{-4}	1.2 ± 0.1	10^{-4}
	$e^+e^- \to e^+e^-\mu^+\mu^-$					
e	6.9 ± 0.1	10^{-3}	6.1 ± 0.1	10^{-1}	5.8 ± 0.3	10^{-1}
μ	4.2 ± 0.1	10^{+1}	4.0 ± 0.1	10^{+1}	4.1 ± 0.4	10^{+1}
ee	2.1 ± 0.2	10^{-6}	2.2 ± 0.1	10^{-4}	1.5 ± 0.3	10^{-4}
μμ	2.14 ± 0.05	10^{+1}	2.01 ± 0.09	10^{+1}	1.45 ± 0.3	10^{+1}
eμ	6.7 ± 0.2	10^{-3}	1.1 ± 0.1	10^{-2}	1.6 ± 0.5	10^{-2}
eeμ	1.3 ± 0.1	10^{-5}	1.6 ± 0.1	10^{-4}	2.4 ± 0.7	10^{-4}
μμe	2.0 ± 0.1	10^{-3}	2.6 ± 0.2	10^{-3}	1.5 ± 0.2	10^{-3}
eeμμ	2.62 ± 0.04	10^{-5}	5.9 ± 0.2	10^{-4}	5.8 ± 0.7	10^{-4}
	$e^+e^- \to \mu^+\mu^+\mu^-\mu^-$					
μ			14.3 ± 0.6	10^{-6}	13.6 ± 2.4	10^{-6}
μμ			11.6 ± 0.6	10^{-6}	11.3 ± 2.1	10^{-6}
μμμ			7.7 ± 0.4	10^{-6}	8.4 ± 1.7	10^{-6}
μμμμ			26.5 ± 0.3	10^{-6}	27.6 ± 1.2	10^{-6}
	$e^+e^- \to \mu^+\mu^-\tau^+\tau^-$					
τ			7.2 ± 0.3	10^{-6}	7.8 ± 1.0	10^{-6}
μ			1.4 ± 0.1	10^{-6}	1.3 ± 0.4	10^{-6}
ττ			7.2 ± 0.2	10^{-6}	6.5 ± 0.6	10^{-6}
μμ			1.7 ± 0.1	10^{-6}	1.8 ± 0.3	10^{-6}
μτ			2.5 ± 0.2	10^{-6}	2.2 ± 0.6	10^{-6}
ττμ			4.9 ± 0.2	10^{-6}	4.9 ± 0.5	10^{-6}
μμτ			3.4 ± 0.2	10^{-6}	2.7 ± 0.5	10^{-6}
μμττ			23.2 ± 0.3	10^{-6}	23.9 ± 0.9	10^{-6}

Table 5

tracks visible	multiperipheral cross section (nb)		QED cross section (nb)		electroweak cross section (nb)	
			$e^+e^- \to e^+e^-e^+e^-$			
ee	2.04 ± 0.08		1.96 ± 0.04		1.7 ± 0.2	
eee	3.3 ± 1.3	10^{-4}	3.2 ± 0.5	10^{-4}	4.8 ± 2.9	10^{-4}
eeee	3.21 ± 0.02	10^{-6}	3.9 ± 0.1	10^{-5}	4.3 ± 0.4	10^{-5}
			$e^+e^- \to e^+e^-\mu^+\mu^-$			
e	1.6 ± 0.2	10^{-4}	5.6 ± 0.1	10^{-1}	5.7 ± 0.2	10^{-1}
μ	5.5 ± 0.2	10^{+1}	5.3 ± 0.2	10^{+1}	5.0 ± 0.5	10^{+1}
ee	2.9 ± 0.3	10^{-7}	6.6 ± 0.3	10^{-5}	8.7 ± 0.8	10^{-5}
$\mu\mu$	2.48 ± 0.07	10^{+1}	2.6 ± 0.1	10^{+1}	2.0 ± 0.3	10^{+1}
$e\mu$	1.23 ± 0.03	10^{-3}	4.5 ± 0.9	10^{-3}	1.2 ± 0.1	10^{-3}
$ee\mu$	1.49 ± 0.05	10^{-6}	3.2 ± 0.2	10^{-5}	3.3 ± 0.4	10^{-5}
$\mu\mu e$	2.6 ± 0.1	10^{-4}	3.0 ± 0.2	10^{-4}	2.7 ± 0.3	10^{-4}
$ee\mu\mu$	3.3 ± 0.1	10^{-6}	1.4 ± 0.1	10^{-4}	2.8 ± 0.2	10^{-4}
			$e^+e^- \to \mu^+\mu^+\mu^-\mu^-$			
μ			2.9 ± 0.1	10^{-6}	6.5 ± 1.2	10^{-6}
$\mu\mu$			2.6 ± 0.1	10^{-6}	25.7 ± 1.4	10^{-6}
$\mu\mu\mu$			1.3 ± 0.1	10^{-6}	10.6 ± 0.8	10^{-6}
$\mu\mu\mu\mu$			5.7 ± 0.1	10^{-6}	38.2 ± 1.6	10^{-6}
			$e^+e^- \to \mu^+\mu^-\tau^+\tau^-$			
τ			2.2 ± 0.1	10^{-6}	3.9 ± 0.9	10^{-6}
μ			0.60 ± 0.03	10^{-6}	1.3 ± 0.4	10^{-6}
$\tau\tau$			2.0 ± 0.1	10^{-6}	22.7 ± 1.2	10^{-6}
$\mu\mu$			0.45 ± 0.02	10^{-6}	3.3 ± 0.4	10^{-6}
$\mu\tau$			0.54 ± 0.04	10^{-6}	1.0 ± 0.2	10^{-6}
$\tau\tau\mu$			0.98 ± 0.04	10^{-6}	7.8 ± 0.5	10^{-6}
$\mu\mu\tau$			0.81 ± 0.04	10^{-6}	3.6 ± 0.4	10^{-6}
$\mu\mu\tau\tau$			5.8 ± 0.1	10^{-6}	38.9 ± 1.2	10^{-6}

θ_o > 25 degrees. This error was obtained by means of a Monte Carlo calculation. In table 4 we give the visible cross sections for the four-lepton production processes for a beam energy of 17.5 GeV and a value of 25 degrees for θ_o. This table contains four columns. The first specifies the visible tracks. The second lists the results for the multiperipheral amplitude alone. The third takes into account all lowest order QED amplitudes whereas the fourth does the complete electro-weak calculation. Next in table 5 we repeat this calculation but now with E_b= 50 GeV.

We conclude that the total cross section for $e^+e^+e^-e^-$ and $e^+e^-\mu^+\mu^-$ final states increases with the beam energy, as expected from the multiperipheral character of the scattering. The main difference in size between the two cross sections is entirely due to the much lower invariant mass accessible by the e^+e^- pair. From the middle lines in table 3 it is seen that in the total cross section the multiperipheral contributions dominate by far. Because of their absence in the $\mu^+\mu^+\mu^-\mu^-$ and $\mu^+\mu^-\tau^+\tau^-$ cases these cross sections are much smaller and decrease with beam energy. Moreover, when considering these final states, we see that Z_0 interchanges are no longer negligible when the beam energies are so high that the denominators of the Z_0 propagators can become small. Looking at the cross sections listed in table 4 we observe that, in the $e^+e^+e^-e^-$ case with two tracks visible, the cross section obtained from two multiperipheral graphs only is in perfect agreement with the result from the complete treatment. However, if we demand all tracks to be visible in the central detector we see that the multiperipheral cross section tends to be too small. In this case, clearly, a complete calculation is necessary. In the $e^+e^-\mu^+\mu^-$ case a clear difference between the multiperipheral and the complete treatment is observed if we require only one e track to be visible. This difference is explained by the contribution of the bremsstrahlung diagrams. When precisely two e tracks are visible again the multiperipheral calculation underestimates the cross section because in this part of phase-space the conversion and annihilation diagrams contribute significantly. The same conclusion applies to the case where all four tracks are visible in the central detector. When we compare the visible cross sections for $e^+e^- \to e^+e^-\mu^+\mu^-$ with the ones published in ref. [1] we find some significant differences. These are due to the fact that in ref. [1] the muons were treated in the ultra-relativistic limit. Furthermore we did not use the single- or double-tag event generators to calculate the cross sections corresponding to many tracks seen in the central detector. Finally it is worthwhile noticing

that in the $\mu^+\mu^+\mu^-\mu^-$ and the $\mu^+\mu^-\tau^+\tau^-$ case the main part of the cross section corresponds to events with four tracks visible in the central detector. These results show that there are regions in phase-space where a complete calculation of all Feynman diagrams contributing in lowest order is necessary.

As expected from table 3 we see no effects due to Z_0 exchange. However at 50 GeV the cross sections do change when the Z_0 is incorporated. Notably the $ee\mu\mu$ cross section is doubled and all cross sections concerning $e^+e^- \to \mu^+\mu^+\mu^-\mu^-$ or $e^+e^- \to \mu^+\mu^-\tau^+\tau^-$ increase significantly.

3. Effects due to the bremsstrahlung subgroup

In this section we study in more detail effects which are caused by the bremsstrahlung subgroup. The first result which we present concerns the muon charge asymmetry. This asymmetry is due to the interference between multiperipheral and bremsstrahlung diagrams and is defined as follows :

$$A = \frac{N(\mu^+,f) + N(\mu^-,b) - N(\mu^+,b) - N(\mu^-,f)}{N(\mu^+,f) + N(\mu^-,b) + N(\mu^+,b) + N(\mu^-,f)} \quad . \qquad (5.1)$$

where $N(\mu^+,f)$ and $N(\mu^+,b)$ denote the number of anti-muons produced in respectively the forward and backward directions. Forward means in the direction of the incoming positron beam, backward in the direction of the incoming electron beam.

We assume that the positron is tagged, that is, we apply cuts on the positron energy and scattering angle. The electron is explicitly untagged. Thus its scattering angle must be small with no energy cut. Finally, the produced muons must both be seen at large angles with respect to the beams. We specified the following parameters :

$E_b = 17.$ GeV , $W^2_{min} = 1$ GeV^2, $q^o_{+,min} = 3.6$ GeV ,
$8.02^o \leq \theta_+ \leq 20.64^o$, $0^o \leq \theta_- \leq 5^o$, $|\cos\theta_\mu| \leq 0.92$.

We used the single-tag event generator described in appendix D and obtained the following results (L stands for the integrated luminosity) :

$N(\mu^+,f) = 7.003 \pm 0.005$ pb $\times$ L
$N(\mu^-,b) = 6.319 \pm 0.002$ pb $\times$ L
$N(\mu^+,b) = 6.212 \pm 0.002$ pb $\times$ L
$N(\mu^-,f) = 6.895 \pm 0.005$ pb $\times$ L

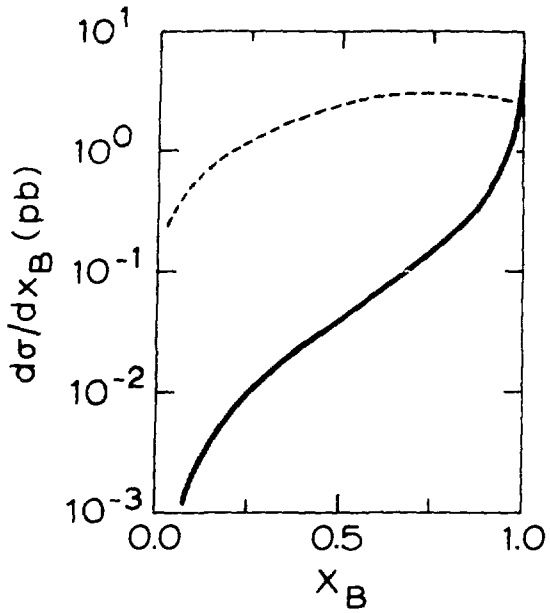

fig. 13

Inserting these cross sections in eq. (5.1) we find the asymmetry :

$A = 0.81\% \pm 0.05\%$.

The experimental results [2] seem to indicate an asymmetry which is compatible with zero but suffers from large statistical errors. There is only one report of a possible large asymmetry but again the errors are quite large due to lack of statistics [3].

The second result is obtained while single-tagging cuts are applied which closely resemble those of the PLUTO experiment [4]. We use :

$E_b = 17.5$ GeV , $\theta_- \leq 1.^\circ$, $10.^\circ \leq$ angle between $\vec{q}_-$ and $\vec{k} \leq 170.^\circ$,

$21.^\circ \leq \theta_+ \leq 39.^\circ$, $q_+^\circ \geq 6.$ GeV , angle between $\vec{p}_+$ and $\vec{k} \geq 21.^\circ$

Next we plot the differential cross section with respect to the Bjorken scaling variable X_B which is of interest because it provides information on the leptonic (or hadronic) structure function of the photon (see chapter II). It is defined as :

$$X_B = \frac{|Q^2|}{|Q^2| + W^2} \, . \qquad (5.2)$$

Here Q^2 is by definition the momentum transfer squared of the particle which

scatters over a large angle, in this case the positron. In order to see clearly the effect of the bremsstrahlung group we keep the contribution from the multiperipheral and the bremsstrahlung group separated. Looking at fig. 13 we see that the multiperipheral graphs give rise to an X_B distribution which is almost flat (for less severe cuts it peaks at lower X_B values). However, the bremsstrahlung contribution is concentrated completely near $X_B = 1$. This effect is a consequence of the different behaviour of the multiperiheral and bremsstrahlung differential cross sections with respect to W. The latter peaks much sharper at low W than the first one. This X_B behaviour agrees nicely with the experimental results on deep inelastic scattering on nearly real photons with $|Q^2|$ values up to 100 GeV^2 [5]. We conclude that the bremsstrahlung diagrams can yield sizeable effects whenever we apply single-tagging cuts which do not exclude the low W region.

4. Radiative corrections

Finally we discuss results on the radiative corrections which were obtained by the use of the event generator described in the previous chapter. Firstly, we calculated these corrections for the no-tagging case. In table 6 we list the total cross section (in nanobarns) with and without radiative corrections at various beam energies. Comparison between these results shows that the radiative corrections are indeed small.

Table 6

Beam energy (GeV)	σ (lowest order multiperipheral)		σ (radiative corrections included)	
10	97.1	±0.3	97.3	±0.5
20	137.2	±0.5	138.7	±0.8
50	202.4	±0.8	202.3	±1.2
100	261.4	±1.0	262.8	±1.6

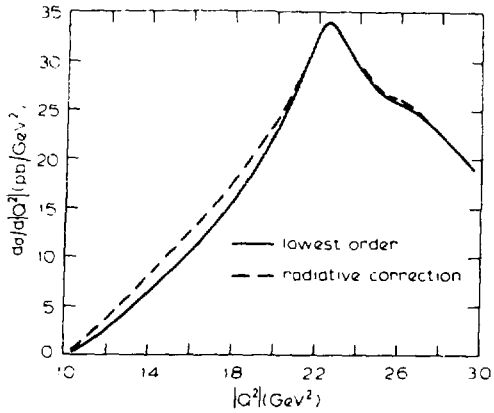

fig. 14

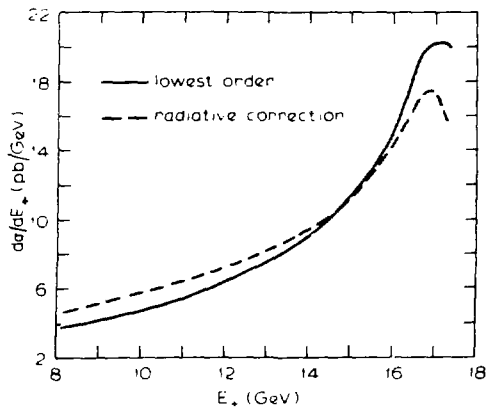

fig. 15

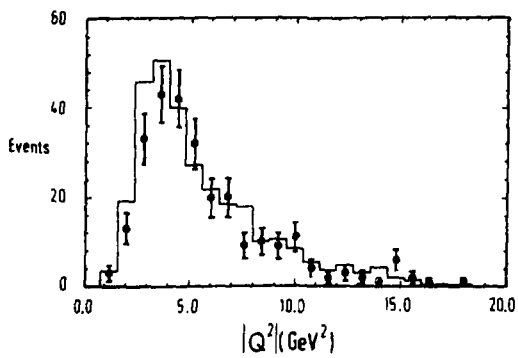

fig. 16

Next we study the radiative corrections on various differential cross sections with large angle tagging conditions. The cuts used resemble very much those applied by the PLUTO experiment [2] :

$E_b = 17.5$ GeV , $W^2_{min} = 1$ GeV^2, $q^o_+ > 8$ GeV , $|\cos\theta_{\mu+}| < 0.996$, $|\cos\theta_{\mu-}| < 0.996$,
0.085 rad $< \theta_+ < 0.8$ rad or $\pi - 0.8$ rad $< \theta_+ < \pi - 0.085$ rad ,
$\theta_- < 0.03$ rad or $\theta_- > \pi - 0.03$ rad.

Calculation of the cross section yields $\sigma_{lo} = 86.28 \pm 0.32$ pb for the lowest order and $\sigma_{rad} = 87.95 \pm 0.35$ pb when the radiative corrections are included. So again we find a small correction on the total cross section. However, when we study differential cross sections the corrections may be larger. As an illustration we show the $d\sigma / d|Q^2_+|$ and the $d\sigma / dq^o_+$ distributions in figs. 14 and 15. In the first plot we observe an increase of the cross section at lower $|Q^2_+|$ values and in the $d\sigma / dq^o_+$ plot event the peak in the cross section is shifted towards lower energies. This shift is caused by the emission of a real photon which carries away some of the available energy. Finally, in fig. 16 a comparison between the experimental and the Monte Carlo $d\sigma / d|Q^2|$ distribution is presented. It contains PLUTO data with cuts imposed that resemble very much those mentioned above [6].

5. Outlook

Finally, we want to mention a few topics concerning two-photon physics which are not dealt with in this thesis but may prove to become important in the future.

- Double multiperipheral contributions to the two-photon cross section

In this case we study the contribution of t-channel diagrams to processes such as : $e^+e^- \to e^+e^-\mu^+\mu^-\mu^-$. When the scattered electron and positron are not detected in the experiment and the energies of the outgoing particles can only be measured with a limited accuracy this process may turn out to be an important background to the process $e^+e^- \to \mu^+\mu^+\mu^-\mu^-$. Although the former process is of order α^6 it can still contribute substantially again because of the large logarithms which occur in the no-tagging case. Of course a precise measurement of the total energy of the four muons could experimentally distinguish between the two reactions.

- Radiative corrections corresponding to graphs depicted in fig. 9.
Especially the extension of the calculation in ref. [7] for at least one highly virtual photon may be important for the study of deep inelastic electron-photon scattering.

- Contribution of processes such as $e^+e^- \to \ell^+\ell^-\nu\bar{\nu}$ to the cross section of four-lepton production processes with only two tracks (i.e. ℓ^+, ℓ^-) visible. These reactions involve either Z_0 or $W^\pm$ exchange and may therefore become of importance at LEP energies.

References

1. F.A. Berends, P.H. Daverveldt and R. Kleiss, Phys. Lett. 148B (1984) 489.
2. B. King, private communication.
3. P. Colas, Thèse de Trosième Cycle, Université de Paris (1983).
4. G. Knies, private communication.
5. M. Pohl, G. Knies, F. Raupach, G. Carnesecchi : Talks given at the 5th Intern. Workshop on Photon Photon Collisions, Aachen, Ed. Ch. Berger, Lectures Notes in Physics Vol. 191, Springer Verlag (1983).
6. PLUTO Coll., Ch. Berger et al., Z. Physik C 27 (1985) 249.
7. F.A. Berends, Z. Kunszt and R. Gastmans, Nucl. Phys. B182 (1981) 397.

APPENDIX A

Throughout this thesis we use the following notations and conventions.

We use units in which $\hbar = c = 1$.

Contravariant four-vectors are denoted by $k^\mu = (k^0, k^1, k^2, k^3) = (k^0, \vec{k})$. The diagonal elements of the metric tensor $g^{\mu\nu}$ are given by $g_{00} = -g_{11} = -g_{22} = -g_{33} = +1$, all other elements are zero. The inner product between two four vectors p^μ and q^μ is denoted as $p \cdot q$.

Summation over repeated indices is always implied.

The 4×4 matrices γ^μ satisfy : $\{\gamma^\mu, \gamma^\nu\} = \gamma^\mu\gamma^\nu + \gamma^\nu\gamma^\mu = 2 g^{\mu\nu} I$ where I is the unit matrix. For the contraction of four-vectors with γ-matrices we write $p_\mu\gamma^\mu = \not{p}$. Finally we define $\gamma^5 = i \gamma^0\gamma^1\gamma^2\gamma^3$.

The Dirac spinors are normalized in such a way that :

$$\sum_{s=\pm 1} u(p,s)\,\bar{u}(p,s) = \not{p} + m \,. \tag{A1}$$

We consider the scattering process between two particles with four-momenta p_a and p_b which produce N particles in the final state with four-momenta $p_1, p_2, \ldots, p_N$. The differential cross section corresponding to this reaction can be written as follows :

$$d\sigma = \frac{1}{2\,(2\pi)^{3N-4}\,\lambda^{\frac{1}{2}}(s, m_a^2, m_b^2)}\,\delta^4\Big(p_a + p_b - \sum_{i=1}^{N} p_i\Big)\,\big|M\big|^2 \prod_{j=1}^{N} \frac{d^3\vec{p}_j}{2\,p_j^0}\,,$$
$$m_a^2 = p_a^2\,,\quad m_b^2 = p_b^2\,,\quad s = (p_a + p_b)^2\,. \tag{A2}$$

Here $|M|^2$ denotes the matrix element squared (spin summed and averaged) which describes the reaction.

Appendix B

In this appendix we shall sketch the derivation of eq. (2.5).

We start with a general expression for the differential cross section :

$$d\sigma = \frac{4\,\alpha^4}{\pi^2}\,\frac{t_+^{\mu\nu}t_-^{\alpha\beta}\,M_{\mu\alpha\nu\beta}}{\left[(p_+\cdot p_-)^2-m_e^4\right]^{\frac{1}{2}}\,Q_+^4\,Q_-^4}\,\frac{d^3\vec{q}_+}{q_+^o}\,\frac{d^3\vec{q}_-}{q_-^o}\,, \tag{B1}$$

$$t_\pm^{\mu\nu} = \tfrac{1}{2}\,(p_\pm^\mu q_\pm^\nu + q_\pm^\mu p_\pm^\nu + \tfrac{1}{2}\,Q_\pm^2 g^{\mu\nu})\,,\quad M_{\mu\alpha\nu\beta} = \int dp_X (2\pi)^4 \delta^4(Q_+ + Q_- - p_X)\,R_{\mu\alpha}R^*_{\nu\beta}.$$

Here we used the Feynman rules to calculate $t_\pm$, dp_X is the invariant phase-space element of the final state X, which we do not need to specify. Moreover we introduced the matrix element $R^{\mu\alpha}$ which describes the process $\gamma\,\gamma \to X$. We now decompose the so-called hadron tensor $M_{\mu\alpha\nu\beta}$ using very general principles, like Lorentz invariance and the hermiticity of $M_{\mu\alpha\nu\beta}$. The former implies that we can expand $M_{\mu\alpha\nu\beta}$ in terms of the photon four-momenta Q_+ and Q_- and the metric tensor $g_{\mu\nu}$. However because of current conservation, that is $Q_+^\mu M_{\mu\alpha\nu\beta} = Q_+^\nu M_{\mu\alpha\nu\beta} = Q_-^\alpha M_{\mu\alpha\nu\beta} = Q_-^\beta M_{\mu\alpha\nu\beta} = 0$, it is more convenient to use the vectors X_+ and X_- and the symmetric tensor $G_{\mu\nu}$, which are defined as follows :

$$X_\pm = Q_\mp - \frac{Q_+\cdot Q_-}{Q_\pm^2}\,Q_\pm\,,\quad G^{\mu\nu} = g^{\mu\nu} - \frac{Q_+^\mu Q_-^\nu}{Q_+\cdot Q_-} - \frac{X_-^\mu X_+^\nu}{X_+\cdot X_-}\,. \tag{B2}$$

The expansion of the hadronic tensor now reads :

$$M^{\mu\alpha\nu\beta} = \sum_{i=1}^{10} V_i(Q_+^2, Q_-^2, W^2)\; I_i^{\mu\alpha\nu\beta}.$$

Here I_i are tensors built up from X_+, X_- and G. The V_i are scalar functions and therefore depend only on Q_+^2, Q_-^2 and $W^2 = (Q_+ + Q_-)^2$. Because of the hermiticity of the hadron tensor they must be real. It is a straightforward exercise to perform the contractions between $t_+^{\mu\nu}t_-^{\alpha\beta}$ and $I_i^{\mu\alpha\nu\beta}$. Therefore what remains to be done is to establish the relation between the functions V_i and the cross sections for $\gamma\,\gamma \to X$. To this end we choose the CM system of the virtual photons as frame of reference and introduce the following polarization vectors $\varepsilon_\lambda^\mu(Q)$ $(\lambda = 0, \pm 1)$ for the virtual photons :

$$\varepsilon_\pm(Q_+) = \frac{1}{\sqrt{2}}\,(0, \mp 1, -i, 0)\,,\quad \varepsilon_o(Q_+) = \frac{1}{\sqrt{-Q_+^2}}\,(|\vec{Q}_+|, 0, 0, Q_+^o)\,,$$

$$\varepsilon_{\pm}(Q_-) = \frac{1}{\sqrt{2}}(0,\pm 1,i,0) \quad , \quad \varepsilon_o(Q_-) = \frac{1}{\sqrt{-Q_-^2}}(-|\vec{Q}_-|,0,0,Q_-^o) \ . \qquad (B3)$$

These polarization vectors satisfy :

$$\sum_{\lambda=0,\pm 1} (-1)^{\lambda} \varepsilon_{\lambda}^{\mu *}(Q)\ \varepsilon_{\lambda}^{\nu}(Q) = g^{\mu\nu} - \frac{Q^{\mu}Q^{\nu}}{Q^2} \ .$$

Using these polarization vectors we define :

$$M_{\lambda_+\lambda_-\lambda'_+\lambda'_-} = \varepsilon_{\lambda_+}^{\mu}(Q_+)\ \varepsilon_{\lambda_-}^{\alpha}(Q_-)\ \varepsilon_{\lambda'_+}^{\nu *}(Q_+)\ \varepsilon_{\lambda'_-}^{\beta *}(Q_-)\ M_{\mu\alpha\nu\beta} \ . \qquad (B4)$$

Thus we have got rid of the components of $M_{\mu\alpha\nu\beta}$ which are abundant because of current conservation. The number of independent components of M can be further reduced if we observe that, because of the rotational symmetry around the collision axis of the two photons, the differential cross section does not depend on $\tilde{\phi}_+$ and $\tilde{\phi}_-$ (the azimuthal angles of respectively the scattered positron and electron) separately but only on $\tilde{\phi}_+ - \tilde{\phi}_-$. Integration over the abundant azimuthal angle yields the relation : $\lambda_+ - \lambda_- = \lambda'_+ - \lambda'_-$. Invariance under space reflexion gives us another constraint :

$$M_{\lambda_+\lambda_-\lambda'_+\lambda'_-} = M_{-\lambda_+-\lambda_--\lambda'_+-\lambda'_-} \ .$$

This leaves us with 19 non-zero components of M which can be classified into one 3×3 matrix corresponding to $\lambda_+ - \lambda_- = 0$,two 2×2 matrices with $\lambda_+ - \lambda_- = \pm 1$ and two 1×1 matrices with $\lambda_+ - \lambda_- = \pm 2$. Now we work out the contractions in eq. (B4) explicitly. Thus we express the V_i functions in terms of the 19 non-vanishing components of $M_{\lambda_+\lambda_-\lambda'_+\lambda'_-}$. These can be in their turn related to either the differential cross section for polarized photons producing the final state X or to interference terms τ . In the former case the helicity must be conserved, that is $\lambda_+ = \lambda'_+$ and $\lambda_- = \lambda'_-$ and we have the following relation :

$$\sigma_{\lambda_+\lambda_-} = \frac{e^4}{4\,|\vec{k}|\,W} M_{\lambda_+\lambda_-\lambda_+\lambda_-} \quad , \quad |\vec{k}| = \frac{\left[(W^2 - Q_+^2 - Q_-^2)^2 - 4\,Q_+^2Q_-^2\right]^{\frac{1}{2}}}{2\,W} \ . \qquad (B5)$$

When the helicity is not conserved we define in a similar way :

$$\tau_{\lambda_+\lambda_-\lambda'_+\lambda'_-} = \frac{e^4}{4\,|\vec{k}|\,W} M_{\lambda_+\lambda_-\lambda'_+\lambda'_-} \ . \qquad (B6)$$

Expressing $d\sigma$ in terms of these photon-photon cross sections and interference terms we find finally :

$$d\sigma = \frac{\alpha^2}{16\pi^4} \frac{|\vec{k}|\, W}{[(p_+ \cdot p_-)^2 - m_e^4]^{\frac{1}{2}}\, Q_+^2 Q_-^2}$$
$$\{ \rho_+^{oo} \rho_-^{oo} \sigma_{LL}(Q_+^2, Q_-^2, W^2) + 2\, \rho_+^{oo} \rho_-^{++} \sigma_{LT}(Q_+^2, Q_-^2, W^2) + 2\, \rho_+^{++} \rho_-^{oo} \sigma_{TL}(Q_+^2, Q_-^2, W^2) +$$
$$4\, \rho_+^{++} \rho_-^{++} \sigma_{TT}(Q_+^2, Q_-^2, W^2) + 2\, |\rho_+^{+-}|\, |\rho_-^{+-}| \cos(2\tilde{\phi})\, \tau_{TT} -$$
$$8\, |\rho_+^{+o}|\, |\rho_-^{+o}| \cos\tilde{\phi}\, \tau_{TL} \} \frac{d^3 \vec{q}_+}{q_+^o} \frac{d^3 \vec{q}_-}{q_-^o} ,$$

$$\rho_\pm^{oo} = 4 \left(\frac{p_\pm \cdot X_\pm}{|\vec{k}|\, W}\right)^2 - 1 , \quad \rho_\pm^{++} = 2 \left[\left(\frac{p_\pm \cdot X_\pm}{|\vec{k}|\, W}\right)^2 + \tfrac{1}{4} + \frac{m_e^2}{Q_\pm^2}\right] , \quad |\rho_\pm^{+-}| = \rho_\pm^{++} - 1 ,$$

$$|\rho_\pm^{+o}| = \left[\, |\rho_\pm^{+-}| (\rho_\pm^{oo} + 1) \,\right]^{\frac{1}{2}}, \quad \cos\tilde{\phi} = - \frac{p_+^\mu p_-^\nu\, G_{\mu\nu}}{\left[\, \tfrac{1}{4} Q_+^2 Q_-^2\, |\rho_+^{+-}|\, |\rho_-^{+-}| \,\right]^{\frac{1}{2}}} ,$$

$$\sigma_{TT} = \tfrac{1}{2} (\sigma_{++} + \sigma_{+-}) , \quad \tau_{TT} = \tau_{++--} , \quad \tau_{TL} = \tfrac{1}{2} (\tau_{oo++} + \tau_{+oo-}) ,$$

$$\sigma_{LT} = \frac{e^4}{4\, |\vec{k}|\, W} M_{0+0+} , \quad \sigma_{TL} = \frac{e^4}{4\, |\vec{k}|\, W} M_{+0+0} , \quad \sigma_{LL} = \frac{e^4}{4\, |\vec{k}|\, W} M_{0000} . \qquad (B7)$$

Appendix C

In this appendix we shall derive eq. (2.2) which expresses the multiperipheral differential cross section in terms of the photon structure functions. To this end we consider the single-tagging case. The e^+ is required to scatter over a large angle ($\Theta_+ >> m_e / E_b$) and thus produces a virtual photon which is far off mass shell. We assume that the other photon is quasi-real. Under these assumptions we can approximate the differential cross section given by eq. (2.9). Making the approximation $Q_-^2 << W^2$ in the factors ρ and ε, we observe that again the flux factor $N(\omega_-)\, d\omega_-$ of the quasi-real photon can be split off. The remaining part describes the interaction between a positron and a quasi-real photon. We write the cross section as follows :

$$d\sigma_{e\gamma \to eX} = \frac{\alpha}{\pi} \frac{q_+^o\,(2 - 2y + y^2)}{|Q_+^2|\, y} \{ \sigma_{TT}(Q_+^2, 0, W^2) + \varepsilon\, \sigma_{LT}(Q_+^2, 0, W^2) \}$$
$$dq_+^o d\cos\Theta_+ ,$$

$$y = \frac{Q_+ \cdot Q_-}{p_+ \cdot Q_-} \simeq 1 - q_+^o \cos^2(\tfrac{1}{2}\Theta_+) \quad , \quad \varepsilon = \frac{2 - 2y}{2 - 2y + y^2} \qquad (C1)$$

We now define the structure functions as follows :

$$\sigma_{TT} = 8\pi^2\alpha\, x \frac{F_T(x, Q_+^2)}{|Q_+^2|} \quad , \quad \sigma_{LT} = 4\pi^2\alpha \frac{F_L(x, Q_+^2)}{|Q_+^2|} \quad , \quad x = \frac{|Q_+^2|}{2\, Q_+ \cdot Q_-} \simeq \frac{|Q_+^2|}{W^2 + |Q_+^2|} ,$$
$$F_2(x, Q_+^2) = 2\, x\, F_T(x, Q_+^2) + F_L(x, Q_+^2) \quad , \quad F_1(x, Q_+^2) = F_T(x, Q_+^2) \quad . \qquad (C2)$$

Substitution in eq. (C1) yields :

$$d\sigma = \frac{8\pi\alpha^2 q_+^o}{Q_+^4\, y} [(1 - y)\, F_2(x, Q_+^2) + x\, y^2 F_1(x, Q_+^2)]\, dq_+^o d\cos\Theta_+ \qquad (C3)$$

Because y tends to be rather small in two-photon experiments, most experiments are only sensitive to the structure function $F_2(x, Q_+^2)$. In analogy to deep inelastic electron-nucleon scattering the variable x is called the scaling variable. As we have seen in sect. 2 of chapter 2, scaling in this variable is violated when the Quark Model is applicable.

Appendix D

In principle, the Monte Carlo event generator described in chapter III can simulate any experimental set-up. However, in this program only the cut on the invariant mass squared of the lepton or quark pair, can be applied without a considerable loss of efficiency. Other cuts, for example on the angles of the produced particles can only be dealt with by first generating events in the complete phase-space and next applying a rejection algorithm to get rid of those events which do not satisfy these cuts. Of course, this may result into a noticeable decrease of the efficiency. Thus for tagging experiments a Monte Carlo event generator which allows the user to specify beforehand the bounds on the scattering angle of the beams, is called for. Therefore we design two new event generators for $e^+e^- \to e^+e^-\mu^+\mu^-$, one of which is well suited for single-tagging, the other for double-tagging. In both generators again all the Feynman diagrams contributing in lowest order are taken into account and the corresponding complete matrix element squared is calculated in the same way as before. However, the subgenerators for the multiperipheral and bremsstrahlung diagrams are now changed in several respects. We first describe the event generator for the single-tagging case.

Here the scattering angle of the positron beam is chosen to be an integration variable so that cuts on this angle can be applied without the use of a rejection algorithm. Next the approximate differential cross sections which are used for the event generation, are changed in order to describe the peaking behaviour of the exact differential cross section in a better and more accurate way. Due to these changes, the performance of this large angle tagging event generator is equal to that of the one described in chapter III in the no-tagging case. The subgenerators for the conversion and annihilation diagrams have not been changed for two reasons. Firstly, in most single-tagging configurations their contribution is negligible compared to the one from the multiperipheral and bremsstrahlung subgenerators. Secondly, the events which are produced by these generators tend to consist of final state particles which are produced at large angles with respect to the beams (see chapter V). Therefore, the cut on the polar angle of the positron beam can easily be accounted for by the application of a rejection algorithm without too much loss of efficiency. For detailed information on this large angle tagging event generator we refer to the Program Write-Up (submitted to Comp.

Phys. Comm.).

In the multiperipheral and bremsstrahlung subgenerator for double-tagging we choose the scattering angles of the beam particles as integration variables. This guarantees that we shall not have to throw away too many events when we impose the double-tagging cuts. Next we carefully tune the approximate differential cross sections, bearing in mind that the virtual photon masses can no longer be neglected. The resulting event generator is only slightly less efficient than the no-tag generator in the no-tagging case. Consequently it enables us to predict accurately tiny cross sections which correspond to very unorthodox regions in phase-space, for example both muons produced at small angles but both beam particles produced at large angles with respect to the beams. Just like in the single-tag generator we do not change the conversion and annihilation subgenerators.

We conclude that we now can calculate the cross section in any part of phase-space by using either the no-tag, the single-tag or the double-tag generator.

Appendix E

In this appendix we show briefly how we can extend the event generator, described in chapter III, so that in lowest order not only all possible virtual photon exchanges but also all possible Z_0 exchanges are accounted for. Since, in principle, each photon can be replaced by a Z_0 the number of diagrams to be considered is multiplied by a factor four. Of course, the contribution of many of these added diagrams is expected to be small because of the large mass of the Z_0 in the propagator. However at LEP energies, especially the conversion and annihilation diagrams can contribute significantly because the Z_0 propagator can become on shell. This effect will show up in, for example, the total cross section for $e^+e^- \rightarrow \mu^+\mu^+\mu^-\mu^-$ at high beam energies. The incorporation of the Z_0 poses two problems.

First of all, there is introduced a vector part v and an axial part a in the coupling with the leptons or quarks. The constants v and a depend on the Z_0 parameters and on the quark or lepton nature of the particles to which the Z_0 couples.

Table E1

fermion type	electric charge Q	weak vector coupling v	weak axial vector coupling a
e, μ, τ	+ 1	(x - 1) / y	- 1 / y
u, c, t	- 2 / 3	(x - 3 / 2) / y	- 3 / (2 y)
d, s, b	+ 1 / 3	(x - 3) / y	- 3 / y

In this table $x = 4 \sin^2\Theta_W$ and $y = 4 \sin\Theta_W \cos\Theta_W$, where Θ_W is the weak mixing angle. We use $M_Z = 88.6$ GeV and $\Gamma_Z = 2.5$ GeV which corresponds to $\sin^2\Theta_W = 0.23$.

Secondly, the propagator of the Z_0 with four-momentum k, mass M_Z and width Γ_Z equals :

$$\frac{g^{\mu\nu} - k^\mu k^\nu / M_Z^2}{k^2 - M_Z^2 + i M_Z \Gamma_Z} . \qquad \text{(E1)}$$

The second term in the propagator gives rise to terms proportional to the masses of the interacting particles. For the known leptons and quarks this

contribution will be negligible. Only for top quarks we can get a significant contribution. In the latter case we need a new calculational scheme besides the introduction of the vector and axial vector couplings v and a.

In order to illustrate which extensions have to be made in the calculation of the complete matrix element squared (cf. chapter III sect. 2) we consider Feynman diagrams where the photon with four-momentum $b_1 p_1 + b_2 p_2$ is replaced by a Z_0. For a given diagram we define the amplitude as follows, while using the same convention as in chapter III sect. 2 :

$$M(p_1,\lambda_1,p_2,\lambda_2,p_3,\lambda_3,p_4,\lambda_4,p_5,\lambda_5,p_6,\lambda_6) = \frac{-ie^4\, T(p_1,\lambda_1,p_2,\lambda_2,p_3,\lambda_3,p_4,\lambda_4,p_5,\lambda_5,p_6,\lambda_6)}{((b_1p_1+b_2p_2)^2 - M_z^2 + iM_z\Gamma_z)\,((b_3p_3+b_1p_1+b_2p_2)^2 - m_3^2)\,(b_5p_5+b_6p_6)^2} \tag{E2}$$

The spinor part T now reads :

$$\begin{aligned} T(p_1,\lambda_1,p_2,\lambda_2,p_3,\lambda_3,p_4,\lambda_4,p_5,\lambda_5,p_6,\lambda_6) = {} & \bar{u}_{\lambda_1}(p_1)\,\gamma_\mu(g_a\omega_- + h_a\omega_+)\,u_{\lambda_2}(p_2) \\ & \bar{u}_{\lambda_3}(p_3)\,\gamma^\mu(g_b\omega_- + h_b\omega_+)\,(b_3(\not{p}_3 + m_3) + b_2(\not{p}_2 + m_2) + b_1(\not{p}_1 + m_1))\,\gamma^\nu u_{\lambda_4}(p_4) \\ & \bar{u}_{\lambda_5}(p_5)\,\gamma_\nu u_{\lambda_6}(p_6) - \bar{u}_{\lambda_1}(p_1)\,(b_1\not{p}_1 + b_2\not{p}_2)\,(g_a\omega_- + h_a\omega_+)\,u_{\lambda_2}(p_2)\,\bar{u}_{\lambda_3}(p_3) \\ & (b_1\not{p}_1 + b_2\not{p}_2)\,(g_b\omega_- + h_b\omega_+)\,(b_3(\not{p}_3 + m_3) + b_2(\not{p}_2 + m_2) + b_1(\not{p}_1 + m_1))\,\gamma^\nu u_{\lambda_4}(p_4) \\ & \bar{u}_{\lambda_5}(p_5)\,\gamma_\nu u_{\lambda_6}(p_6) / M_z^2. \end{aligned} \tag{E3}$$

Here we introduced factors g and h which are defined as follows : $g = v + a$ and $h = v - a$. The subscripts denote the vertices to which the couplings v and a belong. We consider for the moment only the first term. The Z function is defined in an analogous way as in chapter III sect. 2 :

$$\begin{aligned} Z(p_1,\lambda_1,p_2,\lambda_2,p_3,\lambda_3,p_4,\lambda_4,g_a,h_a,g_b,h_b) = {} & \\ \bar{u}_{\lambda_1}(p_1)\,\gamma_\mu(g_a\omega_- + h_a\omega_+)\,u_{\lambda_2}(p_2)\,\bar{u}_{\lambda_3}(p_3)\,\gamma^\mu(g_b\omega_- + h_b\omega_+)\,u_{\lambda_4}(p_4) & . \end{aligned} \tag{E4}$$

Upon substitution of $g = 1$ and $h = 1$ we obtain the Z function defined in eq. (3.4) which was used to calculate photon exchange.
Using the completeness relation of the projection matrices $u_\lambda(p)\,\bar{u}_\lambda(p)$:

$$\sum_{\lambda} u_{\lambda}(p)\,\bar{u}_{\lambda}(p) = \not{p} + m \qquad \text{(E5)}$$

we write the first term in terms of the newly defined Z functions :

$$\sum_{\lambda=\pm 1} \{\, b_3\, Z\,(p_1,\lambda_1,p_2,\lambda_2,p_3,\lambda_3,p_3,\lambda,g_a,h_a,g_b,h_b)$$

$$Z\,(p_3,\lambda,p_4,\lambda_4,p_5,\lambda_5,p_6,\lambda_6,1,1,1,1) +$$

$$b_1\, Z\,(p_1,\lambda_1,p_2,\lambda_2,p_3,\lambda_3,p_1,\lambda,g_a,h_a,g_b,h_b)$$

$$Z\,(p_1,\lambda,p_4,\lambda_4,p_5,\lambda_5,p_6,\lambda_6,1,1,1,1) +$$

$$b_2\, Z\,(p_1,\lambda_1,p_2,\lambda_2,p_3,\lambda_3,p_2,\lambda,g_a,h_a,g_b,h_b)$$

$$Z\,(p_2,\lambda,p_4,\lambda_4,p_5,\lambda_5,p_6,\lambda_6,1,1,1,1)\ \} \qquad \text{(E6)}$$

Next we have to express again the Z function in terms of the S and T matrices. This is performed in a completely similar way as in chapter III sect. 2. We write $u_{\lambda}(p)$ in terms of $\alpha_{\lambda}(p)$ and $u_{-\lambda}(k^{\circ})$. Noticing that $\alpha_{\lambda}(p)$ and $u_{\lambda}(k^{\circ})$ are eigenspinors of ω_{λ}, we get rid of the ω_{-} and ω_{+}. What remains is the following table for the Z function :

Table E2

$$Z\,(\lambda_1,\lambda_2,\lambda_3,\lambda_4) \equiv Z\,(p_1,\lambda_1,p_2,\lambda_2,p_3,\lambda_3,p_4,\lambda_4,g_a,h_a,g_b,h_b)$$

$$Z\,(+,+,+,+) = -2\,\{\, h_a h_b s_{13} t_{24} - g_a h_b \mu_1\mu_2\eta_3\eta_4 - h_a g_b \eta_1\eta_2\mu_3\mu_4 \,\}$$
$$Z\,(+,+,+,-) = -2\,\eta_2\{\, h_a h_b \mu_4 s_{13} - h_a g_b \mu_3 s_{14} \,\}$$
$$Z\,(+,+,-,+) = -2\,\eta_1\{\, h_a g_b \mu_4 t_{23} - h_a h_b \mu_3 t_{24} \,\}$$
$$Z\,(+,+,-,-) = -2\,\{\, h_a g_b s_{14} t_{23} - g_a g_b \mu_1\mu_2\eta_3\eta_4 - h_a h_b \eta_1\eta_2\mu_3\mu_4 \,\}$$
$$Z\,(+,-,+,+) = -2\,\eta_4\{\, h_a h_b \mu_2 s_{31} - g_a h_b \mu_1 s_{31} \,\}$$
$$Z\,(+,-,+,-) = 0$$
$$Z\,(+,-,-,+) = 2\,\{\, g_a h_b \mu_1\mu_3\eta_2\eta_4 - g_a g_b \mu_1\mu_4\eta_2\eta_3 - h_a h_b \mu_2\mu_3\eta_1\eta_4 + h_a g_b \mu_2\mu_4\eta_1\eta_3 \,\}$$
$$Z\,(+,-,-,-) = -2\,\eta_3\{\, h_a g_b \mu_2 s_{41} - g_a g_b \mu_1 s_{42} \,\}$$
$$Z\,(-,+,+,+) = -2\,\eta_3\{\, g_a h_b \mu_2 t_{41} - h_a h_b \mu_1 t_{42} \,\}$$
$$Z\,(-,+,+,-) = 2\,\{\, h_a g_b \mu_1\mu_3\eta_2\eta_4 - h_a h_b \mu_1\mu_4\eta_2\eta_3 - g_a g_b \mu_2\mu_3\eta_1\eta_4 + g_a h_b \mu_2\mu_4\eta_1\eta_3 \,\}$$
$$Z\,(-,+,-,+) = 0$$

$$Z\,(-,+,-,-) = -2\;\eta_4\,\{\,g_a g_b \mu_2 t_{31} - h_a g_b \mu_1 t_{32}\,\}$$
$$Z\,(-,-,+,+) = -2\;\{\,g_a h_b t_{14} s_{23} - h_a h_b \mu_1\mu_2\eta_3\eta_4 - g_a g_b \eta_1\eta_2\mu_3\mu_4\,\}$$
$$Z\,(-,-,+,-) = -2\;\eta_1\,\{\,g_a h_b \mu_4 s_{23} - g_a g_b \mu_3 s_{24}\,\}$$
$$Z\,(-,-,-,+) = -2\;\eta_2\,\{\,g_a g_b \mu_4 t_{13} - g_a h_b \mu_3 t_{14}\,\}$$
$$Z\,(-,-,-,-) = -2\;\{\,g_a g_b t_{13} s_{24} - h_a g_b \mu_1\mu_2\eta_3\eta_4 - g_a h_b \eta_1\eta_2\mu_3\mu_4\,\}$$

Here we notice that in general the new table is no longer symmetric with respect to the interchange of + and −. This is due to the axial part in the coupling of the Z_0.

Now we consider the second term of the spinor part of the amplitude (eq. (E3)) which we shall only need when we consider top quark pair production. We define the function Y as follows :

$$Y\,(p_1,\lambda_1,p_2,\lambda_2,g,h) = \bar{u}_{\lambda_1}(p_1)\,(g\,\omega_- + h\,\omega_+)\,u_{\lambda_2}(p_2)\;. \qquad \text{(E7)}$$

Using again the completeness relation (eq. (E5)) we can write the second term as follows :

$$-\frac{1}{M_z^2}\,\{\,b_1 m_1 Y\,(p_1,\lambda_1,p_2,\lambda_2,g_a,h_a) + b_2 m_2 Y\,(p_1,\lambda_1,p_2,\lambda_2,h_a,g_a)\,\}$$

$$\sum_{\lambda=\pm1}\sum_{\lambda'=\pm1}\Big[\,\Big(\;b_3 b_1 Y\,(p_3,\lambda_3,p_1,\lambda',1,1)\;Y\,(p_1,\lambda',p_3,\lambda,g_b,h_b) +$$

$$b_3 b_2 Y\,(p_3,\lambda_3,p_2,\lambda',1,1)\;Y\,(p_2,\lambda',p_3,\lambda,g_b,h_b)\;\Big)$$

$$Z\,(p_3,\lambda,p_4,\lambda_4,p_5,\lambda_5,p_6,\lambda_6,1,1,1,1) +$$

$$\Big(\;b_2 b_1 Y\,(p_3,\lambda_3,p_1,\lambda',1,1)\;Y\,(p_1,\lambda',p_2,\lambda,g_b,h_b) +$$

$$b_2 b_2 Y\,(p_3,\lambda_3,p_2,\lambda',1,1)\;Y\,(p_2,\lambda',p_2,\lambda,g_b,h_b)\;\Big)$$

$$Z\,(p_2,\lambda,p_4,\lambda_4,p_5,\lambda_5,p_6,\lambda_6,1,1,1,1) +$$

$$\Big(\;b_1 b_1 Y\,(p_3,\lambda_3,p_1,\lambda',1,1)\;Y\,(p_1,\lambda',p_1,\lambda,g_b,h_b) +$$

$$b_1 b_2 Y\,(p_3,\lambda_3,p_2,\lambda',1,1)\;Y\,(p_2,\lambda',p_1,\lambda,g_b,h_b)\;\Big)$$

$$Z\,(p_1,\lambda,p_4,\lambda_4,p_5,\lambda_5,p_6,\lambda_6,1,1,1,1)\;\Big]\;. \qquad \text{(E8)}$$

The function Y can again easily be expressed in terms of the S and T matrices. The result is listed in table E3.

Table E3

$$Y(\lambda_1,\lambda_2) \equiv Y(p_1,\lambda_1,p_2,\lambda_2,g,h)$$

$$Y(+,+) = g\,\mu_2\eta_1^2 + h\,\mu_1\eta_2^2$$
$$Y(+,-) = g\,s_{12}$$
$$Y(-,+) = h\,t_{12}$$
$$Y(-,-) = g\,\mu_1\eta_2^2 + h\,\mu_2\eta_1^2$$

Of course, the calculation of the amplitude with the other or both photons replaced by a Z_0 proceeds in the same way. In the case with both photons replaced by a Z_0 eq. (E3) changes which gives in particular a proliferation of Y terms. Notice that this scheme is again extremely well suited to be translated in a FORTRAN program.

The last problem that has to be solved in order to achieve an efficient event generator concerns the approximate differential cross section which is used for the event generation. When we replace in the event generator described in chapter III the matrix element squared but do not change the approximate differential cross section, the resulting generator will only be efficient at small beam energies. The reason for the inefficiency at LEP energies is the changed peaking structure of the matrix element squared. This can be understood by the observation that whenever a Z_0 replaces a photon, the denominator of the photon propagator, t, is changed into $t - M_z^2 + i\,M_z\Gamma_z$. As a consequence whenever t is positive and sufficiently large, new peaks arise in phase-space. Therefore the approximations used in the conversion and annihilation subgenerators need extensions in order to cope with this additional peaking behaviour. We solve this problem by using again the superposition principle. The conversion and annihilation subgenerator are split into four parts which deal with no Z_0, one Z_0 (two possiblities) or two Z_0 exchanges. When the virtual photon with mass t is replaced by a Z_0 the corresponding approximate differential cross section is chosen to be proportional to $1 / \left((t - M_z^2)^2 + M_z^2\Gamma_z^2 \right)$ instead of $1 / t$. In this way we can achieve efficiencies which are of the same order of magnitude as those in the pure QED case.

Appendix F

In this appendix we list the expressions which result after the contractions between $H_{\mu\nu}$ and respectively $a^{\mu}a^{\nu}$ and $g^{\mu\nu}$ have been performed.

$$H_{\mu\nu}a^{\mu}a^{\nu} = H_{\mu\nu}d_1^{\mu}d_1^{\nu}$$

$$= -32 \{ \frac{(P_{11}^2 + \frac{1}{4} t_1 d_1^2)(P_{22}^2 + t_2(\frac{1}{4} t_2 + m_\mu^2 + m_e^2))}{\Delta_1^2} +$$

$$\frac{(P_{21}^2 + \frac{1}{4} t_1 d_1^2)(P_{12}^2 + t_2(\frac{1}{4} t_2 + m_\mu^2 + m_e^2))}{\Delta_2^2} +$$

$$\{ 2 P_{11}P_{12}P_{21}P_{22} + P_{11}P_{22}\Delta_2\Delta + P_{12}P_{21}\Delta_1\Delta +$$

$$\frac{1}{4} \Delta_1\Delta_2\Delta^2 - 2 P_{11}P_{21}t_2(\frac{1}{4} t_2 + m_\mu^2 + m_e^2) -$$

$$\frac{1}{2} P_{12}P_{22}t_1d_1^2 - \frac{1}{4} d_1^2t_2[(Q_{12} + Q_{22})^2 + \frac{1}{4} (\Delta_1 - \Delta_2)^2] -$$

$$m_e^2t_1(Q_{11} + Q_{21})^2 - \frac{1}{4} m_e^2d_1^2(W^2 - t_1 - t_2)^2 -$$

$$\frac{1}{4} t_1t_2(Q_{11} - Q_{21})^2 + \frac{1}{8} t_1t_2d_1^2(4 m_e^2 + 4 m_\mu^2 - 2 W^2 - t_2) -$$

$$\frac{1}{4} t_1t_2\Delta_o^2) / (\Delta_1\Delta_2) \} / (t_1t_2)^2 , \qquad \text{(F1)}$$

$$H_{\mu\nu}g^{\mu\nu} = -32 \{ \frac{(\frac{1}{2} t_1 + m_\mu^2)(P_{22}^2 + t_2(\frac{1}{4} t_2 + m_\mu^2 + m_e^2))}{\Delta_1^2} +$$

$$\frac{(\frac{1}{2} t_1 + m_\mu^2)(P_{12}^2 + t_2(\frac{1}{4} t_2 + m_\mu^2 + m_e^2))}{\Delta_2^2} +$$

$$\{ - (t_1 + 2 m_\mu^2) P_{12}P_{22} - \frac{1}{2} t_2(Q_{12}^2 + Q_{22}^2) -$$

$$\frac{1}{4} m_e^2[(W^2 - t_1 - t_2)^2 + (\Delta_1 - \Delta_2)^2] -$$

$$\frac{1}{16}\, t_2[(W^2+ t_1+ t_2)^2+ (\Delta_1- \Delta_2)^2] +$$

$$\frac{1}{8}\, t_2[(4\, m_\mu^2- W^2)(4\, m_\mu^2+ 4\, m_e^2+ 2\, t_1+ t_2) +$$

$$W^2(t_2- 4\, m_\mu^2- 4\, m_e^2)]\ ]\ /\ (\Delta_1\Delta_2)\ \}\ /\ (t_1 t_2)^2\ , \qquad \text{(F2)}$$

$$d_1^\mu= a^\mu- \frac{Q_-\cdot a}{Q_-^2}\, Q_-^\mu\ ,\ t_1= Q_-^2\ ,\ t_2= (p_+- q_+)^2\ ,\ W^2= (k_+ + k_-)^2,$$

$$d_2^\mu= p_+^\mu+ q_+^\mu\ ,\ \varepsilon_1^\mu= d_1^\mu+ z_1 Q_-^\mu\ ,\ \varepsilon_2^\mu= d_2^\mu+ z_2(p_+^\mu- q_+^\mu)\ ,$$

$$\Delta = \varepsilon_1\cdot\varepsilon_2\ ,\ \Delta_o= d_1\cdot d_2\ ,$$
$$P_{11}= k_-\cdot\varepsilon_1- \tfrac{1}{2} z_1 t_1\ ,\quad Q_{11}= k_-\cdot d_1\ ,$$
$$P_{12}= k_-\cdot\varepsilon_2- \tfrac{1}{2} z_2 t_2\ ,\quad Q_{12}= k_-\cdot d_2\ ,$$
$$P_{21}= k_+\cdot\varepsilon_1- \tfrac{1}{2} z_1 t_1\ ,\quad Q_{21}= k_+\cdot d_1\ ,$$
$$P_{22}= k_+\cdot\varepsilon_2- \tfrac{1}{2} z_2 t_2\ ,\quad Q_{22}= k_+\cdot d_2\ . \qquad \text{(F3)}$$

The vector a^μ (and d_1^μ) is arbitrary. In the actual calculation the following vectors are used. For the calculation of eq. (4.3) $a = p_- + q_-$ (and in this case $a = d_1$), for the computation of eq. (4.10) the contraction with $H_{\mu\nu}$ is performed with the vectors a being p_-, q_- or k. The $\tilde{p}_-$, $\tilde{q}_-$ and $\tilde{k}$ in eq. (4.11) are in fact the corresponding d_1 vectors.

SAMENVATTING

Het in dit proefschrift beschreven onderzoek heeft tot doel een nauwkeurige beschrijving te geven van zogenaamde twee-foton processen zoals $e^+e^- \to e^+e^-\ell^+\ell^-$ ($\ell = e, \mu, \tau$) welke optreden bij botsingen tussen hoogenergetische electronen en positronen. De naam voor deze processen is ontleend aan het feit dat zij in essentie beschreven kunnen worden door de interactie tussen twee virtuele fotonen. Hierbij stelt men zich voor dat het proces in twee fasen verloopt. Eerst worden de fotonen uitgezonden door het inkomende electron en positron. Vervolgens ondergaan zij een wisselwerking met elkaar waarbij annihilatie plaatsvindt en twee nieuwe deeltjes (ℓ^+, ℓ^-) geproduceerd worden. De theoretische ondersteuning van dit model (de Weizsäcker-Williams benadering) heeft enige tijd de experimentele metingen aan twee-foton reacties goed kunnen verklaren. Spoedig echter werd een betere beschrijving noodzakelijk wegens de toegenomen nauwkeurigheid van de metingen. De quantumelectrodynamische berekening van twee zogenaamde multiperifere Feynman diagrammen gecombineerd met numerieke integratietechnieken bracht aanvankelijk soelaas, echter niet voor lange tijd, want tegenwoordig kunnen experimentatoren zelfs correcties op deze multiperifere beschrijving vaststellen.

De correcties die in dit proefschrift behandeld worden zijn van tweeërlei aard. In de eerste plaats is er een correctie op de multiperifere werkzame doorsnede door toedoen van andere Feynman diagrammen die in laagste orde van de electromagnetische koppelingsconstante α, $O(\alpha^4)$, bijdragen. Deze berekening levert als nevenresultaat de werkzame doorsnede voor zogenaamde vier-lepton productieprocessen zoals $e^+e^- \to \mu^+\mu^-\mu^+\mu^-$, $e^+e^- \to \mu^+\mu^-\tau^+\tau^-$, die tegenwoordig belangstelling van experimentele zijde ondervinden. Een andere correctie die ook tot deze categorie behoort, is de bijdrage van Feynman diagrammen waarbij één (of beide) van de twee virtuele fotonen vervangen is (zijn) door een Z_0 deeltje. Bij LEP energieën kunnen de effecten van deze correcties op de vier-lepton productieprocessen merkbaar worden. In de tweede plaats zijn er de zogenaamde stralingscorrecties welke van hogere orde $O(\alpha^5)$ zijn. Hierbij beschouwt men niet alleen de bovengenoemde twee-foton processen maar ook reacties waarbij in de eindtoestand zich een extra foton bevindt.

Om deze correcties te verdisconteren moeten verschillende problemen

opgelost worden. Enerzijds is de berekening zelf allerminst triviaal: nieuwe, snelle berekeningswijzen van Feynman diagrammen worden nu onontbeerlijk. Anderzijds is de berekening alleen niet voldoende. Immers de correcties zullen hanteerbaar moeten zijn voor experimentatoren, hetgeen een op het experiment gerichte aanpak vereist. Dit probleem kan worden opgelost door gebruik te maken van de Monte Carlo simulatie methode welke in het afgelopen decennium dankzij de snel toegenomen computerfaciliteiten enorme opgang gemaakt heeft. Deze simulatie houdt in dat alle vier-momenta van de deeltjes in de eindtoestand door de computer gegenereerd worden waarbij de waarschijnlijkheidsdichtheid voor het optreden van een bepaalde configuratie van de vier-momenta bepaald wordt door de theorie. Het belangrijkste voordeel van deze methode is het feit dat de verzamelingen van vier-momenta die in overeenstemming met de theoretische voorspelling geproduceerd worden, door de experimentatoren op precies dezelfde wijze behandeld kunnen worden als de echt gemeten verzamelingen van vier-momenta. Dit alles leidt tot een relatief gemakkelijke vergelijking tussen experimentele metingen en theoretische voorspellingen.

In hoofdstuk III van dit proefschrift worden de correcties ten gevolge van andere dan multiperifere Feynman diagrammen besproken. Behalve aan de berekening wordt ook veel aandacht besteed aan het ontwerp van de bijbehorende simulatie-programmatuur. In hoofdstuk IV worden de belangrijkste stralingscorrecties op het proces $e^+e^- \to e^+e^-\mu^+\mu^-$ beschouwd. Tenslotte worden in hoofdstuk V enkele resultaten besproken die verkregen zijn met behulp van de ontwikkelde Monte Carlo programmatuur. Tevens wordt een vergelijking gemaakt met experimentele metingen.

CURRICULUM VITAE

van Piet-Hein Daverveldt, geboren op 22 december 1958 te Geldrop.

Na mijn eindexamen gymnasium β aan het Rijnlands Lyceum te Wassenaar begon ik in 1977 de studie Natuurkunde aan de Rijksuniversiteit te Leiden. Het kandidaatsexamen met bijvakken Wiskunde en Sterrenkunde werd door mij in januari 1980 afgelegd. In april 1982 volgde met lof het doctoraalexamen Natuurkunde met bijvak Wiskunde. Het experimenteel werk voor dit examen werd onder leiding van Prof. Dr. A.N. Diddens en Prof. Dr. D. Harting verricht op het Nationaal Instituut voor Kernfysica en Hoge-energiefysica te Amsterdam. In het laatste jaar van mijn doctoraalstudie begon ik onder leiding van Prof. Dr. F.A. Berends op het Instituut-Lorentz voor Theoretische Natuurkunde het onderzoek van twee-foton processen. In deze periode stelde het Lorentz Fonds mij in de gelegenheid de Herbstschule für Hoch Energie Physik te Maria Laach te bezoeken. Vanaf augustus 1982 tot op heden heb ik, als wetenschappelijk medewerker in dienst van de Stichting voor Fundamenteel Onderzoek der Materie (F.O.M.), eerdergenoemd onderzoek voortgezet. De resultaten hiervan zijn beschreven in dit proefschrift.

Aan het onderwijs droeg ik bij door het geven van enkele werkcolleges. Voorts verzorgde ik enige college-uren fysische informatica. De F.O.M. stelde mij in staat deel te nemen aan de 5th International Workshop on Photon-Photon Collisions te Aken (1983), de NATO Summerschool "Particles and Fields" te Cargèse (1983),de Joint Spring Meeting of the Elementary Particles Physics Sections of Germany, Belgium and The Netherlands te Bielefeld (1984), de Workshop on Two-Photon Physics te Parijs (1984) en de 1984 CERN School of Computing te Aiguablava. In mei 1985 nam ik op uitnodiging van IBM Nederland N.V. deel aan een congres in Rome met als thema "Vector and Parallel Processors for Scientific Computations". Tevens werden diverse werkbezoeken gebracht aan DESY te Hamburg.

LIST OF PUBLICATIONS

1. F.A. Berends, P.H. Daverveldt and R. Kleiss :
Bremsstrahlung contribution to deep inelastic electron-photon scattering.
Z. Physik C 22 (1984) 239

2. F.A. Berends, P.H. Daverveldt and R. Kleiss :
Total and visible cross sections for multilepton events in e^+e^- collisions.
Phys. Lett. 148B (1984) 489.

3. F.A. Berends, P.H. Daverveldt and R. Kleiss :
Radiative corrections to the process $e^+e^- \to e^+e^-\mu^+\mu^-$.
Nucl. Phys. B253 (1985) 421.

4. F.A. Berends, P.H. Daverveldt and R. Kleiss :
Complete lowest order calculations for four-lepton final states in e^+e^- collisions. Nucl. Phys. B253 (1985) 441.

5. F.A. Berends, P.H. Daverveldt and R. Kleiss :
Monte Carlo simulation of two-photon processes; I: Radiative corrections to multiperipheral $e^+e^-\mu^+\mu^-$ production.
Leiden preprint.

6. F.A. Berends, P.H. Daverveldt and R. Kleiss :
Monte Carlo simulation of two-photon processes; II: Complete lowest order calculations for four-lepton production processes in e^+e^- collisions.
Leiden preprint.

7. F.A. Berends, P.H. Daverveldt and R. Kleiss :
Monte Carlo simulation of two-photon processes; III: Complete lowest order calculations for $e^+e^- \to e^+e^-\mu^+\mu^-$ with large angle tagging conditions.
Leiden preprint.

8. F.A. Berends and P.H. Daverveldt :
Effects of an excited muon on $\mu^+\mu^-\gamma$ final states.
Leiden preprint.

Diverse tekeningen in dit proefschrift zijn vervaardigd door de Heer W.F. Tegelaar.